

**SSC-473**

**METHODOLOGY FOR DEFINING  
TECHNICAL SAFE SPEEDS FOR LIGHT  
ICE-STRENGTHENED GOVERNMENT  
VESSELS OPERATING IN ICE**

By J. Dolny

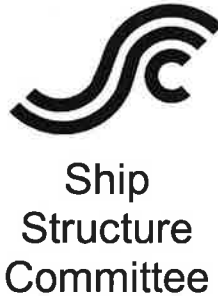


This document has been approved  
for public release and sale; its  
distribution is unlimited.

**SHIP STRUCTURE COMMITTEE**  
**2018**

*Member Agencies:*

American Bureau of Shipping  
Defence Research & Development Canada  
Maritime Administration  
Military Sealift Command  
Naval Sea Systems Command  
Office of Naval Research  
Society of Naval Architects & Marine Engineers  
Transport Canada  
United States Coast Guard



*Address Correspondence to:*

Commandant (CG-ENG-2/SSC)  
ATTN: Executive Director, SSC  
US Coast Guard  
2703 Martin Luther King Jr. Ave SE  
Washington, DC 20593-7509  
Website: <http://www.shipstructure.org>

SSC – 473  
SR – 1475

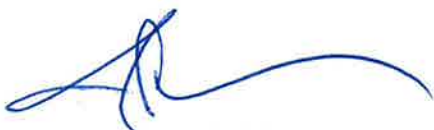
05 October 2017

**METHODOLOGY FOR DEFINING TECHNICAL SAFE SPEEDS FOR LIGHT ICE-STRENGTHENED GOVERNMENT VESSELS OPERATING IN ICE**

With marine traffic in the Arctic on the rise, governments are expanding their maritime presence in the northern seaways and building capabilities to prevent accidents, support emergency responses, search and rescue, and to address issues related to national sovereignty. Despite the declining minimum extent of summer Arctic sea ice, there is still ice present throughout the year and deployments may be in areas infested with ice. Operators of naval ships that may be deployed to the Arctic need a sound methodology to understand the operational limitations of their assets in various ice conditions.

This report provides an overview of several existing approaches for determining operational limitations of ships in various ice conditions. A detailed technical methodology is proposed to determine technical safe speeds for different ice conditions that is founded on modern principles of modeling ice-structure interaction. The focus is on government vessels that are lightly ice-strengthened, which may be required to operate in pack ice conditions as part of an emergency response effort. A case study is presented of a 5000 ton Ice Class PC5 Patrol Vessel to demonstrate the ice capability assessment procedure and the influence of key parameters.

We thank the authors and Project Technical Committee for their dedication and research toward completing the objectives and tasks detailed throughout this paper and continuing the Ship Structure Committee's mission to enhance the safety of life at sea.



J. P. NADEAU  
Rear Admiral, U.S. Coast Guard  
Co-Chairman, Ship Structure Committee



L. C. SELBY  
Rear Admiral, U.S. Navy  
Co-Chairman, Ship Structure Committee

# SHIP STRUCTURE COMMITTEE

RDML John Nadeau  
U. S. Coast Guard Assistant Commandant,  
for Prevention Policy  
Co-Chair, Ship Structure Committee

Mr. H. Paul Cojeen  
Society of Naval Architects and Marine Engineers

Mr. Kevin Kohlmann  
Director, Office of Safety  
Maritime Administration

Mr. Kevin Baetsen  
Director of Engineering  
Military Sealift Command

Mr. Jeffrey Lantz  
Director, Commercial Regulations and Standards  
U.S. Coast Guard

Mr. Albert Curry  
Deputy Assistant Commandant for Engineering and  
Logistics  
U.S. Coast Guard

RDML Lorin Selby  
Chief Engineer and Deputy Commander  
For Naval Systems Engineering (SEA05)  
Co-Chair, Ship Structure Committee

Mr. Howard Fireman  
Senior Vice President  
American Bureau of Shipping

Dr. John MacKay  
Head, Warship Performance, DGSTCO  
Defence Research & Development Canada - Atlantic

Mr. Luc Tremblay  
Executive Director, Domestic Vessel Regulatory Oversight  
and Boating Safety, Transport Canada

Mr. Eric Duncan  
Director,  
Ship Integrity and Performance Engineering Group  
Naval Sea Systems Command

Dr. Thomas Fu  
Director, Ship Systems and Engineering Research Division  
Office of Naval Research

## SHIP STRUCTURE SUB-COMMITTEE

### UNITED STATES COAST GUARD (CVE)

CAPT Ben Hawkins  
Mr. Jaideep Sirkar  
Mr. Charles Rawson

### AMERICAN BUREAU OF SHIPPING

Mr. Craig Bone  
Mr. Daniel LaMere  
Mr. Richard Delpizzo

### SOCIETY OF NAVAL ARCHITECTS AND MARINE ENGINEERS

Mr. Rick Ashcroft  
Dr. Roger Basu  
Dr. Robert Sielski  
Dr. Paul H. Miller

### DEFENCE RESEARCH & DEVELOPMENT CANADA ATLANTIC

Dr. Malcolm Smith  
Mr. Cameron Munro

### MARITIME ADMINISTRATION

Mr. Chao Lin  
Mr. Richard Sonnenschein  
Mr. Todd Ripley  
Mr. Todd Hiller

### TRANSPORT CANADA

Ms. Abigail Fyfe  
Mr. Bashir Ahmed Golam

### UNITED STATES COAST GUARD (FLEET)

CAPT George Leshner  
Mr. Timothy McAllister  
Mr. Frank DeBord  
Mr. Marty Hecker

### NAVSEA/NSWCCD

Mr. David Qualley  
Mr. Gerard Mercier  
Mr. Dean Schleicher  
Mr. Pradeep Sensharma

### MILITARY SEALIFT COMMAND

Ms. Jeannette Viernes

### OFFICE OF NAVAL RESEARCH

Dr. Paul Hess

# PROJECT TECHNICAL COMMITTEE

*The Ship Structure Committee greatly appreciates the contributions of the individuals that volunteered their time to participate on the Project Technical Committee, listed below, and thanks them heartily. They were the subject matter expert representatives of the Ship Structure Committee to the contractor, performing technical oversight during contracting, advising the contractor in cognizant matters pertaining to the contract of which the agencies were aware, and performing technical peer review of the work in progress and upon completion.*

## **Co-Chairs:**

Mr. David Qualley, Naval Sea Systems Command  
Mr. James Webster, Naval Sea Systems Command

## **Members:**

Ms. Karlin Anderson, Naval Surface Warfare Center  
Mr. Nathan Hagan, Naval Surface Warfare Center  
Dr. Paul Hess, Office of Naval Research  
LT Joshua Kapusta, US Coast Guard  
Dr. John MacKay, Defence Research and Development Canada  
Mr. Timothy McAllister, US Coast Guard  
Dr. Pradeep Sensharma, Naval Sea Systems Command  
Dr. Robert Sielski, Consultant  
Mr. Jaideep Sirkar, US Coast Guard  
Dr. Arnold Song, Cold Regions Research Engineering Laboratory  
Dr. Malcolm Smith, Defence Research and Development Canada

## **Ship Structure Committee Co-Executive Directors:**

LT Jonathan Duffett, US Coast Guard  
LT Joshua Kapusta, US Coast Guard

1. Report No. SSC-473	2. Government Accession No.	3. Recipient's Catalog No.	
4. Title and Subtitle Methodology for Defining Technical Safe Speeds for Light Ice-Strengthened Government Vessels Operating in Ice		5. Report Date 28 November 2016	
		6. Performing Organization Code	
7. Author(s) Dolny, John		8. Performing Organization Report No. SR - 1475	
9. Performing Organization Name and Address American Bureau of Shipping 16855 Northchase Drive Houston, TX 77060 US		10. Work Unit No. (TRAIS)	
		11. Contract or Grant No. N00178-04-D-4030-EH02	
12. Sponsoring Agency Name and Address The Ship Structure Committee COMMANDANT (CG-ENG-2/SSC) ATTN (ADMIN ASST/SHIP STRUCTURE COMMITTEE)  US COAST GUARD 2703 MARTIN LUTHER KING JR. AVE SE MAILSTOP 7509 WASHINGTON DC 20593-7509.		13. Type of Report and Period Covered Final Report	
		14. Sponsoring Agency Code	
15. Supplementary Notes Contract issued to ABS by CSC Government Solutions LLC Subcontract Number: S6030036 Task Order No: EH02			
16. Abstract With marine traffic in the Arctic on the rise, governments are expanding their maritime presence in the northern seaways and building capabilities to prevent accidents, support emergency responses, search and rescue, and to address issues related to national sovereignty. Despite the declining minimum extent of summer Arctic sea ice, there is still ice present throughout the year and deployments may be in areas infested with ice. Operators of naval ships that may be deployed to the Arctic need a sound methodology to understand the operational limitations of their assets in various ice conditions. Damaging a ship that has been sent to support and assist a response effort is not acceptable.  This report provides an overview of several existing approaches for determining operational limitations of ships in various ice conditions. A detailed technical methodology is proposed to determine technical safe speeds for different ice conditions that is founded on modern principles of modeling ice-structure interaction. The focus is on government vessels that are lightly ice-strengthened, which may be required to operate in pack ice conditions as part of an emergency response effort. A case study is presented of a 5000 ton Ice Class PC5 Patrol Vessel to demonstrate the ice capability assessment procedure and the influence of key parameters.			
17. Key Words  Safe speed in ice, ice class, naval ships, Arctic		18. Distribution Statement Distribution is available to the public through: National Technical Information Service U.S. Department of Commerce Springfield, VA 22151 Ph. (703) 487-4650	
19. Security Classif. (of this report) Unclassified	20. Security Classif. (of this page) Unclassified	21. No. of Pages 77	22. Price

**CONVERSION FACTORS**  
(Approximate conversions to metric measures)

To convert from	to	Function	Value
<b>LENGTH</b>			
inches	meters	divide	39.3701
inches	millimeters	multiply by	25.4000
feet	meters	divide by	3.2808
<b>VOLUME</b>			
cubic feet	cubic meters	divide by	35.3149
cubic inches	cubic meters	divide by	61,024
<b>SECTION MODULUS</b>			
inches <sup>2</sup> feet	centimeters <sup>2</sup> meters	multiply by	1.9665
inches <sup>2</sup> feet	centimeters <sup>3</sup>	multiply by	196.6448
inches <sup>3</sup>	centimeters <sup>3</sup>	multiply by	16.3871
<b>MOMENT OF INERTIA</b>			
inches <sup>2</sup> feet <sup>2</sup>	centimeters <sup>2</sup> meters <sup>2</sup>	divide by	1.6684
inches <sup>2</sup> feet <sup>2</sup>	centimeters <sup>4</sup>	multiply by	5993.73
inches <sup>4</sup>	centimeters <sup>4</sup>	multiply by	41.623
<b>FORCE OR MASS</b>			
long tons	tonne	multiply by	1.0160
long tons	kilograms	multiply by	1016.047
pounds	tonnes	divide by	2204.62
pounds	kilograms	divide by	2.2046
pounds	Newtons	multiply by	4.4482
<b>PRESSURE OR STRESS</b>			
pounds/inch <sup>2</sup>	Newtons/meter <sup>2</sup> (Pascals)	multiply by	6894.757
kilo pounds/inch <sup>2</sup>	mega Newtons/meter <sup>2</sup> (mega Pascals)	multiply by	6.8947
<b>BENDING OR TORQUE</b>			
foot tons	meter tons	divide by	3.2291
foot pounds	kilogram meters	divide by	7.23285
foot pounds	Newton meters	multiply by	1.35582
<b>ENERGY</b>			
foot pounds	Joules	multiply by	1.355826
<b>STRESS INTENSITY</b>			
kilo pound/inch <sup>2</sup> inch <sup>1/2</sup> (ksi <sup>1/2</sup> /in)	mega Newton MNm <sup>3/2</sup>	multiply by	1.0998
<b>J-INTEGRAL</b>			
kilo pound/inch	Joules/mm <sup>2</sup>	multiply by	0.1753
kilo pound/inch	kilo Joules/m <sup>2</sup>	multiply by	175.3



ABS Technical Report

---

## **Ship Structure Committee**

# **Methodology for Defining Technical Safe Speeds for Light Ice-Strengthened Government Vessels Operating in Ice**

## **Final Report**

November 2016

American Bureau of Shipping  
Incorporated by Act of Legislature of  
the State of New York 1862

Copyright © 2016  
American Bureau of Shipping  
ABS Plaza  
16855 Northchase Drive  
Houston, TX 77060 US

# Contents

Acknowledgements.....	7
1. Introduction .....	8
2. Summary of Safe Speed Issues .....	9
2.1. Ice types .....	9
2.2. Concentration .....	10
2.3. Floe size.....	12
2.4. Ice Strength .....	12
2.5. Ice Class.....	14
2.6. Hull Form.....	15
2.7. Operations .....	16
3. Review of Existing Approaches for Operational Limitations in Ice .....	17
3.1. Risk-based Control Regimes.....	17
3.1.1. Canadian Arctic Ice Regime Shipping System (AIRSS).....	17
3.1.2. IMO Polar Code – POLARIS.....	17
3.2. Safe Speed in Ice .....	23
3.2.1. Russian Ice Passport / Ice Certificate .....	23
3.2.2. Probabilistic Approaches.....	25
3.2.3. Recent Approaches .....	26
4. Technical Methodology for Defining the Safe Speeds in Ice .....	33
4.1. DDePS.....	33
4.2. Case 2a Interaction Scenario.....	35
4.3. Impact Model and Collision Mechanics .....	35
4.4. Ice Crushing Forces .....	37
4.4.1. Modification for Steep Frame Angles .....	39
4.5. Ice Flexural Limit Model.....	43
4.5.1. Updated Flexural Failure Limit Model.....	43
4.6. Structural Limit States and Speed Check Algorithm .....	48
4.6.1. Polar Class Design Limit Load Criteria .....	48
4.6.2. Direct Line Load Criteria.....	49
4.6.3. Large Deflection Criteria .....	52
4.7. DDePS Validation .....	53
5. Case Study – Ice Class PC5 Patrol Vessel.....	54
5.1. Hull Form.....	54
5.2. Hull Structural Design .....	55

5.3.	Finite Element Mesh .....	56
5.4.	Structural Response to Various Patch Loads .....	57
5.5.	Safe Speed Assessment.....	60
5.5.1.	Example DDePS Outputs .....	60
5.5.2.	Safe Speed Results .....	66
6.	Conclusions and Future Work.....	68
7.	References .....	70
Appendix A - Description of Popov Terms .....		73
A.1	Popov Terms for Ship .....	73
A.2	Popov Terms for Ice .....	75

## **Acknowledgements**

This study has been funded by the Ship Structure Committee (SSC). Their support and technical feedback throughout the project is gratefully appreciated.

The approaches and software employed in this study has been developed over many years through collaborative research and development efforts between ABS, BMT Fleet Technology, Memorial University of Newfoundland, and Vard Marine Inc. The authors would like to acknowledge the technical contributions from Dr. Claude Daley and Mr. Andrew Kendrick during the development of these methodologies.

Financial support for previous efforts and ongoing parallel projects have also been provided by United States Coast Guard (USCG), Office of Naval Research (ONR), Defense Research and Development Canada (DRDC), and Transport Canada (TC). The authors would like to specifically acknowledge the support from Mr. Tim McAllister (USCG), Dr. Paul Hess (ONR), Dr. Neil Pegg (DRDC), and Mr. Brad Spence (TC). These efforts have greatly advanced the state-of-the-art in this field and help to promote a continued Canada-US joint interest in Arctic vessel operational safety.

## 1. Introduction

The reduction of ice cover has led to new opportunities for Arctic shipping sea routes, increased destination shipping for the exploration and extraction of natural resources, increased adventure and cruise ship tourism, and more environmental science and charting activity in territorial waters. This growth of maritime activity in Arctic waters potentially increases the probability of an incident occurring in the region. Incidents can occur due to a variety of hazards associated with Arctic operations. Some of the most critical hazards include structural damage from ice collisions, stability casualties from ice accretion, equipment and machinery functionality in low air temperatures, and grounding due to lack of accurate charting.

If a significant incident occurs government ships including combatants, cutters, and auxiliary fleets may be required to respond and provide assistance. It is recognized that the Canadian and American icebreaker fleet is ageing and limited. While both governments have recently announced plans to modernize their icebreaker fleets, the acquisition programs are expected to take many years to complete (earliest estimates suggest 2020 for delivery of the first new Polar Icebreaker). In the meantime there is a need to maintain an active presence in these regions with capabilities to support prevention, emergency response, search and rescue, and to address national sovereignty issues. This may result in the deployment of non-ice strengthened combatants (e.g. destroyer, frigate, and command and control ship) or lightly ice strengthened support and patrol ships to the Arctic. Despite the declining minimum extent of summer Arctic sea ice, there is still ice present throughout the year and these deployments may be in areas infested with ice.

Operators of naval ships that may be deployed to the Arctic need a sound methodology to understand the operational limitations of their assets in various ice conditions. Damaging a ship that has been sent to support and assist a response effort is not acceptable. The risk of structural damage to a ship operating in ice depends on many factors which include the ice conditions (thickness, strength and concentration), the ship's structural particulars (shape of the hull, scantlings and structural arrangement) and the vessel's operations (speed and maneuvering). Safe operations in ice typically rely on a combination of quality ice information, the ability to maneuver around/away from hazards, and adequate structural capacity to resist ice loads which arise the form of forces and pressures on the hull.

This report first addresses the issues associated with the safe speed in general and then outlines a technical methodology to determine technical safe speeds for different ice conditions. The focus is on government vessels that are lightly ice-strengthened, which may be required to operate in light to medium pack ice conditions as part of an emergency response effort. This report provides an overview of the principle issues for safe speed while operating in ice infested water and related issues. It also summarizes several existing approaches for determining operational limitations of ships in various ice conditions. A synthesized methodology is proposed and the detailed technical background is presented. Finally, a case study is presented of a 5000 ton Ice Class PC5 Patrol Vessel to demonstrate the ice capability assessment procedure and the influence of key parameters.

## 2. Summary of Safe Speed Issues

The risk of structural damage to ships operating in ice depend on several factors. The most fundamental line of defense is to simply avoid the ice. Ice avoidance requires quality information about the conditions, whether it be visual observation from the bridge, access to available ice charts, or the use of onboard radar and other ice detection technologies. If ice contact cannot be avoided, the ship itself should have proper materials and structural capacity to resist the ice loads. Ice class ships are strengthened specifically to increase the local structural resistance to ice impact loads. For extreme overload scenarios of the rupture of the shell plating, subdivision and damage stability requirements offer a final line of defense from a catastrophic breach of the hull.

Ship speed and vessel maneuvers are operational considerations that can reduce the risk of structural damage. This section describes each of the key factors that should be considered when establishing safe operational limitations for ships in ice:

- Ice types
- Ice concentrations
- Ice floe size
- Ice strength
- Ship ice class
- Ship hull form
- Operational modes

### 2.1. Ice types

There are many different forms of ice and it is important to be able to distinguish between the different types that may be encountered. Ice cover is rarely uniform or homogeneous in nature. Sea ice is typically found as a mix of ice types, thicknesses and floe sizes at various total ice concentrations. Near the coast, ice may be ‘land fast’, anchored in place by the shoreline or possibly grounded pressure ridges. Further offshore, pack ice typically consists of a mix of ice usually characterized as an ‘ice regime’.

Table 1 describes the standard nomenclature for sea ice ‘stage of development’ established by the World Meteorological Organization (WMO) and adopted by most national ice services. Each stage up to old ice has an associated nominal ice thickness range. The thickness generally increases as the ice is exposed to longer periods of cold temperatures (or Freezing Degree Days). Thicker ice also can become stronger in both compressive and flexural strengths. The codes are used in ice charts and ‘egg codes’ as a way to quickly reference each ice type. Egg codes are further discussed below.

**Table 1: Ice types according to WMO nomenclature**

Stage of Development	Thickness	Code	Stage of Development	Thickness	Code
New Ice	< 10 cm	1	Medium First Year Ice	70 - 120 cm	1●
Nilas, Ice Rind	< 10 cm	2	Thick First Year Ice	> 120 cm	4●
Young Ice	10 - 30 cm	3	Old Ice	--	7●
Grey Ice	10 - 15 cm	4	Second Year Ice	--	8●
Grey - White Ice	15 - 30 cm	5	Multi-Year Ice	--	9●
First Year Ice	30 - 200 cm	6	Ice of Land Origin (Glacial/Icebergs)	--	▲●
Thin First Year Ice	30 - 70 cm	7	Undetermined/Unknown	--	X●
Thin First Year Stage 1	30 - 50 cm	8			
Thin First Year Stage 2	50 - 70 cm	9			

## 2.2. Concentration

Ice can be present in various concentrations usually expressed in tenths coverage. Lower concentrations mean there is more open water to maneuver around hazardous features and the probably of ice contact can be reduced. Higher concentrations initially make it more difficult to identify and differentiate between ice types. Contact with ice in high concentrations becomes unavoidable and ice interactions can hinder maneuverability, in particular for hull forms not optimized for icebreaking.

Winds, currents, and tides cause ice fields to converge and potentially creates ridges as the ice buckles and fractures (i.e. deformed ice). This is known as ‘pressure’ and can persist at different severity levels. High pressure in the ice pack can pose a significant restriction to vessel movement and may ultimately lead to besetment.

Ice concentration is generally reported in terms of areal coverage in tenths. The scale of areal coverage can vary depending on the perspective of the reporting source. From the bridge of a ship, concentration is typically concerning the coverage of ice within the line of site of the ship (up to several kilometers). Ice concentrations reported on ice charts relate to a much larger scale on the order of 10s of kilometers. Figure 1 is provided by the Canadian Coast Guard (2012) in the guide on *Ice Navigation in Canadian Waters* and depicts different concentrations of ice.



Figure 1: Ice concentrations (source CCG)

Ice charting services, for example the Canadian Ice Service (CIS) and the US Naval/National Ice Center (NIC) regularly produce ice charts for different geographical regions. The charts show an analysis of ice conditions based on an integration of data collected from satellite imagery, weather/oceanographic information, and visual observations from ship and aircraft. Charts are typically prepared on a daily, weekly or bi-weekly basis, depending on the region, and use a series of ‘Egg Codes’ to indicate concentration, stage of development, and form of ice (floe sizes). The charts can be used for planning of marine operations as well as for environmental research on the change and variability of ice conditions over time.

An example CIS ice chart is presented in Figure 2 for ‘Approaches to Resolute, mid-October’ in the northwestern part of Baffin Bay. The color codes represent different total concentrations. The ‘Egg Codes’ express concentration as a ratio in tenths describing the area of the water surface covered by ice as a fraction of the whole area. Total concentration includes all stages of development that are present while partial concentration refers to the amount of a particular stage or of a particular form of ice and represents only a part of the total. In this example the total concentration of regime ‘L’ is +9/10ths, or near 100%. The ice regime is comprised of 3/10ths multi-year ice, 5/10ths grey ice (10-15cm), and 1/10<sup>th</sup> new ice (<10cm) following the codes in Table 1.

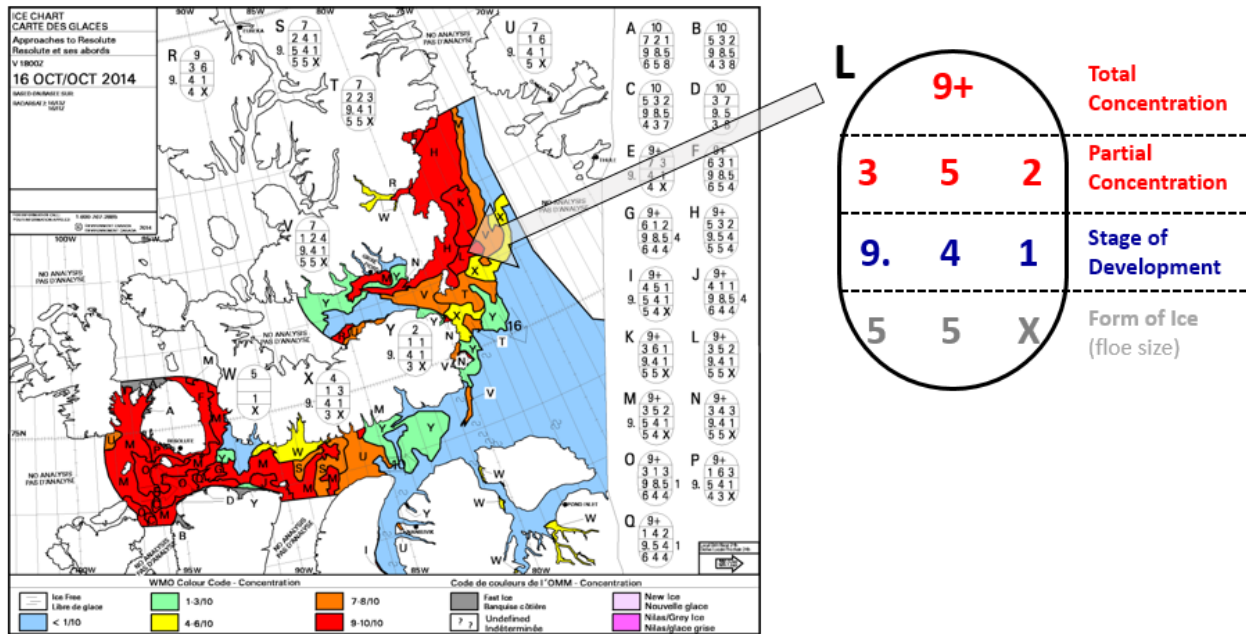


Figure 2: Example ice chart and egg code (courtesy of Canadian Ice Service)

From the bridge of a ship, an 'Egg Code' can also be used to characterize an observation of ice conditions. Bridge observations can be subjective and the quality of the egg code description depends on the experience and skill level of the ice observer. Figure 3 is an example of an ice regime that is approximately 6/10ths total coverage with 4/10ths thick first-year ice (120-200cm), 1/10<sup>th</sup> second year ice, and 1/10<sup>th</sup> multi-year ice (note the dot applies to each ice type listed to its left).

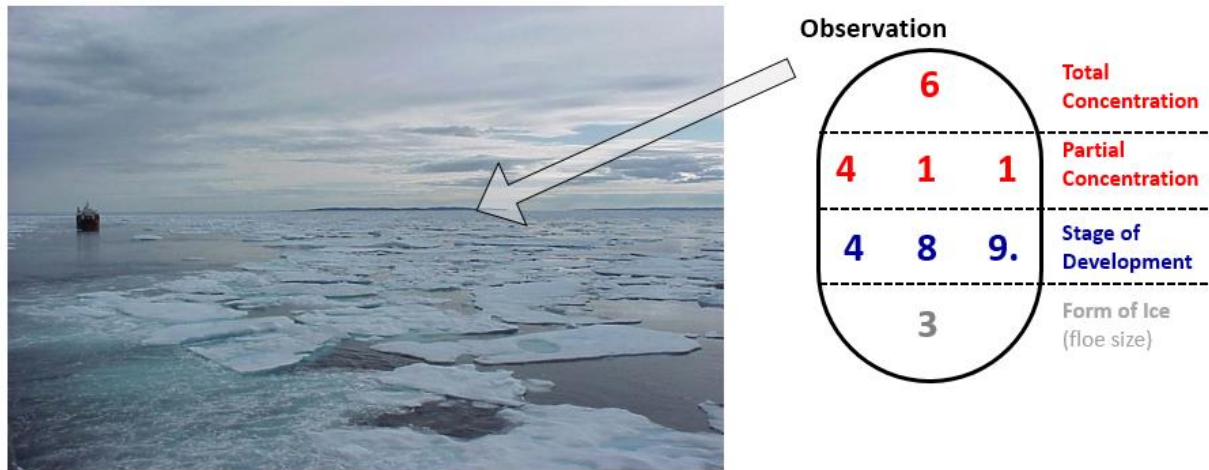


Figure 3: Example ice observation and egg code

### 2.3. Floe size

For operations in pack ice, the mass of the floe will have a direct effect on the loads acting on the ship hull. Floe mass depends on the area of the floe (size) and its thickness. WMO defines ice floe sizes into several categories as shown in Table 2. The range of floe widths for each category is fairly large, e.g. small floes are 20-100m, medium floes are 100-500m, and big floes are 500m – 2km. For most ships once floe sizes get to ~2-4x the ship’s length, the floes become effectively infinite. The categories and floe sizes specified by WMO are not really practical to vessel operations. As will be shown in later in this project, a smaller discretization of floe size is needed.

Table 2: Ice floe sizes

Floe Sizes	Floe Width	Code
Pancake ice		0
Small ice cake; brash ice	< 2 m	1
Ice cake	2 - 20 m	2
Small floe	20 - 100 m	3
Medium floe	100 - 500 m	4
Big floe	500 - 2000 m	5
Vast floe	2 - 10 km	6
Giant floe	> 10 km	7
Fast ice, growlers, or floe-bergs		8
Icebergs		9
Undetermined or unknown		X

### 2.4. Ice Strength

Ice crushing strength and flexural strength can greatly influence the severity of ice loads on ships. Both terms are critical inputs to the technical method that will be applied in this project. Previous studies have highlighted the influence of ice strength on the local ice loads during impacts and the ultimate safe speed envelopes for different ship types (ABS, 2015; Dolny, Yu, Daley, & Kendrick, 2013; VARD, 2015). It’s important to consider realistic ice strength parameters when carrying out a ship-specific analysis.

Various measurement data has been collected to study the variations in ice crushing strengths across different regions of the Arctic and for different types of ice. Unfortunately crushing strength is a challenge to define and measurement techniques can vary. Timco and Weeks (2010) provided a comprehensive review of the engineering properties of sea ice and assessed the state of knowledge of various physical and mechanical properties. Two common methods for measuring the crushing strength of sea ice include uniaxial compressive sample tests and in-situ borehole jack tests which measure the failure load (and stress) for ice under compression. Test setups can vary and confining stresses can be introduced which can affect the strength results. Several researchers have studied the relationships between borehole and uniaxial tests. Kendrick & Daley (2011) offer a brief discussion of the different methods and how they relate to loads on ship hulls.

The ice impact model used in the IACS Polar Rules (Daley, 2000) and the model used in the technical method proposed later in this report consider crushing strength as a nominal average pressure to crush ice on a contact area of  $1\text{m}^2$ , or  $P_0$ , together with an inverse exponential function of area,  $ex = -0.1$ . This ‘process’ pressure-area representation of ice strength is derived from field measurements collected from instrumented ship panels and is one available ice crushing model.

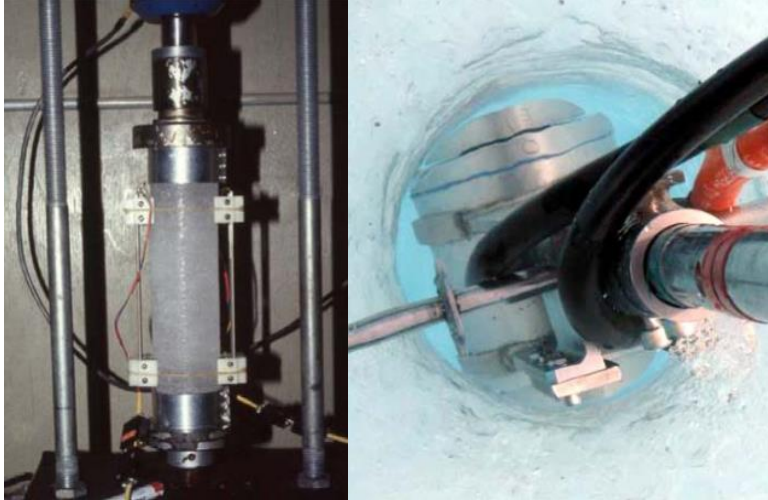


Figure 4: Typical ice compressive strength testing methods - uniaxial crushing (left) and in-situ borehole tests (right) [from Timco & Weeks, 2010]

The pressure-area approach to characterize ice crushing strength lends itself to the development of an ice load pressure patch which is used to establish the minimum required structural scantlings in the rules. This is quite different from uniaxial strength values reported in the literature from field and laboratory experiments. Other ice crushing models exist and have been used to determine ice loads on ship structures. For example section 3.2.1 briefly describes the Kheisin-Kurdyumov hydrodynamic model of ice-structure interaction that is utilized in the Russian rules and ice passport derivations.

Ice flexural strength is another practical parameter that is important to ice engineering problems, in particular ice loads on ship hulls, although it is not considered a basic material property. The basic concept of an icebreaking hull form is to introduce hull angles such that the flexural failure of an ice sheet limits the maximum ice crushing force on the hull. Flexural strength is typically measured using a simple beam bending or a cantilever beam tests. Typically for performance trials of icebreaking ships, target flexural bending strengths are between 0.5MPa – 0.75MPa.

Ice strength can be highly variable and is not currently reported on ice charts. From the bridge of a ship, ice strength is also quite difficult to judge. In the deterministic methodology outlined in this report, conservative process-pressure area relationships are generally selected for the crushing terms, with  $P_o$  ranging from 2MPa – 6MPa. Figure 5 shows a few different model pressure area relationships compared with the strength models assumed for each IACS Polar Class.

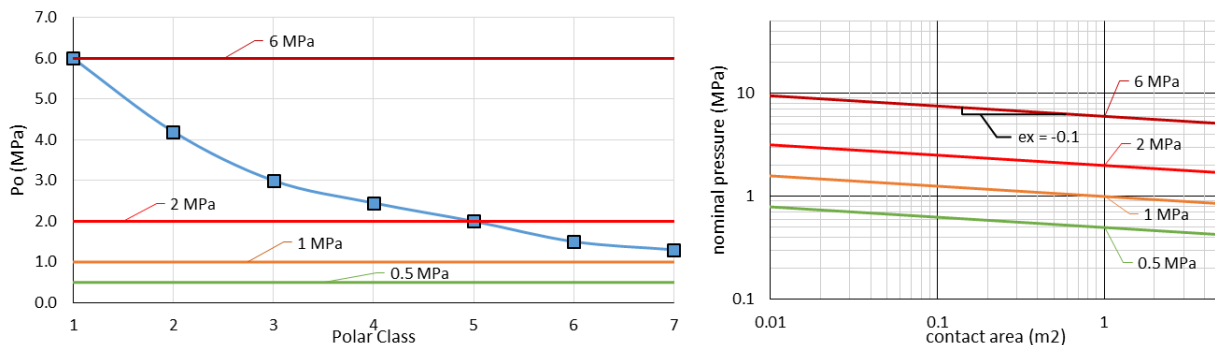


Figure 5: Typical ice crushing parameters

## 2.5. Ice Class

Ice class requirements have been developed by classification societies and maritime authorities based on decades of service experience and history of ships operating in ice. Currently two principle sets of ice class rules are available and used in practice:

- 1) Finnish-Swedish Ice Class Rules (FSICR, or Baltic Rules)
- 2) International Association of Classification Societies - Unified Requirements for Polar Ships (IACS Polar UR, or Polar Rules).

The FSICR were originally developed and primarily intended for winter navigation in the Baltic Sea although they are applicable to several other areas where first-year sea ice is prevalent. Four (4) ice classes have been established by the Finnish and Swedish maritime authorities and are essential to the robust winter navigation system that exists in the region. The requirements for structural scantlings and machinery have been calibrated many times over the years based on empirical data and service history. Table 3 describes each of Baltic ice classes along with the assumed level ice thickness used in the design point for structural strength.

**Table 3: Finnish-Swedish Ice Class Rules with nominal descriptions**

FS Ice Class	Description	Level Ice Thickness (for structural design)
IA Super	Navigating in difficult ice conditions without the assistance of icebreakers	1.0m
IA	Navigating in difficult ice conditions, with the assistance of icebreakers when necessary	0.8m
IB	Navigating in moderate ice conditions, with the assistance of icebreakers when necessary	0.6m
IC	Navigating in light ice conditions, with the assistance of icebreakers when necessary	0.4m

Prior to the development of the IACS Polar Rules, classification societies each had their own unique set of ice classes for ships intended for Arctic operations. In 2008, the International Association of Classification Societies (IACS) finalized the Polar Class Unified Requirements, the result of a long term harmonization effort between IACS members and several coastal administrations. Seven (7) Polar Classes were defined based on descriptions of nominal ice conditions as shown in Table 4. The intent of the highest Polar Class PC1 is to offer the capability for a ship to operate year-round in all Polar waters, subject to due caution by the crew. The lowest two Polar Classes, PC7 and PC6, were intentionally set to approximately correspond to FS Class 1A and 1A Super, respectively, however the Polar Rules consider old ice inclusions and their design points have been shown to slightly exceed those of the Baltic counterparts. Riska and Kämäräinen (2012) offer a detailed comparison between the background and history of Polar Rules and FSICRs and their respective design points.

**Table 4: IACS Polar Class Rules with nominal descriptions**

Polar Class	Ice Description (based on WMO Sea Ice Nomenclature)
PC1	Year-round operation in all Polar waters
PC2	Year-round operation in moderate multi-year ice conditions
PC3	Year-round operation in second-year ice which may include multi-year ice inclusions.
PC4	Year-round operation in thick first-year ice which may include old ice inclusions
PC5	Year-round operation in medium first-year ice which may include old ice inclusions
PC6	Summer/autumn operation in medium first-year ice which may include old ice inclusions
PC7	Summer/autumn operation in thin first-year ice which may include old ice inclusions

One unique aspect of the IACS Polar Rules was the philosophy that the design ice load can be rationally linked to a design ship-ice interactions scenario. The selected design scenario is a glancing impact with a thick level ice edge and a mathematical model was developed for calculating ice load parameters for the bow region. The IACS Polar Rules model forms the basis of the technical methodology proposed later in this report.

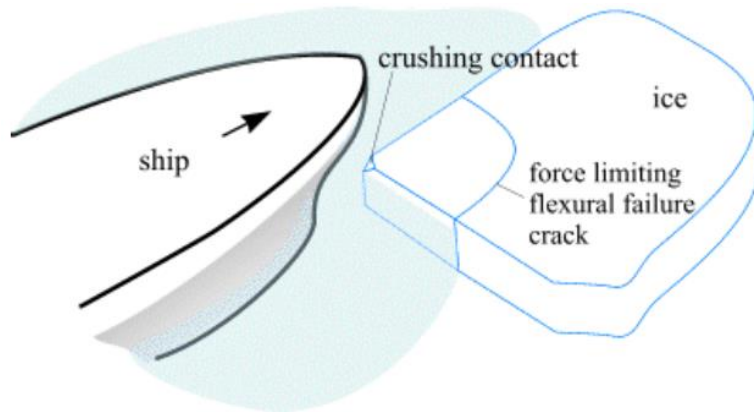


Figure 6: IACS Polar Rules design scenario - glancing impact with thick level ice edge

Any ship has some notional capacity to transit a certain amount of ice cover safely, though for a standard open water ship the safe thickness is quite thin. As ice strengthening (i.e. ice class) is added to the hull, it becomes capable of handling thicker ice. Since the ice class rules are intended to provide a set of construction standards, the compliance with an ice class does not provide a full representation of the ship's structural capabilities or limitations in various ice environments or operational modes. Additional analysis procedures are often sought by prudent designers, builders and owners to quantitatively place bounds on the ships' structural capabilities. This project proposed one possible synthesized technical analysis procedure.

## 2.6. Hull Form

There is a vast range of potential ship hull forms, whose hull (bow) angles have a strong influence on ice loads. Figure 7 presents sketches of three different bow forms - a non-icebreaking form (typical of naval platforms), a moderate icebreaking form (in this example a Polar Class patrol vessel) and a heavy icebreaking bow (Polar Class cargo ship).

Icebreaking bows are generally designed to promote ice failure in bending (i.e. flexural failure). During level icebreaking an icebreaking bow will ride over the ice and exert enough downward force to induced flexural failure. This tends to reduce the local loads on the ship compared with pure crushing of the ice. Icebreaking hull forms are also typically optimized to clear the ice away from propellers and underwater appendages and reduce surface drag of the ice on the aft section of the hull.

Non-icebreaking bow forms are designed for open water performance. Typically at the waterline they have more vertically sided surfaces (low  $\beta$  angles) which result in promoting more crushing behavior. Some open water ships, e.g. naval platforms, tend to have fine waterline entrance geometries (low  $\alpha$  angles). Others, e.g. large tankers, may have very blunt bow forms which high  $\alpha$  angles. These features can play a significant role on the nature of local ice pressures.

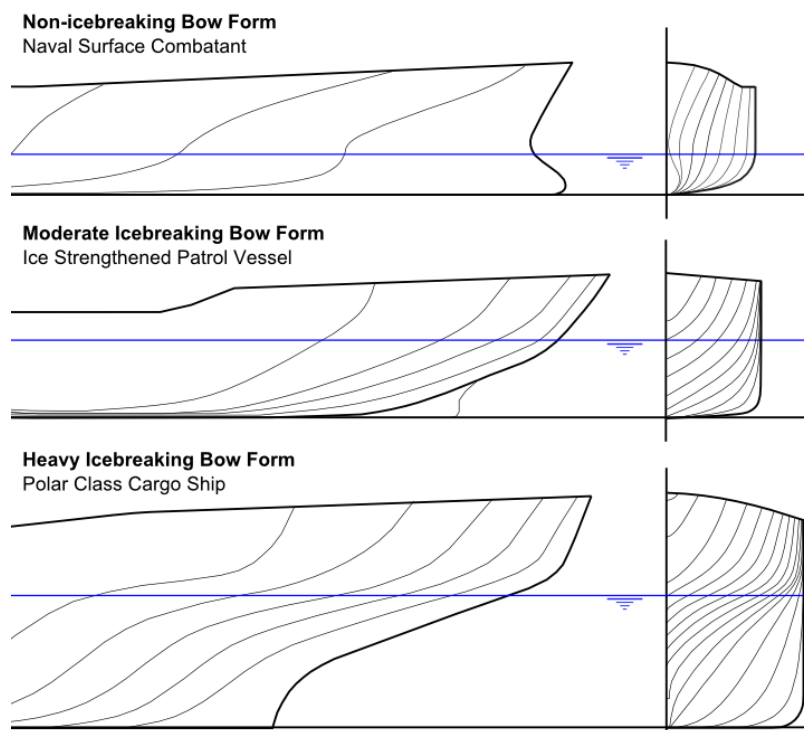


Figure 7: Sketches of different bow forms

## 2.7. Operations

Different modes of operation and different ice regimes will generate different magnitudes of ice impact forces. Ships that only encounter first-year ice will experience lower impact forces than a ship encountering old ice. Icebreakers with heavy ice strengthening that are required to ram ice features aggressively will obviously incur higher impact forces that would otherwise damage ships with lighter or no ice strengthening. The Canadian Coast Guard's publication on *Ice Navigation in Canadian Waters* (2012) offers some practical information about operations in ice and also includes guidance for non-icebreaking ships.

Speed is a fundamental operational consideration that can control the risk of damage to a ship. General guidance is to enter the ice pack at very low speeds to carefully receive the initial impacts. Once the vessel is into the pack, speed can be increased gradually to maintain headway and control of the ship, but the speed should not increase beyond the point at which the ship might suffer ice damage. The technical methodology presented in this report aims to offer quantitative guidance on estimating speeds that approach the limit of structural damage in different types of ice.

Additional guidance on ice operations typically focuses attention to the applied power in areas of weak ice or open leads, pools, etc. where the speed might unnoticeably increase to dangerous levels, posting extra lookouts on the bridge, the use of searchlights after dark, ballast control to protect a bulbous bow, rudders, propellers, etc., and turning in ice and in channels. All of these are critical to safe operations in ice and rely on competent and experienced ice navigators. However these topics are outside the scope of this project.

### 3. Review of Existing Approaches for Operational Limitations in Ice

Different methods are available for determining operational limitations of ships in ice. An approach that has been applied by regulatory authorities, is the use of risk control methodologies and access control regimes. The Canadian Arctic Ice Regime Shipping System (AIRSS) and the IMO's POLARIS are two examples of risk-based control methodologies which link a vessel's ice class, or lack thereof, to actual ice conditions and provide guidance on whether or not it is safe to operate. These systems don't explicitly deal with safe operating speeds but offer a quick assessment of the risk level for operations in ice.

More specific safe speed analyses methods have been proposed which link the ship's actual structural capacity to ice loads that arise from different operational impact scenarios. One such methodology will be presented in detail in this report. The following sections provide a review of several existing approaches to establish operational limitations for ships in ice.

#### 3.1. Risk-based Control Regimes

##### 3.1.1. Canadian Arctic Ice Regime Shipping System (AIRSS)

The Canadian Arctic Ice Regime Shipping System (AIRSS) was developed through collaborative efforts between Canadian government agencies and industry and introduced in the 1990s. AIRSS involves comparing the actual ice conditions along a route to the structural capability of the ship. The system recognizes that realistic ice conditions tend to manifest in an 'ice regime' which is composed of any mix or combination of ice types, including open water.

Under AIRSS, the decision to enter a given ice regime is based on the quantity of dangerous ice present, and the ability of the vessel to avoid the dangerous ice along the route to (and from) its destination. Every ice type (including Open Water) has a numerical value which is dependent on the ice class of the vessel. This number is called the Ice Multiplier (IM). The value of the Ice Multiplier reflects the level of danger that the ice type poses to the particular category of vessel.

For any ice regime, an Ice Numeral (IN) is the sum of the products of the concentration (in tenths) of each Ice Type, and the Ice Multipliers relating to the Type or Class of the ship in question. These multiplications are repeated for as many Ice Types and each of their respective concentrations that may be present, including Open Water. Ice Numerals can be calculated from ice conditions observed on the bridge or from ice 'egg codes' typically found on ice charts. The Ice Numeral is therefore unique to the particular ice regime and ship operating within its boundaries. To use the system, the master or ice navigator needs to identify the ice types and concentrations along the route.

An Ice Numeral produced by AIRSS provides a binary go/no-go instruction to the operator. A negative IN means the vessel is restricted from operating while a positive IN permits vessel operations. No speed guidance is provided by AIRSS, although intuitively, higher IN would generally permit higher safe speeds.

##### 3.1.2. IMO Polar Code – POLARIS

The International Maritime Organization (IMO) recently developed a harmonized methodology for assessing operational limitations in ice called the *Polar Operational Limit Assessment Risk Indexing System* (POLARIS). POLARIS was published as a recommendatory IMO Circular in 2016 and is intended to be a supplement to the IMO International Code for Ships Operating in Polar Waters (Polar Code). This system incorporates experience and best practices from the Canadian AIRSS system and additional input provided by several coastal administrations with experience regulating marine traffic in ice conditions. Similar to

AIRSS, the basis of POLARIS is an evaluation of risk posed to the ship by ice conditions using the WMO nomenclature and the ship’s assigned ice class (or lack thereof).

POLARIS can be used for voyage planning or on-board decision making in real time on the bridge although, as with any methodology, it is not intended to replace an experienced Master’s judgment. POLARIS assesses ice conditions based on a Risk Index Outcome (RIO) determined by the following simple calculation:

$$RIO = (C_1 \times RV_1) + (C_2 \times RV_2) + (C_3 \times RV_3) + (C_4 \times RV_4)$$

Where;

- $C_1 \dots C_4$  - concentrations of ice types within ice regime
- $RV_1 \dots RV_4$  – corresponding risk index values for a given Ice Class (see Figure 8)

The Risk Values (RV) are a function of ice class, season of operation, and operational state (i.e., independent operation or icebreaker escort). An example table of preliminary RVs for winter independent operations in Figure 8. Risk levels increase with increasing ice thickness and decreasing ice class. POLARIS provides RVs for the seven IACS Polar Classes, four Finnish-Swedish Ice Classes, and non-ice strengthened ships.

A positive RIO indicates an acceptable risk level where operations may proceed while a negative RIO indicates an increased risk level, potentially to unacceptable levels. Criteria is established, as shown in Table 5, for negative RIOs that suggest the operations should either stop to be reassessed or proceed cautiously with reduced speeds (IMO terminology is “subject to special consideration”).

**Table 5: POLARIS risk index outcome (RIO) criteria**

RIO <sub>SHIP</sub>	Ice classes PC1-PC7	Ice classes below PC 7	Color Code
20 ≤ RIO	Normal operation	Normal operation	
10 ≤ RIO < 20			
0 ≤ RIO < 10			
-10 ≤ RIO < 0	Elevated operational risk	Operation subject to special consideration	
-20 ≤ RIO < -10	Operation subject to special consideration	Operation subject to special consideration	
-30 ≤ RIO < -20			

IMO has agreed on ‘recommended speed limits’ for POLARIS RIOs that fall into the ‘elevated operational risk’ category (i.e. RIOs between 0 and -10), however operations in such ice regimes are only permitted for Polar Class ships. These are not intended to be hard and fast speed limits and shipboard ice load measurement systems and/or ice trials can be used to calibrate the recommended speeds.

**Table 6: POLARIS recommended speed limits for ‘elevated operational risk’**

Ice Class	Recommended Speed Limit
PC1	11 knots
PC2	8 knots
PC3-PC5	5 knots
Below PC5	3 knots

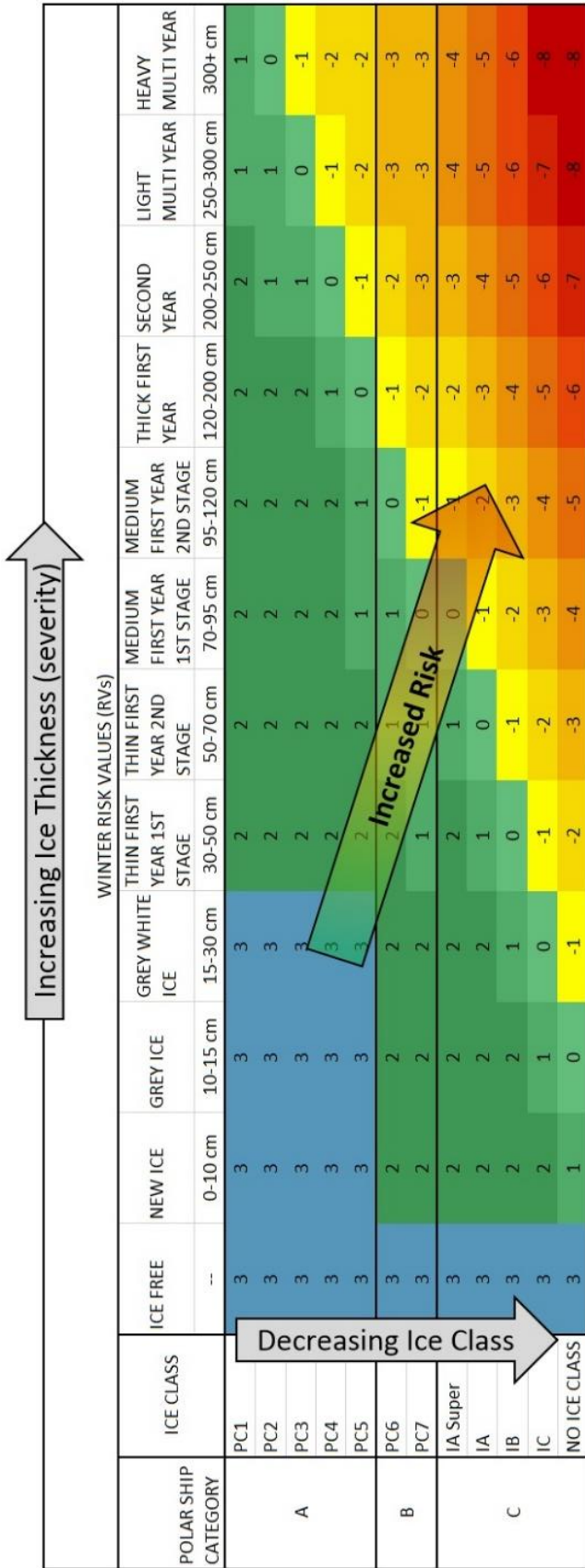


Figure 8: POLARIS risk values (RVs)

As an example demonstration, POLARIS is applied to consider the risks of a non-ice strengthened ship operating in the Alaska region using publically available ice chart data. Figure 9 shows four regional ice charts available for offshore Alaska (Chukchi Sea, Beaufort Sea, Bering Sea West, and Bering Sea East). The charts are typically published several times per week. The black lines in the figure depict the superimposed ice regimes from all October charts between 2010 and 2015 (approximately 40 charts per region). An example of one Chukchi Sea regional ice chart for late October 2012, a relatively severe ice year, is shown in Figure 10 for reference.

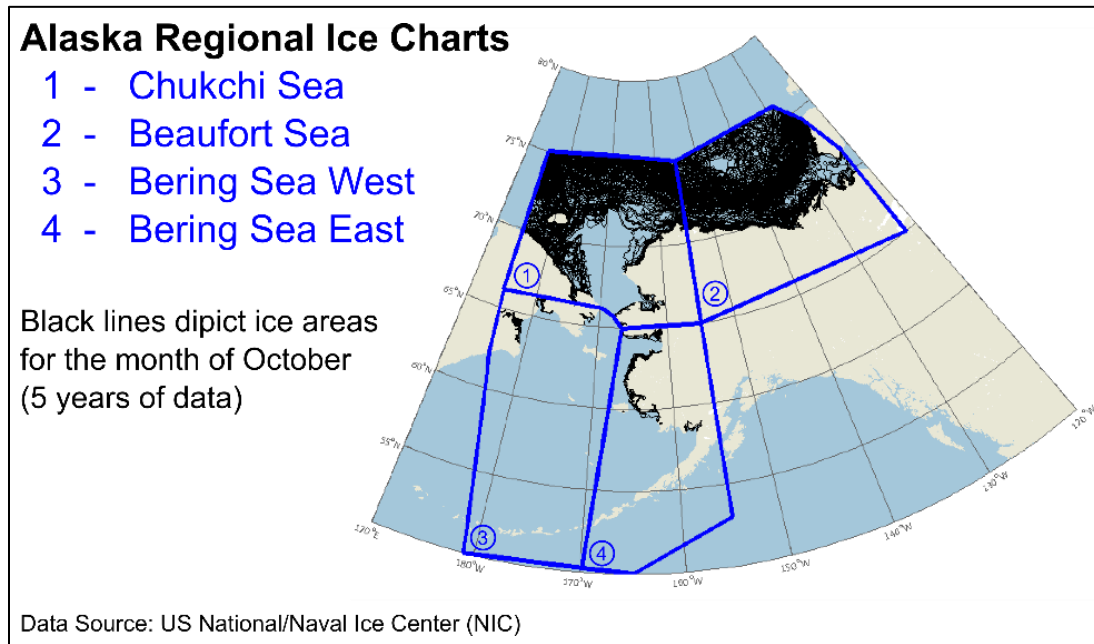


Figure 9: Alaska regional ice charts

The maps in Figure 11 present the results of POLARIS calculations using the historical ice charts from the US National/Naval Ice Center (NIC). The data was assembled and overlaid on a 0.5 x 0.5 lat/long grid and processed on a monthly basis. ‘Minimum’ RIOs were computed based on the last 10 years of data (2004-2014) and plotted according to the color coded criteria scale described above.

The outcomes highlight geographical areas in the Alaska region with elevated risk levels (orange and red areas indicate RIOs below -10) at different times of the year. It can be seen that there are large areas of the Bering Sea and Arctic Alaskan waters where operations of non-ice classed ships in the summer months is permitted under POLARIS, even in the worst ice years. These ‘Minimum RIO’ plots reflect the worst ice conditions from the past 10 years.

POLARIS can be a useful tool for evaluating risks for ships operating in ice conditions and makes use of ice chart data that is publically available. However, the results are only dependent on ice thickness and concentration and don’t offer any practical guidance related to ship speed. The direct calculation approach discussed and applied in this project takes into account many more factors that contribute to the structural risk of ships in ice; namely floe size, ice strength, ship strength and ship speed.

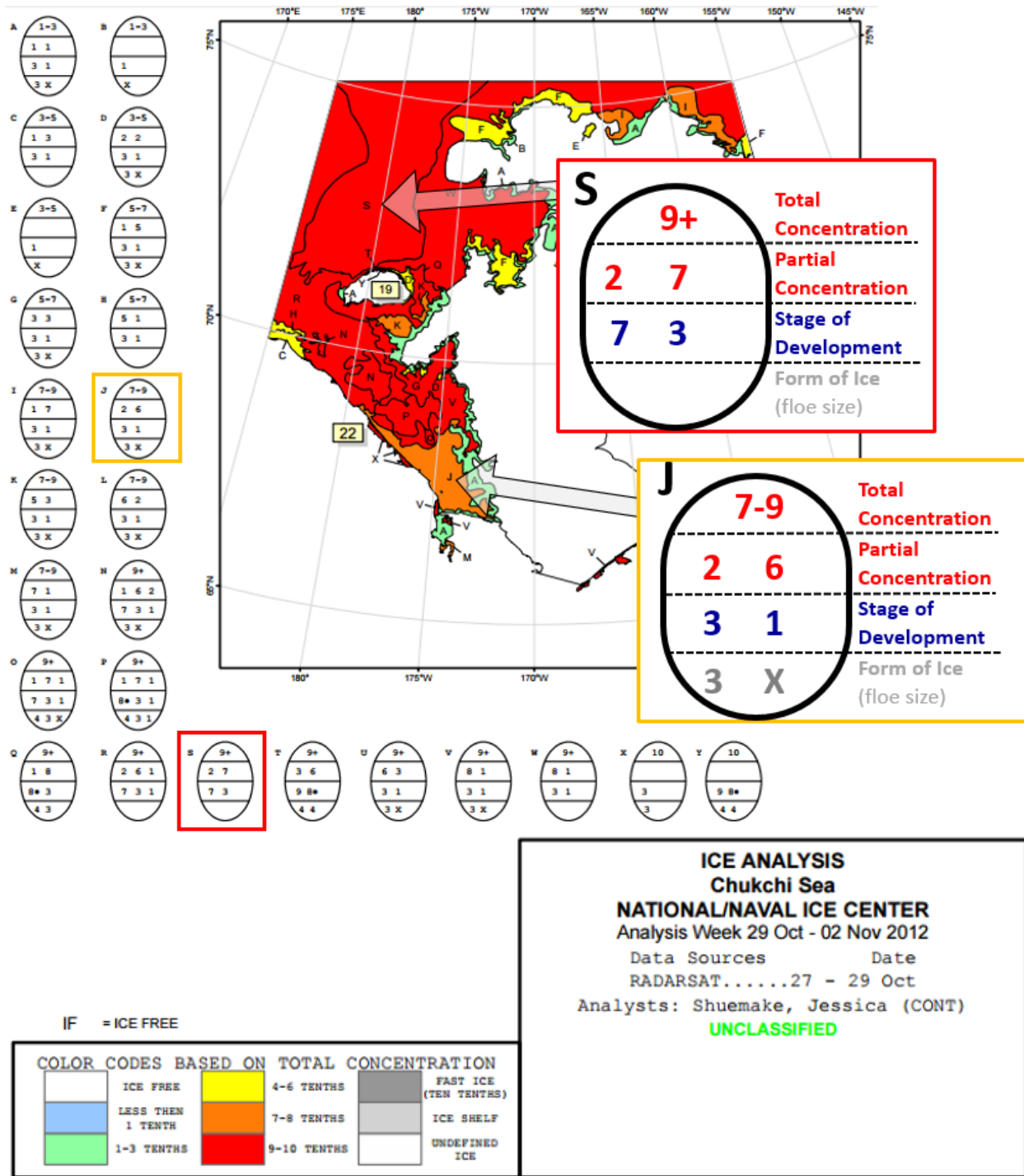


Figure 10: Chukchi Sea Ice Chart (29 October 2012, source: NIC)

# Monthly **Minimum** POLARIS Risk Outcomes (10 years)

Non-ice classed ship

Ice data source: US National/Naval Ice Center (NIC)

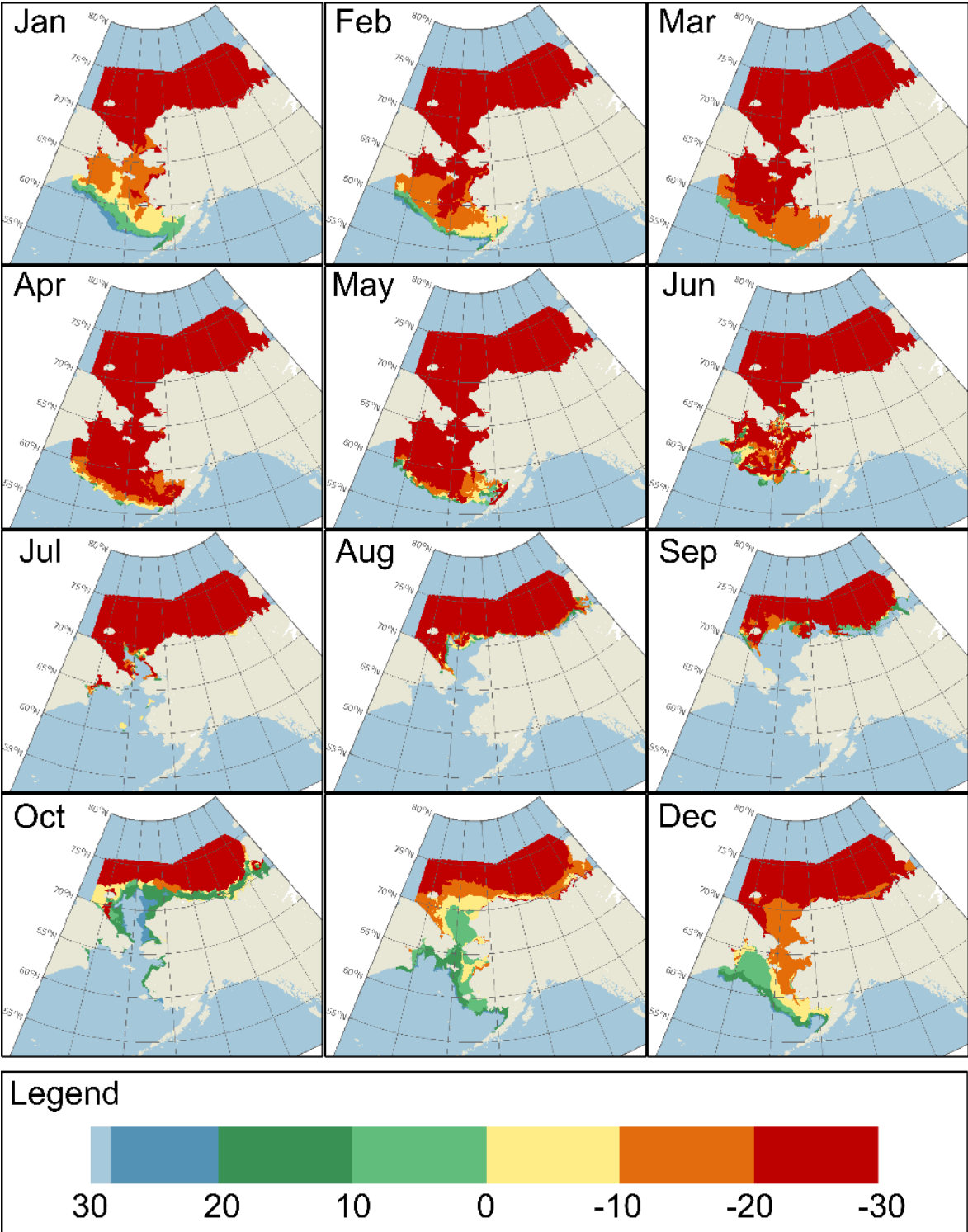


Figure 11: Monthly minimum POLARIS RIOs for non-ice classed ships

## 3.2. Safe Speed in Ice

The idea of a ship-specific analysis procedure to determine safe navigating speeds in ice conditions is not novel. The earliest concepts of safe speeds were likely postulated by Russian scientists sometime in the 1960s and 1970s during the development of transportation regulations for ships operating in the Russian Arctic. The Ice Passport (often referred to as the Ice Certificate), was first introduced in the mid-1970s. One of its major components is the regulation of speed to mitigate the risk of hull damages due to ice. The Ice Passport contains safe speed guidance as a function of the ship's actual structural configuration and anticipated ice conditions. This is the only known existing regime which quantitatively considers the safe speed of ships in ice however its full technical background is not widely available nor accepted.

Other technical approaches to the concept of safe speed also exist in the literature. Some are based on probabilistic approaches while others rely on purely deterministic analysis. Several recent efforts have adopted the ice-ship interaction model and structural response criteria used in the IACS Polar Rules with some modifications that permit safe speed assessments. An overview of available safe speed in ice technical approaches are described in the following sections.

### 3.2.1. Russian Ice Passport / Ice Certificate

Maxutov and Popov (1981) provided a description of Ice Certificate requirements in one of the earliest available publications on its technical basis. They defined the safe limit speed as “the maximum speed under given ice conditions which ensures safe navigation”. This limit speed, depicted by simple diagrams (such as the one presented in Figure 12), is determined by the available installed power and limitations in the hull structure. In addition to the limit speeds, other operational guidance is provided by the Ice Passport such as the minimum safe distance in the convoy and ice pressure resistance capabilities. The authors clearly note that while the Ice Certificate can provide the operator useful guidance, it cannot consider every possible ice condition or operating mode and the overall recommendation of operator due caution should be maintained.

In the late 1990s, at the request of Canadian authorities, a detailed report was prepared describing the scientific basis and methodology of the Ice Passport applied to CCG Pierre Radisson (Likhomanov et al., 1997; Likhomanov, Timofeev, Stepanov, & Kashtelyan, 1998). The report included the ice load model procedures and the formulations to express the load-bearing capacity of framing members. The technical approach for safe speed guidance in the Ice Passport begins by establishing attainable (i.e. performance) speed curves in ice ( $v_{ship}$  vs.  $h_{ice}$ ). Empirical and semi-empirical ice resistance formulations for level solid ice, hummocked ice covered in deep snow, high concentration pack ice, and cake ice are formulated considering the full installed main engine power. These attainable speed curves may also be established by model tests or ice trials.

Critical state curves are developed to represent the load bearing capacity of local hull structural members. Expressed in terms of pressure,  $p$ , and load height,  $b$ , these limit states are derived using analytical beam theory or numerical finite element analyses (linear elastic and nonlinear static) of actual ship grillages. Two separate criteria are applied, first yield (zero plastic deformations) and the ultimate state (the formation of plastic hinges).

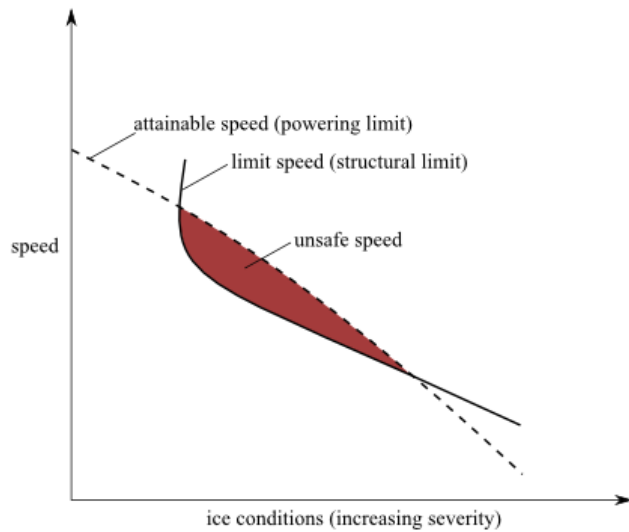


Figure 12. Sketch of safe speed diagram [from Maxutov and Popov (1981)]

The ice load parameters used to develop safe speed curves in the ice passport are based on Kurdyumov and Kheisin’s velocity-dependent hydrodynamic model for local contact pressure (1976) coupled with Popov-type collision mechanics (Popov, Faddeyev, Kheisin, & Yalovlev, 1967). This was one of the first analytical models that produced the basic ice load parameters from a given set of input conditions. Kurdyumov and Kheisin modeled ice crushing using a concept of viscous extrusion and “specific failure energy”. It assumed that ice crushing involves the formation of a near-uniform layer of fine granular material that is then extruded. A viscous extrusion model was used to model the process and describe the pressures.

This crushing model presents two difficulties. The first, a practical challenge, is the need to numerically integrate the model to obtain a solution. This is because viscous extrusion includes velocity effects, which prevent the equations from being solved analytically. Another problem with the viscous extrusion model is that the pressure patterns it predicts are quite smooth, almost uniform. Empirical evidence from testing on ships and in labs has shown the ice pressure are highly non-uniform, and typically contain peaks of very high pressures inside the contact zone.

Figure 13 illustrates the difference between the Kurdyumov-Khesin model and the pressure-area model utilized in DDePS. With a pressure-area model the pressure is just a function of area which is just a function of the normal penetration. This permits the crushing energy to be expressed in terms of only one independent variable, the penetration. The Kurdyumov-Khesin model requires the time derivative as well, adding a significant level of difficulty to the problem. Further, it is widely felt by Canadian and European ice experts that the empirical evidence does not support the Kurdyumov-Khesin model.

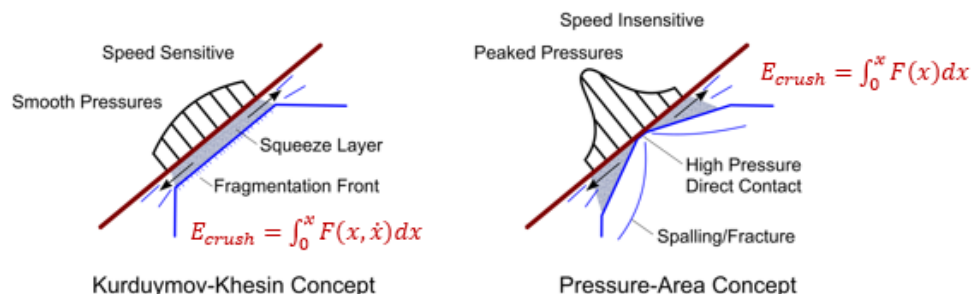


Figure 13: Comparison of original Popov ice pressure model with DDePS pressure area model

To develop the safe speed curves for an ice passport, the model described above is used to calculate the load parameters ( $\rho$  and  $b$ ) over a range of ship speeds ( $v_{ship} = 2- 20$  knots), ice thickness ( $h_{ice} = 0.25 - 4.0$  m), floe size (50 m, 100 m, and infinite level ice), and impact locations (locations on the bow under two draft conditions). A solution scheme is devised to find the speed and ice thickness combinations corresponding to points on the critical state curves.

Examples of safe speed guidance found in a typical ice passport are provided in Figure 14. This example is for a Baltic 1C cargo ship. The left side graph is for 6/10ths concentration and the right is for +9/10ths. The safe speed curve (green) is the same in both cases, however the attainable speed (performance) is reduced for higher concentrations.

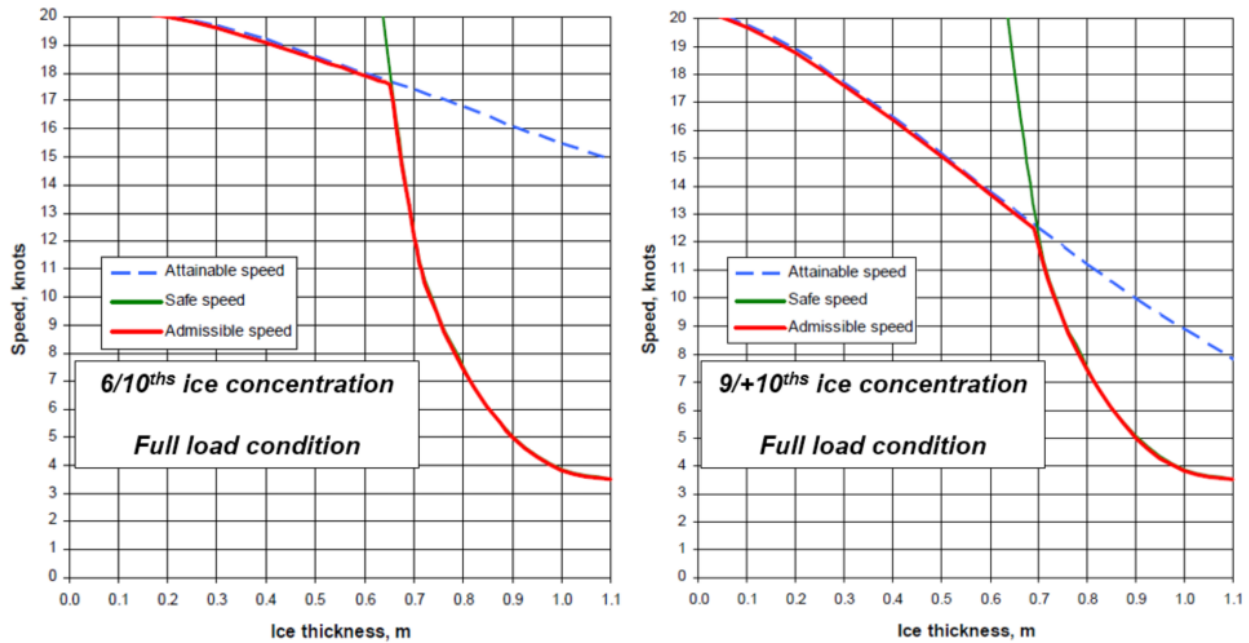


Figure 14: Examples safe speed guidance from a Russian ice passport (source: CNIIMF)

### 3.2.2. Probabilistic Approaches

Tunik et al. (1990) and Tunik (2000) recognized that the safe speed concepts applied in the Ice Passport hinged on pure deterministic analyses. He warned that compounding the most severe combinations of conservatively assumed critical parameters can ultimately lead to even higher levels of conservatism in the safe speeds. As an alternative, a conceptual probabilistic approach to safe speed analysis was offered. The approach is described in Figure 15. The impact location on the hull and the environmental ice parameters are treated as random variables and an analysis procedure is proposed to find the probability of load levels which exceed different structural damage levels. Available distributions of ice concentrations, thickness, floe size and mechanical properties are utilized; however, it is noted that the parameters can vary significantly between regions.

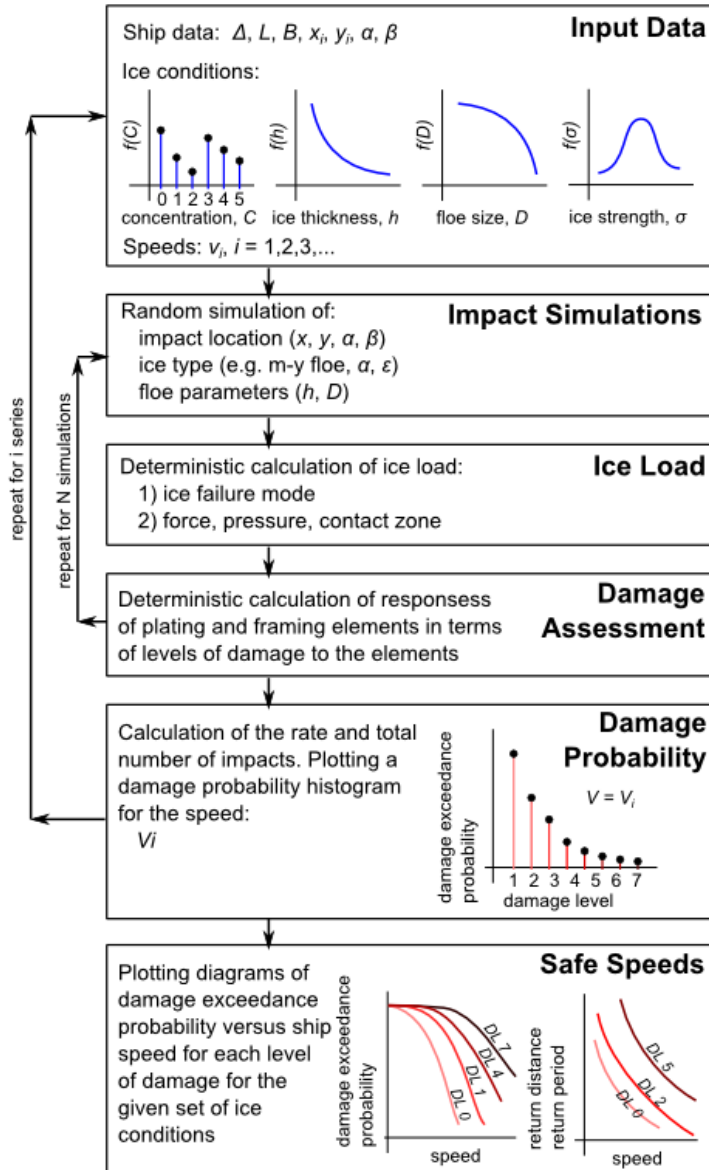


Figure 15: Probabilistic concept for safe speed in ice [from Tunik et al. (1990)]

### 3.2.3. Recent Approaches

The approaches discussed so far each consider the hydrodynamic model of ice-solid body impact combined with Popov collision mechanics. This model is generally considered as the standard Russian practice and has been employed for over 40 years. Recently, alternative models have been utilized, many of which are tied directly to the pressure-area relationship which underlies the technical background of the Polar UR, which is described in more detail later in this paper.

Daley & Liu (2010) addressed ship ice loads in pack ice by modifying the Polar UR model to consider finite ice floes. Specifically, they explored the secondary impacts (i.e. reflected collisions) on the midbody following bow glancing events. Limiting speeds were established comparing the reflected load parameters with UR design values for sample PC7 ships. This analysis demonstrated that secondary midbody collisions can be critical, especially for thick ice. While the structure was not directly analyzed, this study demonstrated the importance of considering off-design ship-ice interaction scenarios.

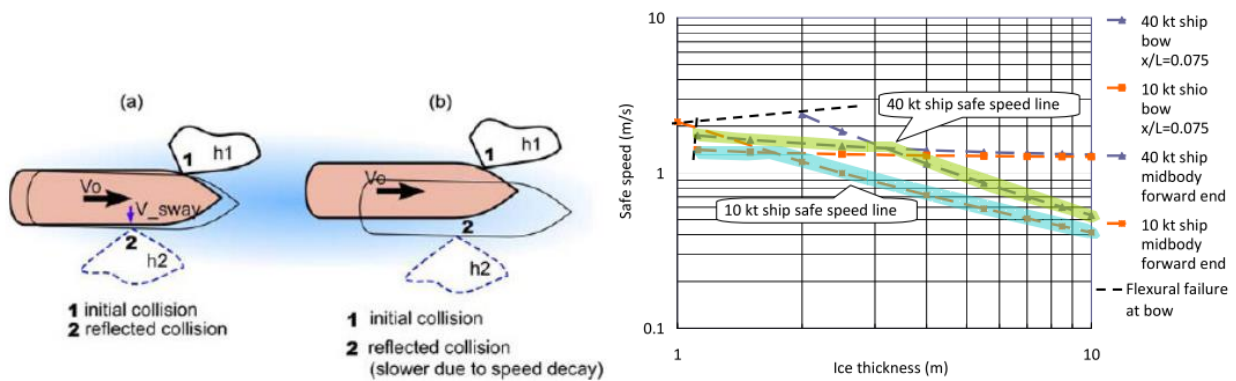


Figure 16: Left – reflected collision scenarios, Right - computed safe speed limits for PC7 ships (10kt and 40kt) in 200m floes [from Daley & Liu (2010)]

Daley & Kim (2010) studied ice collision forces considering structural deformation assuming a linearized plastic component of the structural response. An additional component (structural indentation energy) was introduced to the energy balance in the mathematical model. To some degree, this approach circumvents the assumption of a rigid body. A regression analysis of grillages subjected to point loads using the nonlinear finite element analysis method was used to develop this plastic component. Limiting ship speeds were established against various masses of icebergs for different allowable deformation levels. The inclusion of structural deformation into the impact model is a fairly novel concept. It was shown to play a moderate role in the ice load mechanics and could be a direction for a safe speed regime.

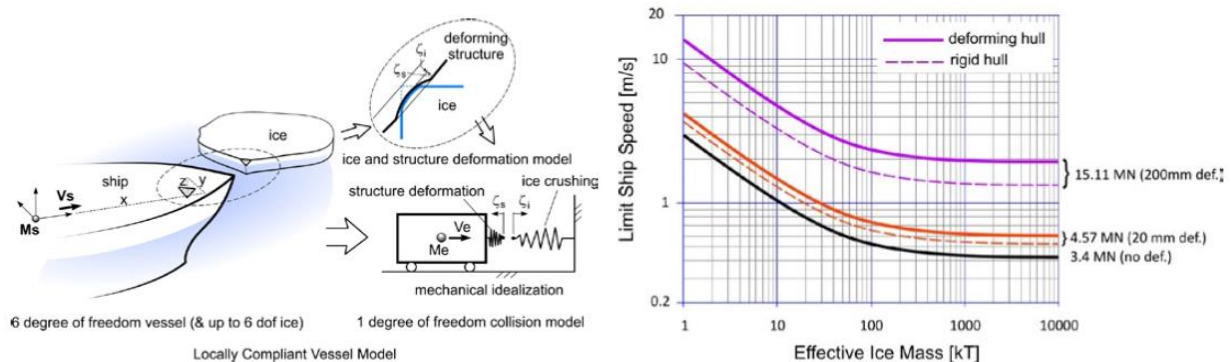


Figure 17: Left – model concept for considering locally compliant structure, Right – example safe speed envelopes for iceberg collisions considering structural deformation [from Daley & Kim (2010)]

#### BMT Fleet Study on Safe Speeds in Ice

In a technical report by BMT Fleet Technology, Daley, Kendrick, & Quinton (2011) examined the use of the IACS Polar Rules design ice load scenario for developing safe speed in ice curves for ships. One notable modification was an update to the flexural failure limit. The authors recognized the limitations of a static flexural limit in the Polar Rules and proposed an extension the model which included a horizontal force component, friction, and dynamic effects. The quasi-plastic structural response assumptions based on IACS UR limit states for plating and frame strength were applied to establish vessel speeds which resulted in the structure being loaded up to the design conditions. The result was “technical safe speed” curves for bow glancing collisions.

In a PhD thesis by Sazidy (2014), the dynamic factors involved in the contact between a ship side and ice were studied in more detail, particularly relating to flexural ice failure. Sazidy initially explored the ice edge behavior using LS-Dyna, a commercially available explicit dynamic finite element program. The program was able to model the ice edge crushing and flexural response in a time-history analysis that accounts for and can demonstrate dynamic effects. Figure 18 shows an example LS-Dyna simulation of a shoulder collision with an ice wedge on an elastic foundation.

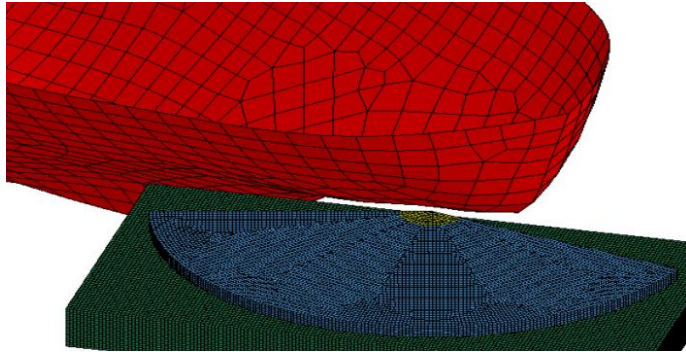


Figure 18: LS-Dyna model of a shoulder collision with an ice wedge on an elastic foundation

Later, the numerical model was compared to several available analytical and semi-empirical mathematical models of ship-ice breaking (including Kashteljan, Lindqvist, Vartsa and Daley) and a new empirical equation was formulated for a velocity-dependent flexural failure limit. The equation was cross-checked against data collected from full scale impact tests of a landing craft bow installed on the tug Rauma I. The results of that comparison, plotted in Figure 19, show fairly good agreement. This model is used in the proposed technical methodology described later in this report.

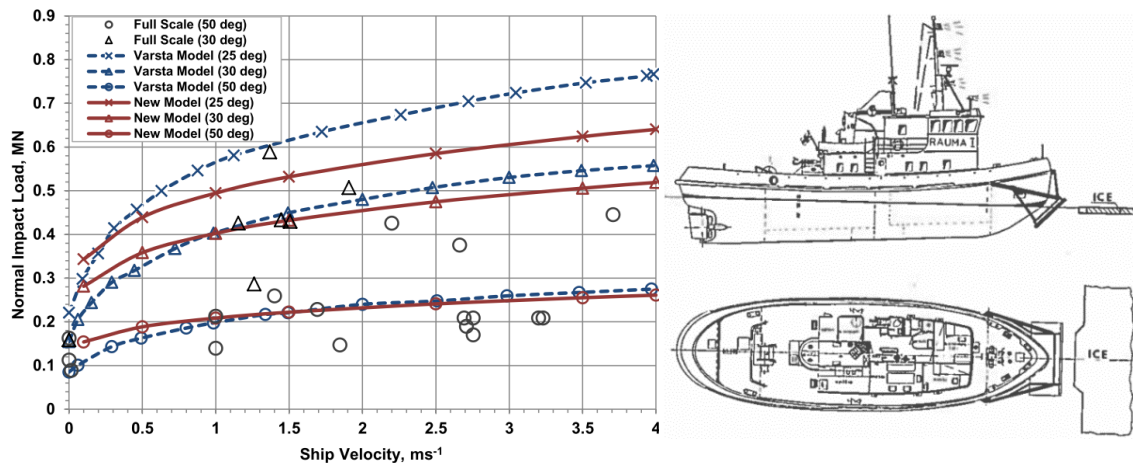


Figure 19: Cross-check of velocity dependant ice flexural failure model with full scale test data [from (Sazidy, 2014)]

#### Finnish/Swedish Submission to IMO

In a position paper submitted by Finland and Sweden to IMO during the development of the Polar Code, Kolari & Kurkela (2012) considered the case of a bow glancing collision with a spherical glacial ice mass. Their model solved a system of motion equations in the time domain estimating hydrodynamic effects by added mass terms, and adopted a pressure-area model for the treatment of ice crushing strength. The safety criterion used is the elastic response similar to that of the Russian Ice Passport for safe speeds. Their model was applied for different framing scantlings on the commercial ship – MV Eira. Some sample results along with a depiction of the model are shown in Figure 20.

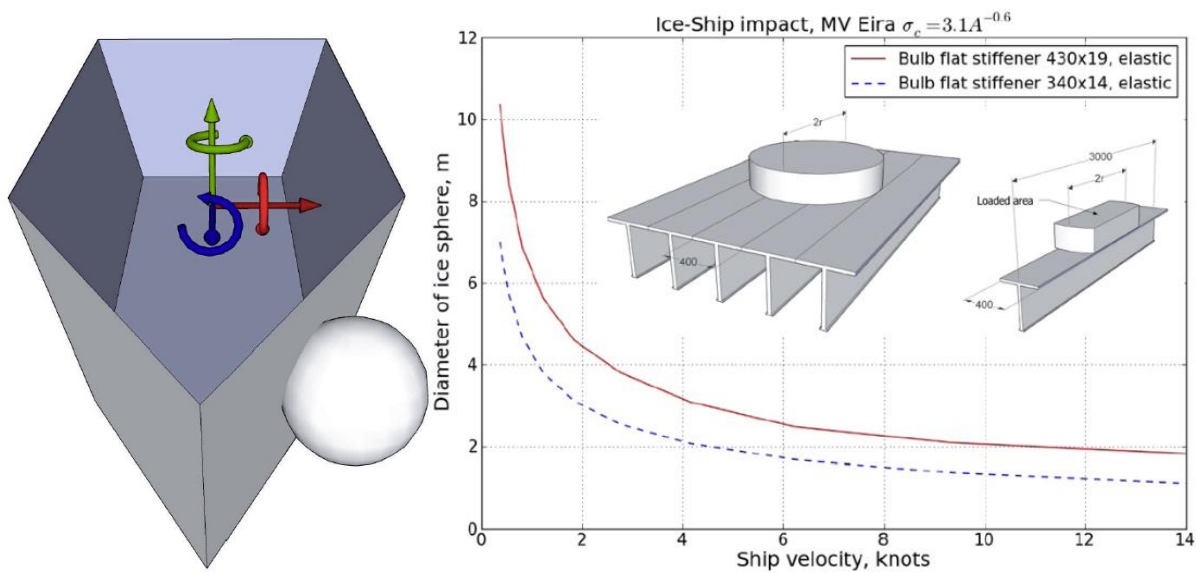


Figure 20: Safe speed assessment concept by Kolari & Kurkela (2012)

*VARD Study for Transport Canada*

VARD Marine with support from ABS carried out a project for Transport Canada in 2015 that explored how speed could be incorporated into current and future ice damage prevention/risk mitigation methods, including Transport Canada’s existing ice damage prevention system, the Arctic Ice Regime Shipping System (AIRSS). The objective of the project was improved safety and operability of shipping in the Arctic by applying technical analysis tools (i.e. DDePS) as input towards the further development and refinement of the AIRSS system. DDePS was used to explore the sensitivity of results to various parameters and assumptions including hull form, ice class, ship mass-to-ice mass ratios, and ice strength terms.

An example set of results which demonstrate the influence of ice strength and ice class on the technical safe speed curves are shown in Figure 21 for a 100,000 ton ship with an icebreaking bow form. Three sets of ice strength properties were used, and categorized as “weak”, “medium” and “strong”. The “strong” ice strength parameters correspond with the assumed parameters for “IACS PC 1” (i.e. multi-year ice), while the weak ice used the crushing strength for “IACS PC 7” and a lower flexural strength, typical of first-year sea ice. The superimposed PC design points represent the speed-thickness combination assumed in each Polar UR class factor. In this example the sensitivities to ice strength and the ship’s ice class are shown to be fairly significant.

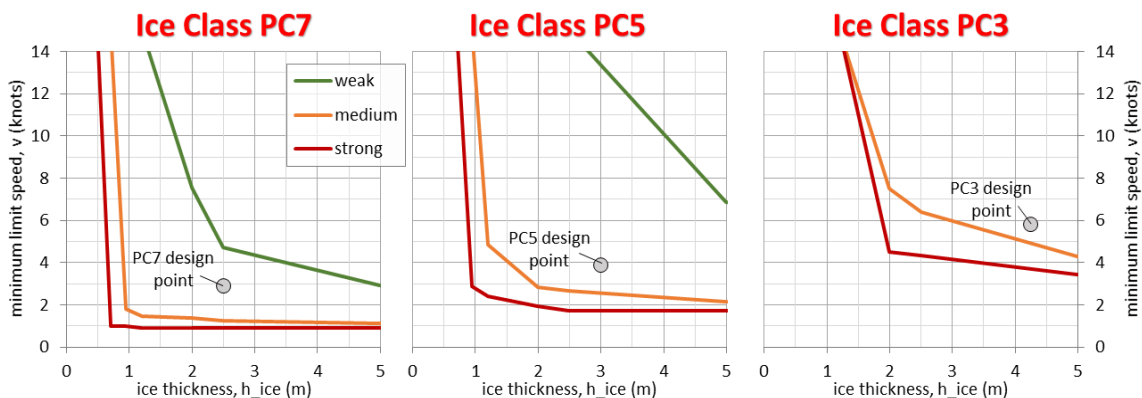
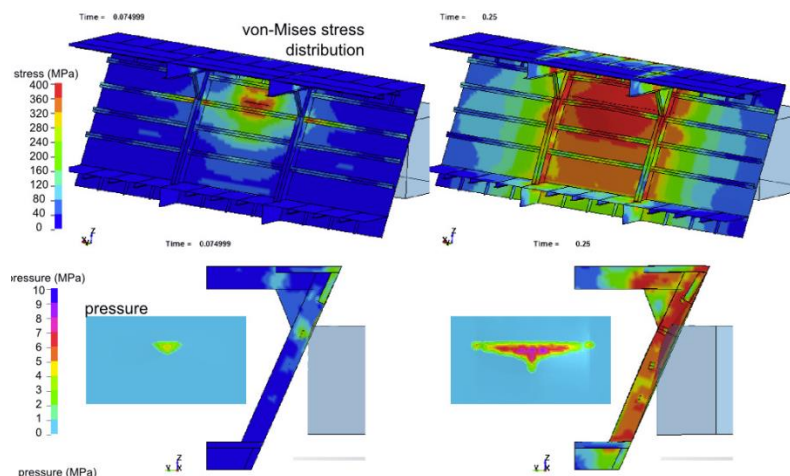


Figure 21: Example safe speed results demonstrating the sensitivities to ice strength and the ship's ice class [from VARD (2015)]

### ABS Study on USCG WMSL Class Cutters

In 2015, ABS carried out an engineering evaluation of the USCG WMSL Class National Security Cutter's structural capacity for operations in ice covered waters (ABS, 2015). Some results of the study were published in a technical paper by DeBord et al. (2015). State-of-the-art analytical and numerical methodologies of ship-ice interaction, collision mechanics, and structural response were exercised to develop estimates of the ship's operational capabilities and limitations in various ice conditions and considering different tolerance levels for structural damage. The work involved the advancement of key elements such as mechanics of "thin ice" and structural compliance which strongly influence the operational limits for this class of vessel. It was recognized that traditional ice-ship interaction models are based on several assumptions which are valid for heavy ice class hulls; structures are considered rigid and the 'design' ice is usually assumed to be thick and strong. However when analyzing lighter ship structures, attention must be given to aspects such as: structural indentation energy, variable floe sizes, rate effects on ice flexural failure modes, structural steel strain-rate sensitivities, dynamic moving ice load actions, and rupture.

The WMSL Class ice operational assessment included an extensive analysis of the bow structural arrangement using plastic limit state capacity equations and a nonlinear explicit finite element analysis procedure. Figure 22 is one example numerical model of the ice indentation process considering a deformable structural grillage typical of the ship's bow waterline region. This model was developed to obtain relationships between ice indentation, impact force, and structural deformation that could be used to estimate the relative energies expended into ice crushing and structural plastic damage. The figure shows an ice edge indenting into the structure at a normal speed of 1.5 m/s. Cross-sectional views show the relative deformation of the structure and ice. Contour plots represent the von-Mises stress distributions in the plating and frames at different moments during the indentation process and upon unloading. The development of plastic regions are evident (shown in red) as the indentation progresses, even early in the simulation.



**Figure 22: Numerical simulation considering deformable structure and ice crushing**

The results of the analysis were used to establish limiting conditions or "technical safe speeds" for the ship in different ice regimes. Limit conditions were determined by comparing loading terms (force, pressure, line load, etc.) against different representations of capacity or strength, i.e. limit states. The loading terms were produced by a model of ship-ice interaction (DDePS) and the capacity was represented in several different ways; from a simple model of the notional elastic limit or plastic hinge formation, to

more complicated models that take into account detailed structural scantlings and large deformation response mechanisms (such as the model described above).

Figure 23 presents example results for the ship impacting 10 diameter ice floes (often referred to as ‘cake ice’). Two different safe speed curves are specified. The more restrictive curve (blue) represents the plastic limit of the structure, where there is no observable damage. The red dashed curve utilized the results of the numerical simulations and represents speeds which might plastically deform the structure up to 5 cm. The results suggest that operational speeds in cake ice of thicknesses greater than 25 cm (termed ‘grey ice’) would have to be kept very low (under 5 knots) if no plastic damage was tolerable. However, the results also provide insight to the potential consequences of operating more aggressively. In certain operational situations such as search and rescue or emergency response, tolerance for relatively minor plastic damage can add considerably to the ability to move in marginal ice.

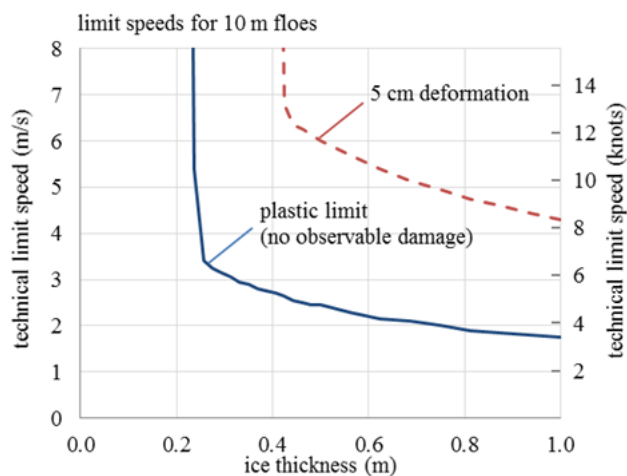


Figure 23: Technical safe speeds for the USCG WMSL Class cutter impacting ‘cake’ ice floes

*DRDC Study on Ice Impact Capability of a Notional Destroyer*

In a parallel effort to the USCG study described above, Daley (2015) exercised a similar methodology to estimate operational capabilities and limitations for a non-ice strengthened notional destroyer in ice conditions. The ship is a concept warship and features a fine open water hull form and relatively light local structures as shown in Figure 24.

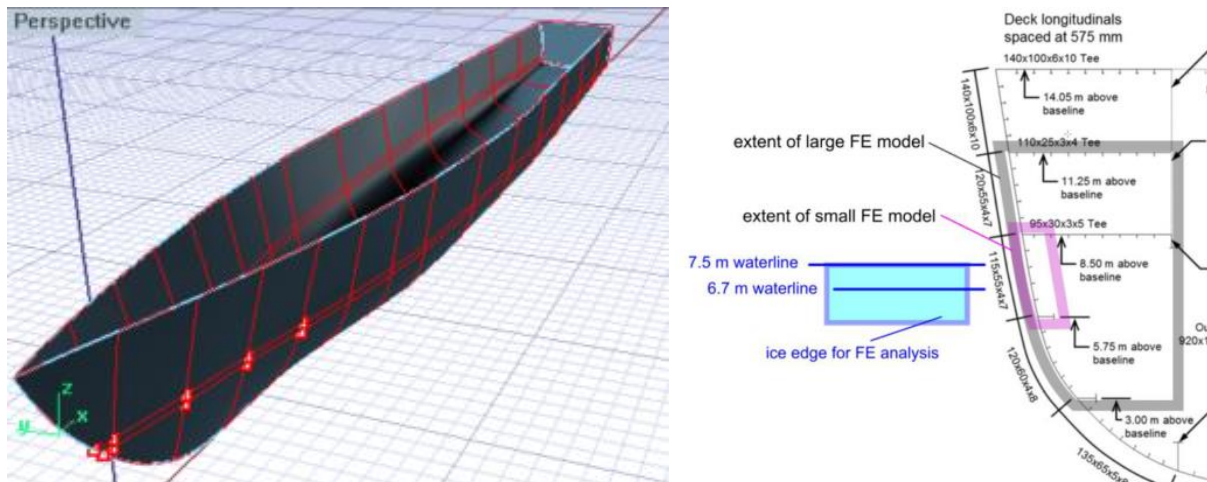


Figure 24: DRDC Notional Destroyer

DDePS calculations and numerical simulations of ice structure interaction were carried out to determine the effects of ice impacts for a variety of collisions cases. Example screenshots from the numerical simulations are presented in Figure 25. These were used to estimate the role of structural compliance in the ice crushing process. A variety of load cases were modeled numerically including framing, plating, web frame, and various moving load scenarios. This effort demonstrated a novel approach to model the structural response to ice loads.

An excerpt of the final results are provided in Figure 26. The left-hand side plot shows the technical speed limitations for the ship considering *no* structural indentation energy and taking into account the IACS Polar UR plastic limit states for the frames (i.e. direct limit states). It shows that the vessel could only operate in the lightest of ice conditions without risking structural damage. The right-hand side plot shows the results considering the structural indentation energy and allowable permanent deformations up to 10cm. The study was used to demonstrate that this arrangement has structural plastic reserve and if employed cautiously would allow the ship to impact moderate ice with a minor damage consequence.

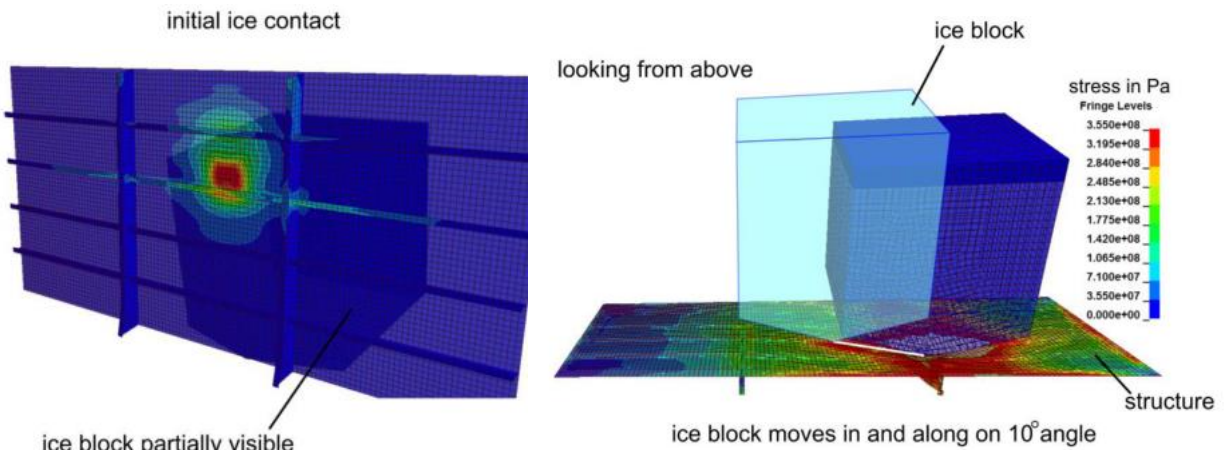


Figure 25: Numerical simulations of ice-structure interaction [from Daley (2015)]

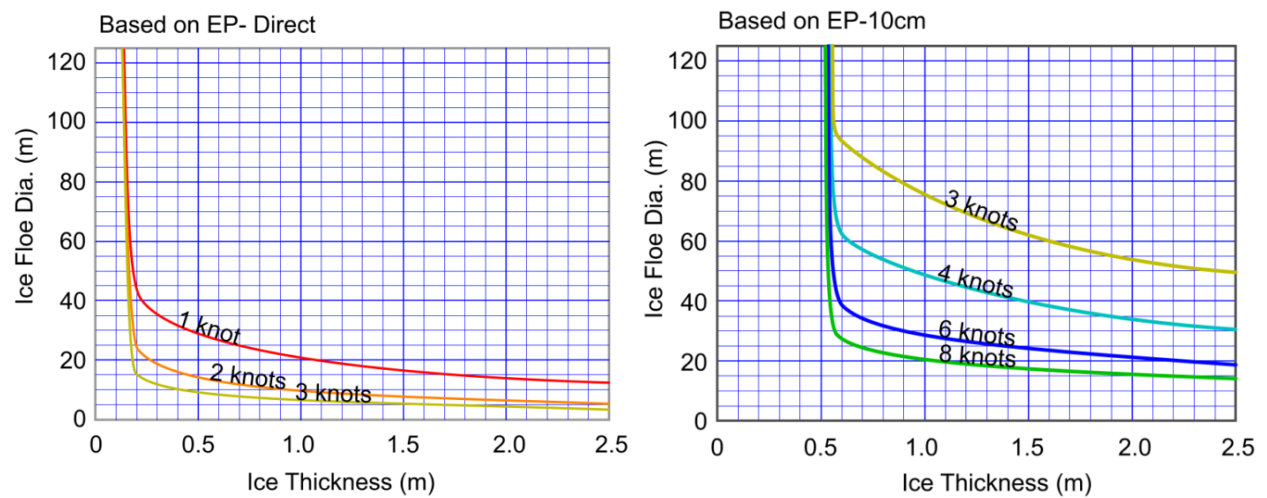


Figure 26: Technical safe speeds up to direct limit state (left) and 10cm permanent deformations (right) [from Daley (2015)]

## 4. Technical Methodology for Defining the Safe Speeds in Ice

The previous section described several different methodologies that have been applied to establish operational limitations for ships in ice. Simplified risk-based control systems, e.g. AIRSS and POLARIS, provide go/no-go guidance based on the ice class of a ship and the expected ice conditions but don't offer any quantitative assessment of safe operating speeds. Ship-specific analysis methods link a ship's actual structural capacity to ice loads that arise from different operational impact scenarios. However, different ice load models and different structural response criteria have been used and no standard methodology currently exists.

Operators of naval ships that may be deployed to the Arctic need a sound and transparent methodology to quantify the operational limitations of their assets in various ice conditions. This section outlines the detailed technical background of a proposed synthesized approach. The methodology is principally comprised of four building blocks highlighted in Figure 27. First, an interaction scenario is identified and selected to form the core ice impact model. Next the mechanics of the ship-ice collision process are solved. This requires an implementation of ice strength models for both ice crushing and flexural failure modes. Finally structural strength models are selected as limit conditions to determine the safe speed envelope curves.

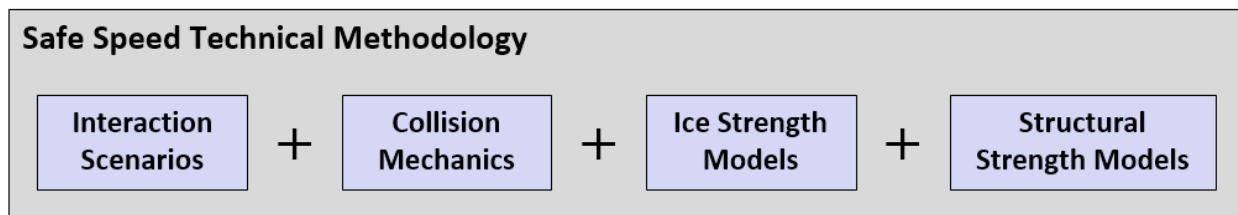


Figure 27: Building blocks of a safe speed technical methodology

This technical methodology is implemented in an updated version of the software tool, Direct Design for Polar Ship (*DDePS*), now called ***DDePS\_2a\_Safe\_Check*** (latest version v3.4). This software tool allows a user to explore damage estimates and develop safe speed envelope curves based on deterministic impact scenarios for a specific ship. It builds upon the original *DDePS Case 2a* (glancing impact with a wedge edge) by incorporating a number of technical elements and user features combined with various structural limit checks.

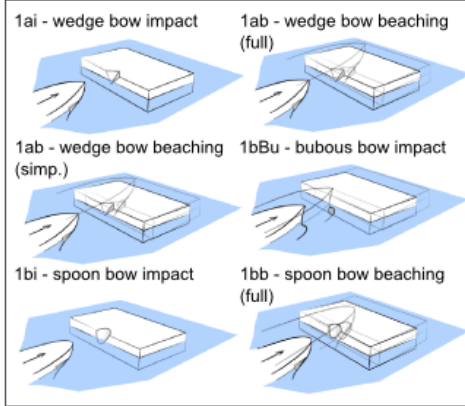
### 4.1. DDePS

Direct Design for Polar Ships (*DDePS*)<sup>1</sup> is a Microsoft Excel based spreadsheet tool capable of modeling a large set of ship-ice interaction scenarios. The impact models, described in several technical reports by BMT Fleet Technology and ABS (Kendrick & Daley, 2006a, 2006b, 2009; Daley & Liu, 2009) are based on the same overall methodology found in the IACS Polar Class Unified Requirements, but consider a wide range of scenarios, including infinite and finite ice floes. 25 total cases are available, each with as many as 25 user input variables. A complete list of available *DDePS* interaction scenarios are provided in Figure 28. For safe speed assessments, *Case 2a* is the selected scenario.

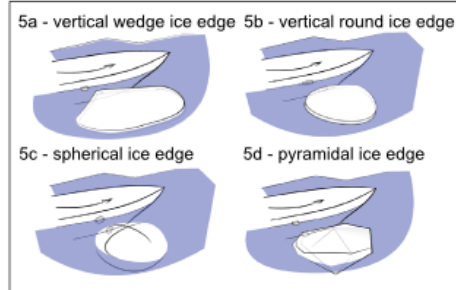
Figure 29 shows a list of the input variables that are used in a typical *DDePS* calculation and the output parameters that a user would obtain.

<sup>1</sup> DDePS is a proprietary software tool used in the assessment for this project.

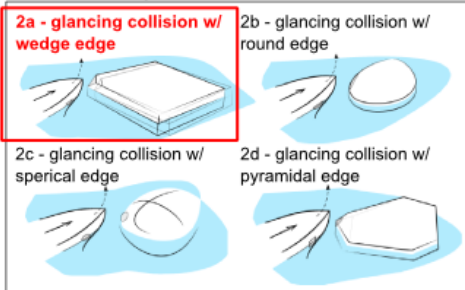
**Case 1 - Head on Ramming Collisions**



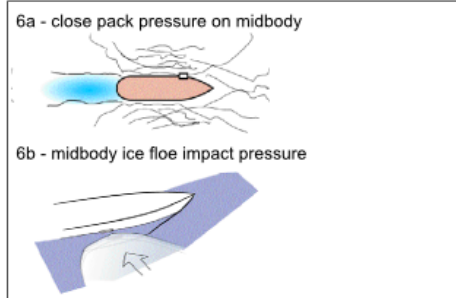
**Case 5 - Glancing Midbody Collisions**



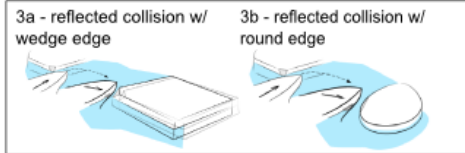
**Case 2 - Glancing Collisions**



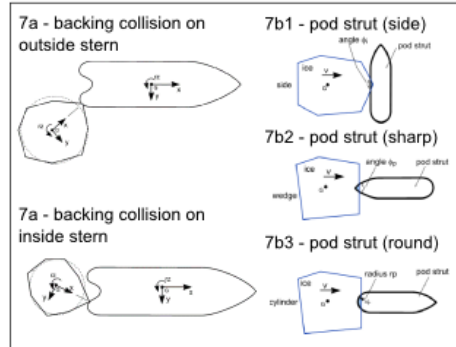
**Case 6 - Pressure**



**Case 3 - Reflected Collisions**



**Case 7 - Stern & Pod Collisions**



**Case 4 - Wedging Ram**

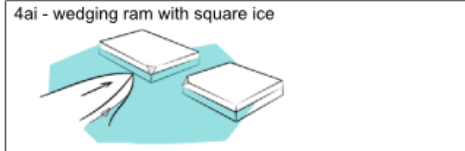


Figure 28: DDePS collision scenarios

Inputs			
Ship Particulars	Hull and Structural	Ice Parameters	Collision Conditions
<ul style="list-style-type: none"> <li>• Length (L)</li> <li>• Beam (B)</li> <li>• Draft (T)</li> <li>• Block coefficient (<math>C_B</math>)</li> <li>• Displacement (M)</li> <li>• etc.</li> </ul>	<ul style="list-style-type: none"> <li>• Impact locations</li> <li>• Hull angles</li> <li>• Plating and framing dimensions</li> <li>• Spacing (s)</li> <li>• Span (a)</li> </ul>	<ul style="list-style-type: none"> <li>• Floe size</li> <li>• Thickness</li> <li>• Strength (flexural and crushing)</li> <li>• Edge angle</li> <li>• Failure models</li> </ul>	<ul style="list-style-type: none"> <li>• Impact speeds (forward, sway, yaw, etc.)</li> <li>• Orientation</li> <li>• Impact location</li> </ul>
Outputs			
Popov Collision Terms	Ice Load Parameters	Structural Checks	
<ul style="list-style-type: none"> <li>• Directional cosines</li> <li>• Added mass terms</li> <li>• Gyration terms</li> <li>• Effective collision mass and energies</li> <li>• Impulse</li> </ul>	<ul style="list-style-type: none"> <li>• Ice indentation</li> <li>• Normal force (F)</li> <li>• Pressure (p)</li> <li>• Load height (b)</li> <li>• Load width (w)</li> <li>• Line load (Q)</li> </ul>	<ul style="list-style-type: none"> <li>• Elasto-plastic (onset of minor deformations)</li> <li>• Overload scenarios (large deformations)</li> </ul>	

Figure 29: Typical inputs and outputs for DDePS\_2a\_Safe\_Check

## 4.2. Case 2a Interaction Scenario

For the purposes of evaluating technical safe speeds for ships in ice, *DDePS Case 2a* - glancing collision with a wedge-shaped ice edge on the bow shoulder - is a reasonable impact scenario to form the core model. A simplified version of the bow glancing scenario with the edge of a thick level ice sheet (original Case 2a), was selected for the IACS Polar Class Unified Requirements design ice load model (Daley, 2000). In the rules, the ice is assumed infinitely large with strength and thickness terms fixed within Class Factors for each Polar Class notation. In the model presented here, ice can be treated as finite sized floes, allowing for investigation of pack ice speed limitations for ships. Figure 30 is a sketch of the assumed scenario for the safe speed evaluation.

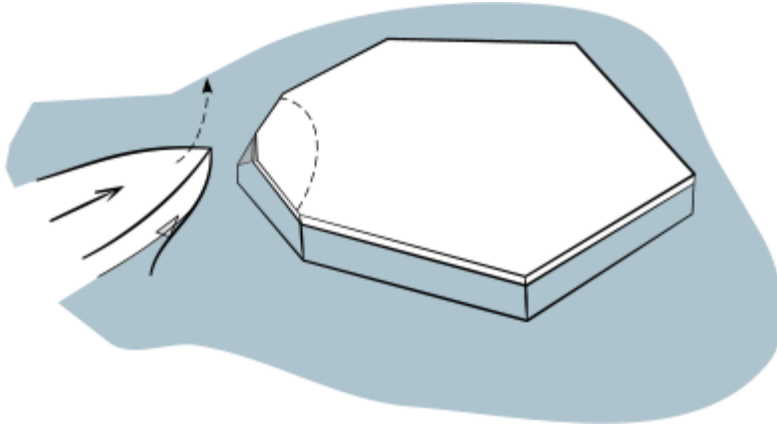


Figure 30: Safe speed collision scenario

The total force during the impact event is limited by one of two limit conditions. When the ship impacts an ice feature, the force increases as the hull penetrates the ice. This penetration will cease if either the ship runs out of energy (in other words – relative normal speed between the ice and ship becomes zero) or the downward component of the force causes the ice to fail in flexure. The maximum structural impact force is determined either by a ‘momentum limit’ or by a ‘flexural failure limit’. Therefore two models are required to determine the impact force: a crushing impact force model and a flexural force limit model. The following sections describe the detailed derivation of the ice impact model, ice crushing parameters, and flexural failure models.

## 4.3. Impact Model and Collision Mechanics

The DDePS 2a model computes ice forces and ship responses for a glancing collision with an ice edge. Both finite sized and infinite floes (level ice sheet) may be considered. The core method originates from Popov (1967) with an update by Daley (1999). Most earlier applications of the Popov model adopted the Kurdyumov-Khesin hydrodynamic ice crushing model to resolve the local contact pressure (Kurdyumov & Khesin, 1976a). That model is rate sensitive and can only be solved by numerical integration. The updated model by Daley uses a simple pressure-area relationship to resolve the local contact pressure and has a closed-form analytical solution (i.e. an equation). The update makes it possible, and fairly simple, to implement the calculation in a spreadsheet. The model assumes that all motions are the result of an impulse along the normal to the shell at the collision point. Currently, no sliding friction, hull curvature, or buoyancy forces are considered in the collision mechanics solution. The only hydrodynamic effect considered is the added mass of the surrounding water. These assumptions are reasonable for single quick transient ship-ice impact situations.

The six motion equations for a general rigid body in 3D space can be converted into one motion equation (1) along the normal of the contact surface;

$$F_n = M_e \cdot \ddot{\zeta} \quad (1)$$

Where

$\zeta$  is the ice indentation from the initial contact point along the normal of the shell

$\ddot{\zeta}$  is net normal acceleration at the point of contact (i.e., the second time derivative of the ice penetration)

$M_e$  is the effective (or reduced) mass of the ship-ice impact system.

$$M_e = \frac{1}{\frac{1}{M_{e_{ship}}} + \frac{1}{M_{e_{ice}}}} \quad (2)$$

$M_{e_{ship}}$  and  $M_{e_{ice}}$  are the effective mass of the ship and ice respectively at the contact point and can be obtained from equations (3) and (4). The full derivations and assumptions are provided in Appendix A.

$$M_{e_{ship}} = \frac{1}{\frac{l^2}{M_{sx}} + \frac{m^2}{M_{sy}} + \frac{n^2}{M_{sz}} + \frac{\lambda^2}{I_{sx}} + \frac{\mu^2}{I_{sy}} + \frac{\nu^2}{I_{sz}}} \quad (3)$$

$$M_{e_{ice}} = \frac{1}{\frac{li^2}{M_{ix}} + \frac{mi^2}{M_{iy}} + \frac{ni^2}{M_{iz}} + \frac{\lambda i^2}{I_{ix}} + \frac{\mu i^2}{I_{iy}} + \frac{\nu i^2}{I_{iz}}} \quad (4)$$

The various mass terms refer to the various degrees of freedom. For example  $M_{sx}$  is the ship's mass plus added mass in surge, and  $I_{iy}$  is the mass moment of inertia of the ice floe in pitch. The ice floe is assumed to be oriented normal to the point of contact, somewhat simplifying the analysis, as shown in Figure 31. For the purposes of computing the mass and moments of inertia, the ice floe is idealized as a square with uniform thickness. The wedge shape at the impact point is simply used for the contact model.

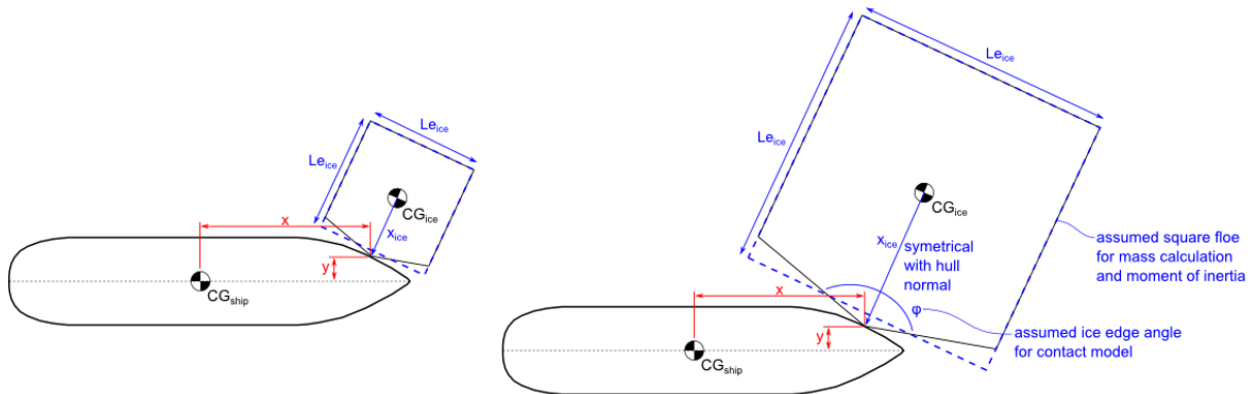


Figure 31: Diagram of ship-ice impact scenario in DDePS\_2a\_Safe\_Check

The situation is reduced to one in which one body is initially moving (the impacting body) and the other is at rest (the impacted body). The solution is found by equating the available (effective) kinetic energy with the energy expended in ice crushing:

$$KE_e = IE_i \quad (5)$$

The left side of equation (5) - kinetic energy,  $KE_e$  - is calculated using the following equation.

$$KE_e = \frac{1}{2} M_e V_n^2 \quad (6)$$

The available kinetic energy is the difference between the initial kinetic energy of the impacting body and the total kinetic energy of both bodies at the point of maximum force. If the impacted body has finite mass it will gain kinetic energy. Only in the case of a direct (normal) collision involving one infinite (or very large) mass will the effective kinetic energy be the same as the total kinetic energy. In such a case all motion will cease at the time of maximum force.

The right side of the equation - indentation energy,  $IE_i$  - is the integral of the indentation force  $F_n$  over the crushing indentation displacement  $\zeta_n$ ;

$$IE_i = \int_0^{\zeta_c} F_n d\zeta_n \quad (7)$$

#### 4.4. Ice Crushing Forces

The solution of the energy equations requires that force is described as a function of indentation. By using an ice 'process' pressure-area relationship, it is possible to derive a force-indentation relationship. This assumption means that ice force will depend only on indentation, and the maximum force occurs at the time of maximum penetration. The collision geometry is the ice/structure overlap geometry which describes the development of nominal contact area,  $A$ . The average pressure  $P_{av}$  in the nominal contact area  $A$  is related to the nominal contact area as;

$$P_{av} = P_o A^{ex} \quad (8)$$

The above equation is a 'process' pressure area model (in contrast to a 'spatial' pressure area model). It describes the development of the average contact pressure (and its nominal contact area) throughout the ice indentation process.  $P_o$  is the average pressure at  $1 \text{ m}^2$  and  $ex$  is a constant. These terms are used to characterize the ice crushing strength and are determined empirically.

Another form of a pressure-area relationship is a 'spatial' pressure area model which describes the spatial variation of pressure distributed over a contact area at an instantaneous point in time. This type of model is not explicitly used in this methodology.

The ice force is related to the nominal contact area. The relationship between the normal indentation and nominal contact area can be found for each specific contact situation. For the case of a general wedge edge geometry, as shown in Figure 32, the contact area can be expressed as;

$$A = \zeta_n^2 \left( \frac{\tan(\phi/2 - \theta) + \tan(\phi/2 + \theta)}{2 \sin(\beta') \cos^2(\beta')} \right) \quad (9)$$

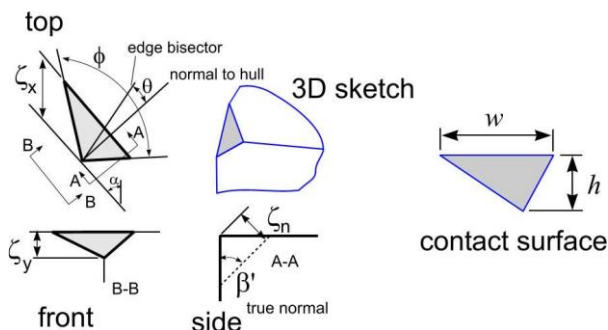


Figure 32: General wedge edge interaction geometry

For simplicity if we assume the wedge angle is normal to the hull, i.e.  $\theta = 0$ , areas can be expressed as;

$$A = \zeta_n^2 \left( \frac{\tan(\phi/2)}{\sin \beta' \cos^2 \beta'} \right) \quad (10)$$

The total normal force can then be expressed as;

$$F_n = P_{av} A = P_o A^{1+ex} \quad (11)$$

Combining equations (10) and (11), the impact force can be stated as a function of indentation as follows;

$$F_n = P_o \zeta_n^{2+2ex} \left( \frac{\tan(\phi/2)}{\sin \beta' \cos^2 \beta'} \right)^{1+ex} \quad (12)$$

After grouping shape terms, the normal force is expressed as;

$$F_n = P_o f a \zeta_n^{fx-1} \quad (13)$$

Where the shape parameters are as follows;

$$fx = (3 + 2 ex) \quad (14)$$

$$fa = \left( \frac{\tan(\phi/2)}{\sin(\beta') \cos^2(\beta')} \right)^{1+ex} \quad (15)$$

These indentation parameters are only valid for the ice contact shape shown in Figure 32 (see Daley, 1999). The ice indentation energy can be obtained by integrating the force over the depth of normal penetration;

$$IE_i = \int_0^{\zeta_c} F_n d\delta_n = \frac{P_o}{3 + 2ex} \left( \frac{\tan(\phi/2)}{\sin \beta' \cos^2 \beta'} \right)^{1+ex} \zeta_n^{3+2ex} \quad (16)$$

Finally, the indentation energy can be stated as;

$$IE_i = \frac{P_o}{fx} f a \zeta_n^{fx} \quad (17)$$

By equating the ice indentation energy to the effective kinetic energy, the normal penetration  $\zeta_n$  (or ice penetration  $\zeta_c$ ) can be expressed as;

$$\zeta_n = \zeta_c = \left( \frac{KE_e \cdot fx}{P_o \cdot fa} \right)^{1/fx} \quad (18)$$

The width and height of the nominal contact area can be represented as functions of ice crushing penetrations as shown in equations (19) and (20):

$$W_z = \frac{2 \zeta_c \tan(\phi/2)}{\cos(\beta')} \quad (19)$$

$$H_z = \frac{\zeta_c}{\sin(\beta') \cos(\beta')} \quad (20)$$

In DDePS and the Polar Rules design ice load model, a simple patch translation is performed to convert the triangular load patch (caused by the geometric ship-ice overlap) to a rectangular load patch that is more applicable for structural analysis. The rectangular patch is then further reduced, maintaining a constant aspect ratio, to account for load concentration as ice edges spall off. This is illustrated in Figure

33 and dimensions for the final load patch width  $w$  and height  $b$  are derived in equations (21) through (24).

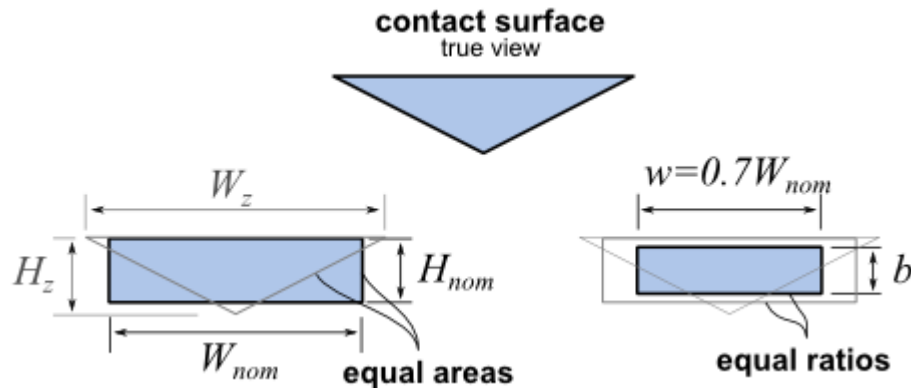


Figure 33: Translation and reduction of true contact surface to rectangular patch load

$$AR = W_z/H_z = 2 \tan(\phi/2) \sin(\beta') \quad (21)$$

$$W_{nom} = W_z/\sqrt{2} \quad (22)$$

$$w = 0.7 \cdot W_{nom} \quad (23)$$

$$b = w/AR \quad (24)$$

#### 4.4.1. Modification for Steep Frame Angles

For interactions at locations with steep frame angles (i.e. low  $\beta'$ ) the vertical component of the indentation depth may exceed the thickness of the ice sheet. This situation tends to arise when the crushing strength of the ice is weak and the frame angle is not large enough to produce an effective downward force to break the ice in flexure. For this scenario, sketched in Figure 34, a correction to the contact area is implemented into DDePS to treat the contact as a trapezoidal shape. The full derivation of this correction is provided in this section.

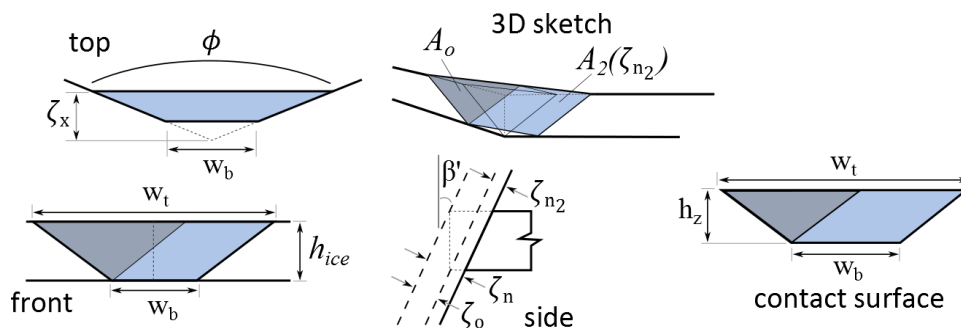


Figure 34: Interaction geometry for trapezoidal contact areas

The indentation depth for the maximum triangular contact area is taken as:

$$\zeta_o = h_{ice} \sin \beta' \quad (25)$$

Following equation (10), that contact area at  $\zeta_o$  is simply:

$$A_o = \frac{\zeta_o^2 \tan(\phi/2)}{\sin \beta' \cos^2 \beta'} \quad (26)$$

And the indentation energy required to crush the ice to a depth of  $\zeta_o$  is:

$$IE_o = \frac{P_o}{f_x} f_a \zeta_o^{fx} \quad (27)$$

If the ship's available effective kinetic energy is greater than the indentation energy required to crush the ice to a depth of  $\zeta_o$ , an additional contact area,  $A_2$ , is computed as a function of the continued indentation,  $\zeta_{n_2}$ .

$$A_2(\zeta_{n_2}) = W_b * H \quad (28)$$

Where,

$$H = \frac{h_{ice}}{\cos \beta'}, \quad W_b = \frac{2 \zeta_{n_2} \tan(\phi/2)}{\cos \beta'} \quad (29)$$

$A_2$  can be expressed and simplified as:

$$A_2(\zeta_{n_2}) = \frac{2 \zeta_{n_2} \tan\left(\frac{\phi}{2}\right) h_{ice}}{\cos^2 \beta'} = C_t \zeta_{n_2} \quad (30)$$

Where,

$$C_t = \frac{2 \tan\left(\frac{\phi}{2}\right) h_{ice}}{\cos^2 \beta'} \quad (31)$$

Therefore the total area of the trapezoidal contact area can be expressed as a function of the continued indentation beyond  $\zeta_o$ .

$$A_{trap}(\zeta_{n_2}) = A_o + A_2(\zeta_{n_2}) = A_o + C_t \zeta_{n_2} \quad (32)$$

Recalling equation (11) and the assumed process pressure-area relationship, the normal force for a given indentation depth over the trapezoidal area is:

$$F_n = P_{av} A_{trap}(\zeta_{n_2}) = P_o (A_o + C_t \zeta_{n_2})^{1+ex} \quad (33)$$

The ice indentation energy in the trapezoidal domain,  $IE_{i2}$ , can be obtained by integrating the force from equation (33) over the depth of normal penetration beyond  $\zeta_o$ .

$$IE_{i2} = \int_0^{\zeta_{n_2}} F_n d\delta_n = \int_0^{\zeta_{n_2}} P_o (A_o + C_t \zeta_{n_2})^{1+ex} d\zeta_{n_2} = P_o \frac{(A_o + C_t \zeta_{n_2})^{2+ex}}{C_t (2+ex)} \Big|_0^{\zeta_{n_2}} \quad (34)$$

This reduces to:

$$IE_{i2} = \frac{P_o}{C_t (2+ex)} [(A_o + C_t \zeta_{n_2})^{2+ex} - (A_o)^{2+ex}] \quad (35)$$

By equating the ice indentation energy,  $IE_{i2}$ , to the available effective kinetic energy,  $KE_{e2}$ , the normal indentation beyond  $\zeta_o$ , is determined by equation (36)

$$\zeta_{n_2} = \frac{\left(\frac{KE_{e2} C_t (2+ex)}{P_o} + A_o^{2+ex}\right)^{\frac{1}{2+ex}} - A_o}{C_t} \quad (36)$$

Where,

$$KE_{e2} = KE_e - IE_o \quad (37)$$

Finally the total normal indentation depth is taken as:

$$\zeta_c = \zeta_{n_2} + \zeta_o \quad (38)$$

The dimensions of the true (idealized) trapezoidal contact area can be represented as functions of ice indentations as shown in equations (39) through (41)

$$W_{zt} = \frac{2 \zeta_c \tan(\phi/2)}{\cos(\beta')} \quad (39)$$

$$W_{zb} = \frac{2 \zeta_{n_2} \tan(\phi/2)}{\cos(\beta')} \quad (40)$$

$$H_z = \frac{h_{ice}}{\cos(\beta')} \quad (41)$$

Figures 35 and 36 show the effect of this correction on nominal contact area and normal force for a sample scenario (thin ice, 75 cm thick with  $\beta' = 10^\circ$ ). As the indentation increases, the assumption of triangular contact area becomes invalid. The development of area is quite different if the transition to a trapezoidal shape is considered. It should be noted that the flexural failure and momentum limits are not shown on these plots. In some cases, these force limiting mechanisms (which depend on ice thickness, floe size, ice strength, hull form and ship speed) will contain this issue within indentation ranges where this is irrelevant.

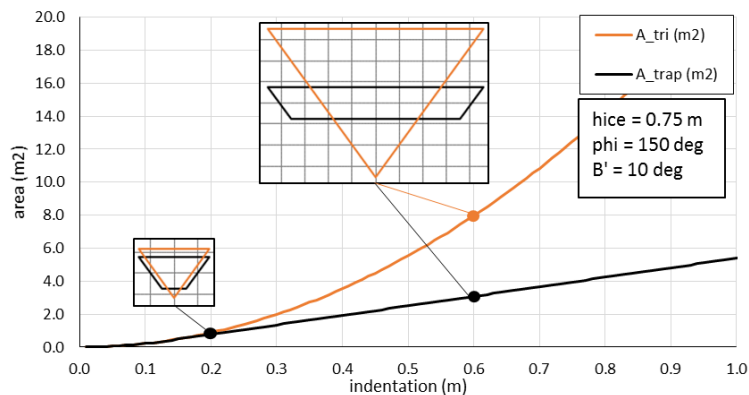


Figure 35: Contact area vs. indentation considering corrected trapezoidal contact shape

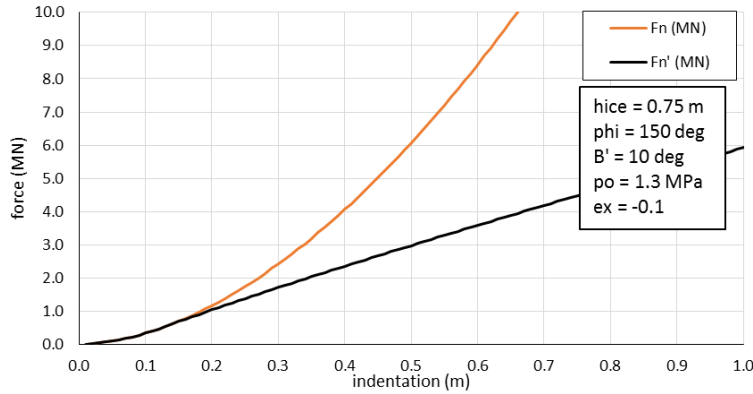


Figure 36: Normal force vs. indentation considering corrected trapezoidal contact shape

The patch shape is translated to a rectangle and reduced to account for load concentration and edge spalling while maintaining the same force. This process, similar to the triangular shape transformation describe earlier, is illustrated for the trapezoidal case in Figure 37.

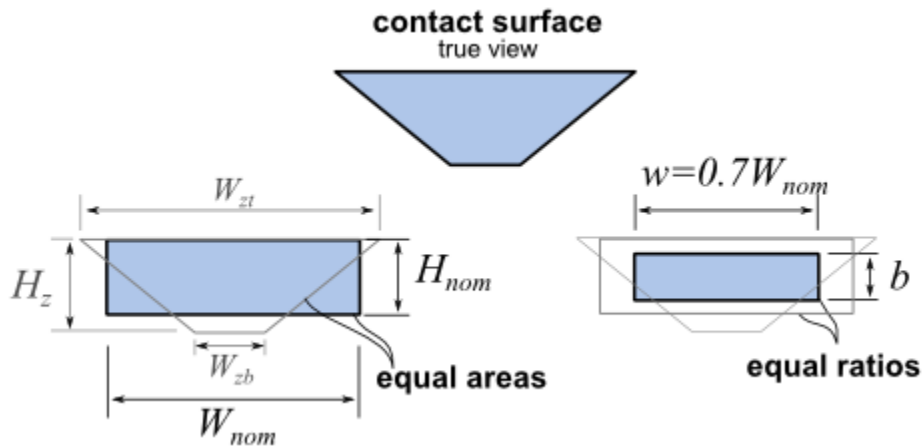


Figure 37: Translation and reduction of trapezoidal contact surface to rectangular patch load

The final load patch width  $w$  and height  $b$  are derived in equations (42) through (46).

$$AR = W_{zt}/H_z \quad (42)$$

$$A_z = \frac{1}{2} H_z (W_{zt} + W_{bt}) \quad (43)$$

$$W_{nom} = \sqrt{A_z \cdot AR} \quad (44)$$

$$w = 0.7 \cdot W_{nom} \quad (45)$$

$$b = w/AR \quad (46)$$

## 4.5. Ice Flexural Limit Model

In the IACS Polar Rules (2007) there is a simple quasi-static flexural limit force. The Polar Rules were formulated this way because they only need to apply to the design cases in the rules, which is always very thick ice. In such cases the quasi-static assumptions are quite valid. The same model is available in DDePS. The force normal to the ship's hull at the point of impact with the ice feature is limited to;

$$F_{n,UR} = \frac{1.2 \cdot \sigma_{flex} \cdot h_{ice}^2}{\sin(\beta')} \quad (47)$$

Where,

1.2 is a constant (assuming a wedge angle of 150°)

$\sigma_{flex}$  is the flexural strength of the ice

$h_{ice}$  is the ice thickness

$\beta'$  is the angle measured from the vertical axis of the ship's hull at the point of impact (i.e. the normal frame angle)

Since the normal force is only a function of the flexural stress of the ice, we may say that the vertical force is simply:

$$F_v = 0.46 \cdot \sigma_{flex} \cdot h_{ice}^2 \cdot \phi \quad (48)$$

The Polar Rules flexural limit is not valid for cases of thinner ice and higher speeds. As a result, a new model is needed for the purposes of safe speed evaluation, especially for naval ships. This is further explained in the following section.

### 4.5.1. Updated Flexural Failure Limit Model

For the more general cases of thinner ice and higher speeds, the IACS Polar Rules flexural force limit model is extended as shown below to include horizontal force, friction and dynamic effects. These necessary enhancements, developed by Daley and Kendrick (2011), are critical to a safe speed assessment.

#### *Horizontal Stress*

Horizontal impact force causes compression stress in the ice feature. This compressive stress negates (or relieves) a portion of the tensile flexural stress in the top of the ice, thereby causing an apparent increase in the flexural capacity of the ice sheet. The horizontal stress  $\sigma_{comp}$  is given by:

$$\sigma_{comp} = F_h / A_{ice} \quad (49)$$

Where,

$F_h$  is the horizontal force from both the normal and friction forces

$A_{ice}$  is the cross sectional area of the ice feature

$A_{ice} = \phi l h_{ice}$  (see Figure 38)

$\phi$  is the ice edge angle

$l = 10 h_{ice}$  is the length of the ice cusp

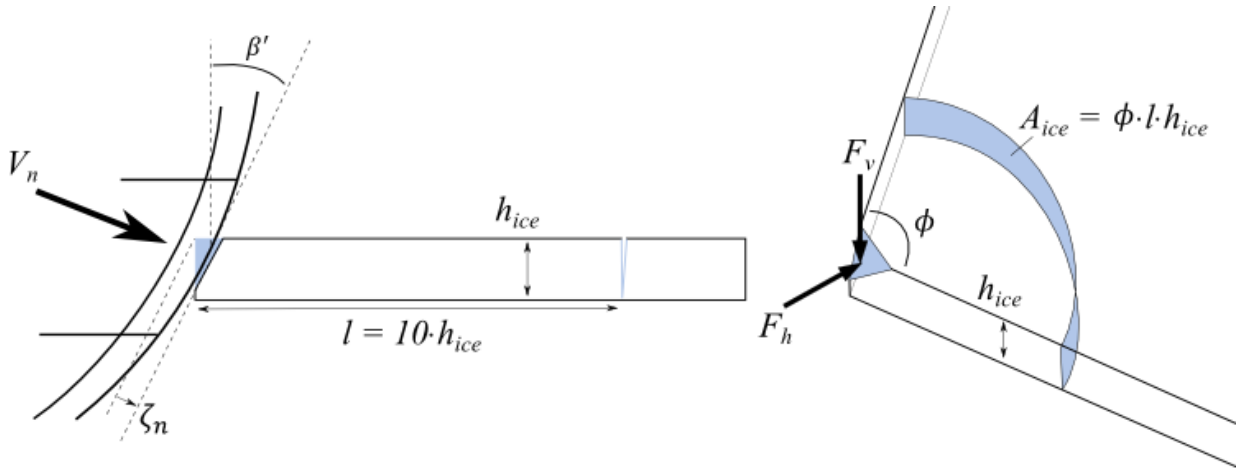


Figure 38: Geometry of flexural failure and ice cusp

#### Friction

Hull-ice friction is important because it affects the horizontal impact force, which influences the flexural force limit. Figure 39 shows that the horizontal component of both the normal and frictional forces are additive. The consideration of friction tends to increase the horizontal force (compressive stress) and decrease the vertical force (bending stress) in the ice during impact.

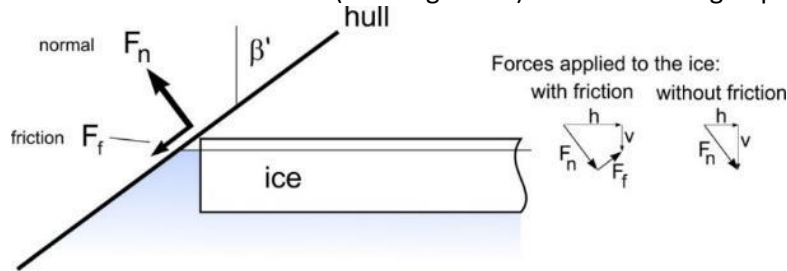


Figure 39: Hull-ice Contact showing Normal and Frictional Forces

When including friction, the horizontal force is;

$$F_h = F_n \cdot \cos(\beta') + \mu F_n \cdot \sin(\beta') \quad (50)$$

Where,

$\mu$  is the Coulomb friction factor

When including friction, the vertical force is;

$$F_v = F_n \cdot \sin(\beta') - \mu F_n \cdot \cos(\beta') \quad (51)$$

#### Design Normal Force

The total stress in the ice is given by:

$$\sigma_{total} = \sigma_{bend} - \sigma_{comp} \quad (52)$$

From  $F_v$  and  $F_h$  above we get:

$$\sigma_{total} = \frac{F_n \cdot (\sin(\beta') - \mu \cos(\beta'))}{C h_{ice}^2 \phi} - \frac{F_n \cdot (\cos(\beta') + \mu \sin(\beta'))}{10 h_{ice}^2 \phi} \quad (53)$$

Solving for the normal force, and substituting  $\sigma_{flex}$  for  $\sigma_{total}$  to get the design normal force:

$$F_n = \frac{C \cdot \sigma_{flex} \cdot h_{ice}^2 \cdot \phi}{(\sin(\beta') - \mu \cos(\beta')) - C/10 \cdot (\cos(\beta') + \mu \sin(\beta'))} \quad (54)$$

This design equation should be approximately equivalent to Polar Rules equation. Using a wedge angle of 150 degrees, a friction factor of 0.1 and  $\beta'$  of 45 degrees, the value of C needed to make the formula equivalent to the Polar Rules is 0.39. So the Formula for normal quasi-static force including friction effects becomes:

$$F_n = \frac{0.39 \cdot \sigma_{flex} \cdot h_{ice}^2 \cdot \phi}{(\sin(\beta') - \mu \cos(\beta')) - 0.039 \cdot (\cos(\beta') + \mu \sin(\beta'))} \quad (55)$$

*Dynamic Effects by Daley and Kendrick*

The following method was developed by Daley and Kendrick (2011) to include the dynamic support effects of water under the ice feature. While several authors (Colbourne, 1989; Valanto, 1996) have indicated a velocity dependence in the force required to break ice in bending, no analytical solutions were found to describe the phenomena. In response to the need for a practical analytical solution to this issue, a simple Froude scaling based method was developed. This method was offered as a starting point, with an understanding of the need for further improvement.

The dynamic effects of the water support arise from velocity dependent drag and acceleration dependent added mass; of which, the added mass effects are believed to dominate. Dynamic support effects are incorporated in the flexural force by scaling the design normal force (given above) with the ratio of Froude Numbers (raised to a power). A 'quasi-static' Froude Number is postulated, below which the "static" flexural case given above is used. For higher Froude numbers the flexural force is multiplied by a factor representing dynamic effects.

Previous experiments (Colbourne, 1989) suggest that the dynamic effects are related to Froude Number, a supposition that seems reasonable as Froude scaling will typically produce dynamic similitude. Further, Colbourne suggested that while the dynamic support increases with increasing Froude Number, the rate of change of this increase decreases with increasing Froude Number. Therefore linear scaling based on some static case would not be appropriate. Considering this, the following approach was adopted:

$$F_{nd} = \frac{0.39 \cdot \sigma_{flex} \cdot h_{ice}^2 \cdot \phi \cdot Kd}{(\sin(\beta') - \mu \cos(\beta')) - 0.039 \cdot (\cos(\beta') + \mu \sin(\beta'))} \quad (56)$$

Where,

$$Kd = \left(\frac{FN}{FN_s}\right)^n \text{ or } 1 \quad \text{whichever is greatest} \quad (57)$$

$F_n$  is the quasi-static normal force as given above

$F_{nd}$  is the dynamic normal force

$FN$  is the Froude Number for the dynamic case

$$FN = Vn / \sqrt{g \cdot h_{ice}} \quad (58)$$

$Vn$  is the speed in the direction normal to the plane of impact with the ice feature

$$Vn = V_{ship} \sin(\alpha) \cos(\beta')$$

$g$  is acceleration due to gravity

$h_{ice}$  is the ice thickness

$FN_s = V_{static} / \sqrt{g \cdot h_{ice}}$  is the Froude number for the static case (assume 0.1)

$V_{static}$  is the maximum speed in the direction normal to the plane of impact with the ice feature at which the impact may be considered "static"

$n$  is the scale factor modifying exponent (0.33 chosen here)

Based on experience, a “static” Froude number of  $FN_s = 0.1$  was chosen. This implies that the maximum speed at which an impact may be considered “static”,  $V_{static}$ , is dependent on ice thickness  $h_{ice}$  which is a reasonable assumption.

Figure 40 shows the normal crushing force (blue), the modified flexural force limit (green) and the IACS URII flexural force limit (red). Note that the horizontal portion of the green line represents the case without dynamic scaling (i.e.,  $V < V_{static}$ ).

For any given speed, the design normal force is the minimum of the crushing force and the flexural force limit. If the IACS URII flexural force model is used (red line) it would appear that the design normal force would be constant for ever increasing velocities; implying that the ship can travel ever faster through the ice feature without increasing hull loading. The modified flexural force model (green line) exhibits increasing design normal force with increasing velocity.

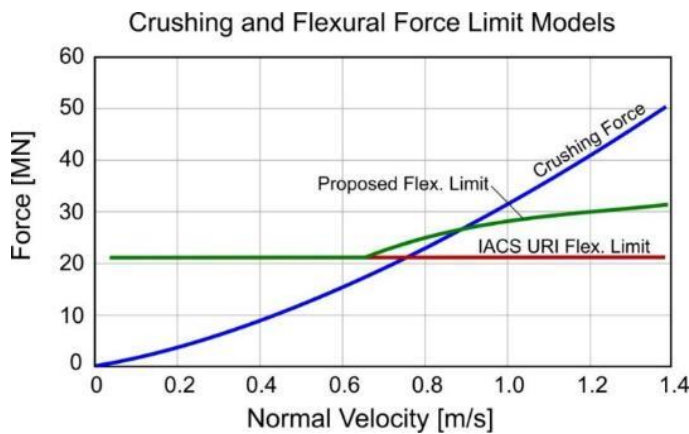


Figure 40: Illustration of Crushing and Flexural Force Models

*Updated Dynamic Effects based on work by Sazidy*

M.S. Sazidy (Sazidy, Daley, & Colbourne, 2014; Sazidy, Daley, Colbourne, & Wang, 2014) studied the dynamic factors involved in the contact between a ship side and ice. Figure 41 illustrates the type of analysis that was used to study dynamic effects. The ice edge was modelled using LS-Dyna, which is a commercially available explicit time-integration finite element program. The program was able to model the ice edge crushing and flexural response in a time-history analysis that accounts for, and can demonstrate, dynamic effects.

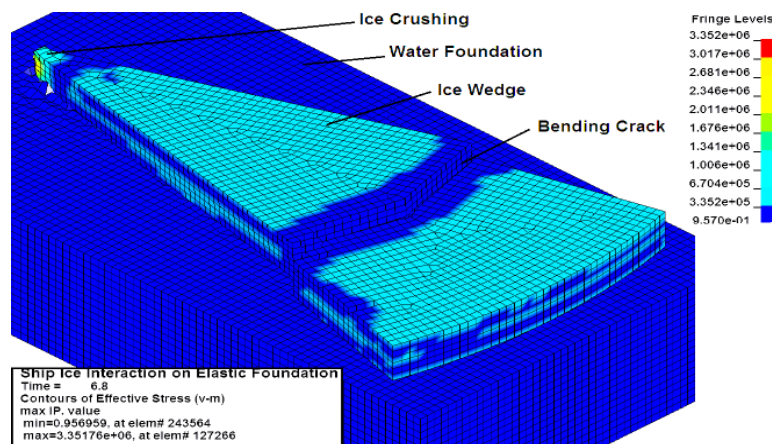


Figure 41: Simple ice wedge breaking pattern (Sazidy, Daley, Colbourne, et al., 2014)

Equation (59) is the new flexural failure model of vertical impact force for dynamic ice wedge breaking.

$$F_{vd} = 0.29 n_w^{-0.3} \sigma_f h^2 \theta K_v \quad (59)$$

where  $n_w$  is the number of wedges. The dynamic factor  $K_v$  is defined as:

$$K_v = 1 + 2.57 \sin \alpha \cos \beta' (\theta/n_w)^{0.2} FN^{0.26} \quad (60)$$

where Froude Number ( $FN$ ) is defined in equation (58). The normal impact force can be expressed in the following form:

$$F_{nd} = \frac{F_{vd}}{\sin \beta'} \quad (61)$$

Sazidy's analysis did not take friction into account, although it did implicitly take the effect of the horizontal stress into account. As a result equation (56) and (61) are not quite comparable. Sazidy's formulation can be adjusted to be compatible with equation (56) by making the following change.

$$F_{nd} = \frac{0.284 n_w^{-0.3} \sigma_f h^2 \theta K_v}{(\sin(\beta') - \mu \cos(\beta')) - 0.0284 \cdot (\cos(\beta') + \mu \sin(\beta'))} \quad (62)$$

The flexural limit models are a function of many parameters. Figure 42 shows a comparison of the static and dynamic equations for a set of selected parameters (also listed in the figure). In DDePS\_2a\_SafeCheck several flexural failure limit options are available. This figure highlights the following:

- static – equation (47)
- dynamic2 – equation (62)

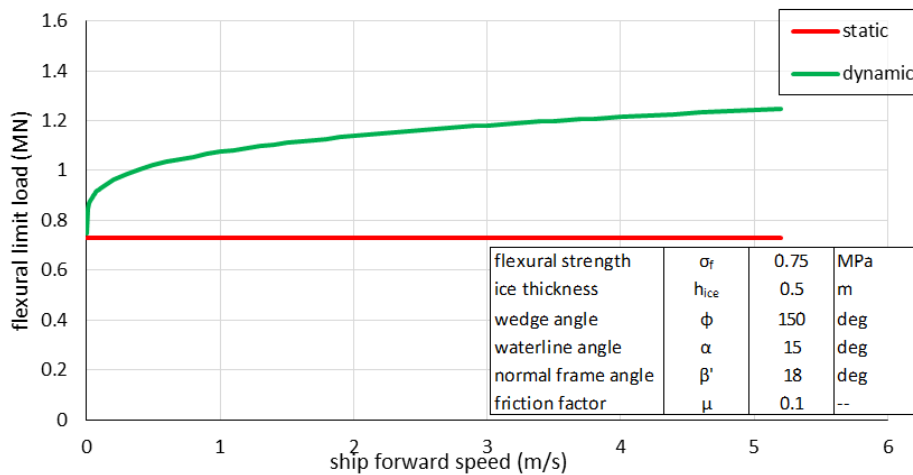


Figure 42: Comparison of static and dynamic flexural failure limits

## 4.6. Structural Limit States and Speed Check Algorithm

A variety of methods exist for establishing limiting conditions that can be used to determine technical safe speeds for ships in ice. In principle, each method compares a loading term against a representation of capacity or strength, i.e. a limit state. The loading term is produced by a model of ship-ice interaction, in this case DDePS following the derivations in the previous sections of this report. The model solves for ice load parameters as a function of many inputs describing an interaction scenario. The inputs are a combination of ship speed, impact location, ice thickness, floe size, and ice strength terms (flexural and crushing strength).

The capacity can be represented in several different ways; from complicated models that take into account detailed structural scantlings and response mechanisms, to simple criteria which anchor the limits on a notional design point. The selection of suitable limit states is a key area for debate with regard to safe speeds. *DDePS\_2a\_Safe\_Check* offers three different criteria to assess structural capacity (i.e. limit states) against the applied ice load for a given scenario. Each of these methods are further described in the following sections.

1. Polar Class Design Limit Load Criteria
2. Direct Line Load Criteria
3. Large Deflection Criteria

### 4.6.1. Polar Class Design Limit Load Criteria

Perhaps the simplest representation of capacity, but perhaps more conservative, is the design ice load for a certain “reference” Polar ice class (if applicable). Instead of considering the structural capacity directly based on actual scantlings, limit speeds can be established by comparing the loading terms against the design ice load of a selected Polar Class. This approach offers a surrogate to a detailed structural analysis but assumes the structure is built exactly to the design load (for the selected Polar Class) and the associated minimum requirements with no additional strengthening (i.e. no over design). In reality this is almost never the case. Due to practicalities of design, shipbuilding constraints, corrosion and abrasion allowances, etc. most designs inherently have some level of over design. For polar class ships (or ships with equivalent strengthening levels) the limit state can be expressed in terms of the design force for a certain “reference” polar ice class. Instead of considering the structural capacity directly, limits speeds are established when the loading term ( $Q_{load}$ ) exceeds the design line load of a selected Polar Class ( $Q_{UR}$ ).

$$v_{lim}(h) = v_i(Q_{load} > Q_{cap}) - \Delta v \quad (63)$$

Where,

$$Q_{cap} = Q_{UR} \quad (64)$$

To start, the load model is used to calculate the maximum design ice line load (from 4 bow locations) according to the specified Polar Class notation. The design point parameters for the specified polar class are assumed (infinite ice,  $V_{ship}$ ,  $h_{ice}$ ,  $P_o$ , and  $\sigma_f$ ). The model is then reapplied with the user specified ice conditions and speed is incrementally increased until the limit condition is exceeded. A graphical representation of the process is shown in Figure 43.

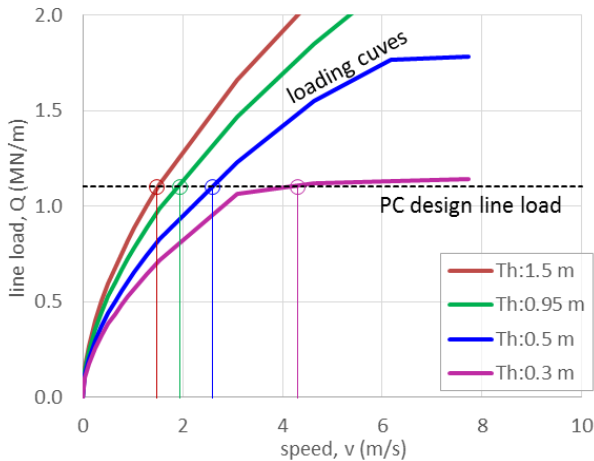
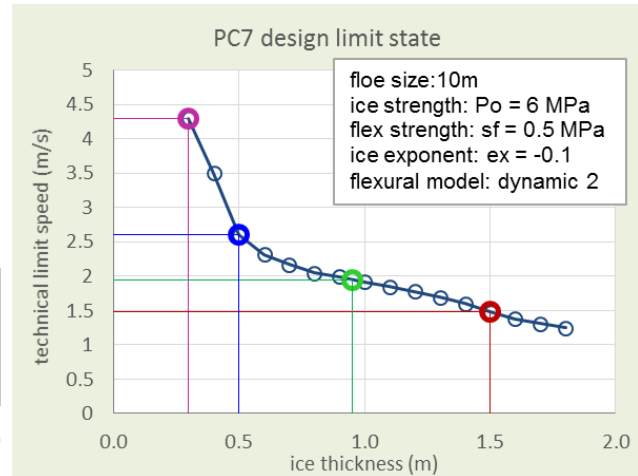


Figure 43: Description of PC design load criteria



#### 4.6.2. Direct Line Load Criteria

Models which take into account the detailed structural scantlings can be applied to determine the direct capacity of the plating, a frame or grillage arrangement. For instance, the plastic limit state models which form the technical background behind in the IACS Polar Class Unified Requirements can be implemented as capacity equations for establishing technical safe speeds. This method was presented and applied in Dolny et. al (2013) and is implemented into *DDePS\_2a\_Safe\_Check*. Limit speeds are established by incrementally increasing the speed until the loading term ( $Q_{load}$ ) exceeds the structural capacity ( $Q_{cap}$ ) for a given interaction scenario (speed, impact location, ice thickness or floe size, strength parameters, etc.). This limit condition is described by equation (65) and illustrated graphically in Figure 44.

$$v_{lim}(h) = v_i(Q_{load} > Q_{cap}) - \Delta v \quad (65)$$

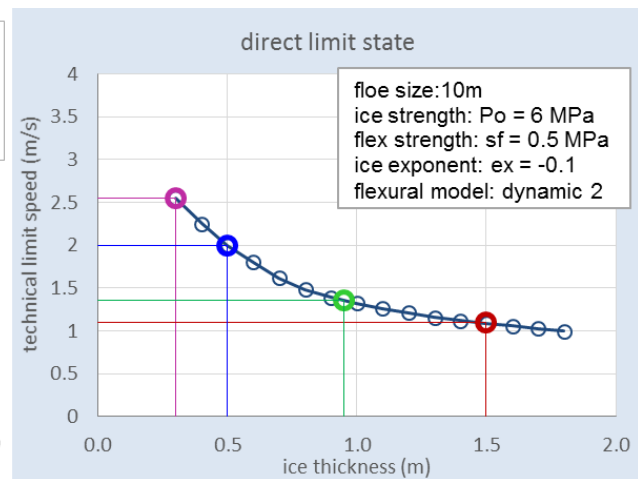
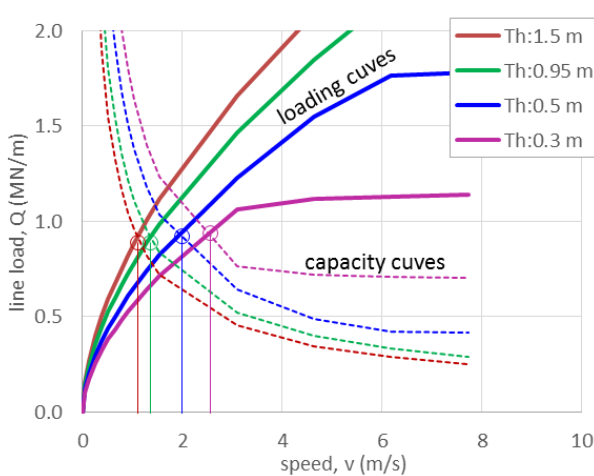


Figure 44: Description of direct limit load criteria

$Q_{cap}$  is calculated from the equations (66) and (67), and is based on the technical background for the plastic structural limit states adopted by the IACS Polar Class Unified Requirements. These limit states define the point where denting begins to occur. Therefore, the speeds computed by this approach are set such that there will be no observable deformation of the hull. Several plastic limit mechanisms, expressed in terms of pressure and taking into account the actual structural dimensions, are considered. The capacity of a frame can be considered as the minimum of limit pressures for each mechanism.

$$p_{cap} = \min(p_1, p_2, \dots, p_n) \quad (66)$$

When combined with the ice load model, which requires the applied load height, the frame capacity can be expressed in terms of a line load capacity as shown in equation (67). Line load is used as the basis for comparison and establishing the technical safe speed limits because it is the closest parameter that relates to the load encountered by a single frame.

$$Q_{cap} = \frac{F_{cap}}{S} = p_{cap} \cdot b \quad (67)$$

The structural limit states adopted by the Polar Rules provide a set of analytical expressions for the capacity of primary stiffening members (Daley, 2002a, 2002b; Daley, Kendrick, & Appolonov, 2001; Kendrick & Daley, 2000). These models were derived on the basis of energy methods and make use of plastic limit analysis. They were validated against extensive numerical simulations and physical experiments. Conceptual sketches of the limit states are shown in Figure 45.

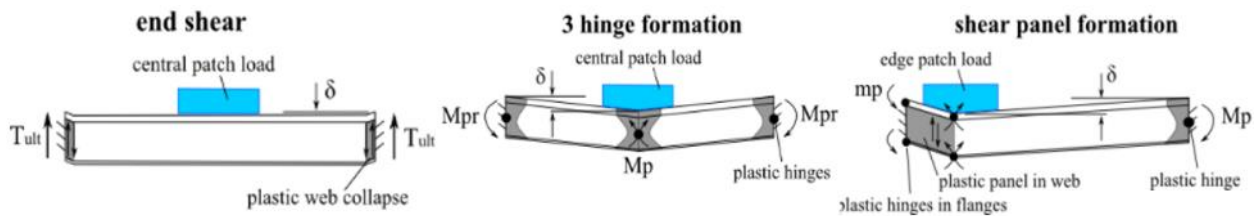


Figure 45: Structural limit states for frames subjected to lateral patch loads

The following sections present capacity equations, in terms of limit pressures, for transverse and longitudinal framing orientations. It should be understood that these notional “capacities” are in reality well below any ultimate strength due to strain hardening, membrane and many other effects. A robust structure can support 5-10 times the UR design load, as shown by extensive FE and experimental work (Daley & Hermanski, 2009; Kim, Dolny, & Daley, 2015; Manual, Gudimelta, Daley, & Colbourne, 2013). A sketch of an ice load patch applied to transverse framing is provided in Figure 46.

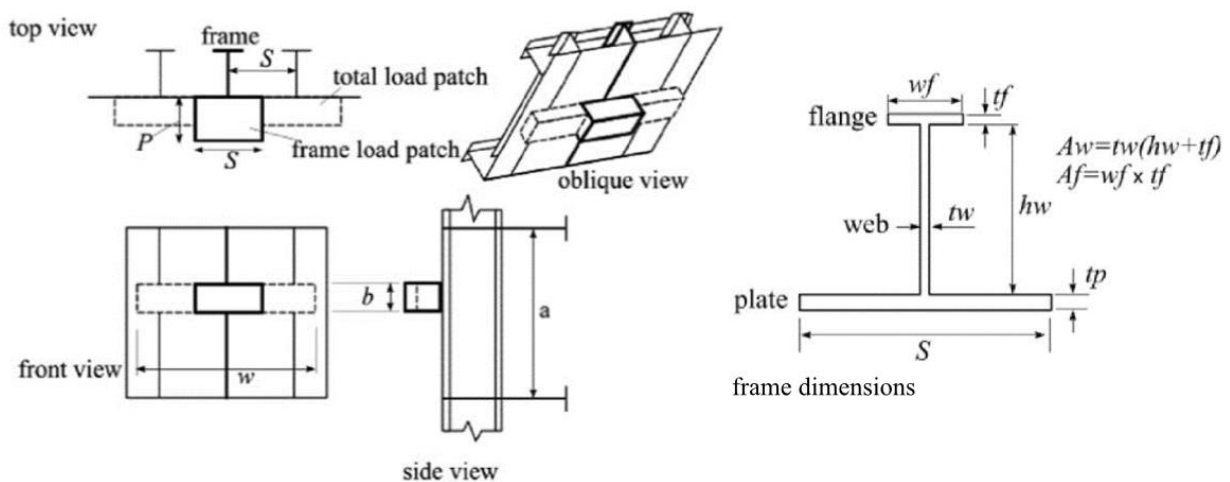


Figure 46: Sketch of ice load applied to transverse framing

### Transverse framing

The limit state capacities used in the IACS Polar Rules are described below. The pure shear collapse limit in which a transverse frame will fail by shear at the supports due to a central load patch is shown in equation (68).

$$p_{lim, shear} = \frac{2 A_s \sigma_y}{b s \sqrt{3}} \quad (68)$$

Where,

$A_s$  is the effective shear area of the frame [ $A_s = (h_w + t_f) * t_w$ ]

$\sigma_y$  is the yield strength of the material

$b$  is the load height

$s$  is the frame spacing

Equations (69) and (71) consider pressure applied as a central load patch which causes the formation of three plastic hinges (one central and two end hinges) under bending. The frame is considered to have two fixed supports ( $j = 2$ ). For case 1 (69), the total bending capacity is reduced based on a relatively simple quadratic shear-moment interaction.

$$p_{lim, c1} = \frac{1}{12 Z_{pns} + 1} \sigma_y Z_p \frac{4}{b s a \left(1 - \frac{b}{2a}\right)} \quad (69)$$

Where,

$a$  is the frame span

$Z_p$  is the effective plastic section modulus of the frame

$$Z_p = (t_f * w_f) * \left(\frac{t_f}{2} + h_w + \frac{t_p}{2}\right) + (t_w * h_w) * \left(\frac{h_w}{2} + \frac{t_p}{2}\right)$$

$Z_{pns}$  is normalized plastic section modulus, squared, described in (70)

$$Z_{pns} = \left[ \frac{Z_p}{A_s a \left(1 - \frac{b}{2a}\right)} \right]^2 \quad (70)$$

Case 2 (71) includes a modification in which the bending capacity is reduced only by the loss of web capacity.

$$p_{lim, c2} = \frac{[2 - kw + kw \sqrt{1 - 48 Z_{pns} (1 - kw)}]}{12 Z_{pns} kw^2 + 1} \sigma_y Z_p \frac{4}{b s a \left(1 - \frac{b}{2a}\right)} \quad (71)$$

Where,

$kw$  is the ratio of web section modulus to the total plastic section modulus [ $kw = Z_w / Z_p$ ]

$$Z_w \text{ is the web section modulus } \left[ Z_w = (t_w * h_w) * \left(\frac{h_w}{2} + \frac{t_p}{2}\right) \right]$$

A fourth limit state (72) considers the case of an off-center (end case) or asymmetric load in which plastic hinges form in the flanges along with a shear panel in the web near the load and a large plastic hinge at the far end.

$$p_{lim,asy} = \left[ \frac{(t_w * h_w)}{\sqrt{3}} + \frac{Z_p}{l} f_z \right] \frac{\sigma_y}{b s \left(1 - \frac{b}{2a}\right)} \quad (72)$$

The capacity of the transverse frame can be considered as the minimum of the four limit states provided above.

$$p_{cap} = \min(p_{lim,c1}, p_{lim,c2}, p_{lim,asy}, p_{lim,shear}) \quad (73)$$

#### Longitudinal Framing

The longitudinal framing limit states are based on the same principles as the transverse cases however the relative orientation of the load patch is simply rotated. The pure shear collapse limit in which a longitudinal frame will fail by shear at the supports due to a central and symmetrical load patch is shown in equation (74).

$$p_{lim,shear} = \frac{2 A_o \sigma_y}{w_{1L} b_{1L} \sqrt{3}} \quad (74)$$

For longitudinal frames, the effective load patch height is taken as:

$$b_{1L} = \min(b, s) \quad (75)$$

The effective load patch width is taken as:

$$w_{1L} = \min(w, a) \quad (76)$$

Equations (77) considers a central and symmetrical load patches which causes the formation of three plastic hinges (one central and two end hinges) under bending. The frame is considered to have two fixed supports ( $j = 2$ ).

$$p_{lim,c1} = \frac{1 + \frac{j}{2} \sqrt{3(j^2 - 4) Z_{pnsL} + 1}}{3 j^2 Z_{pnsL} + 1} \sigma_y Z_p \frac{4}{w_{1L} b_{1L} a \left(1 - \frac{w_{1L}}{2a}\right)} \quad (77)$$

Where,

$$Z_{pnsL} = \left[ \frac{Z_p}{A_s a \left(1 - \frac{w_{1L}}{2a}\right)} \right]^2 \quad (78)$$

The capacity of the longitudinal frame can be considered as the minimum of the two limit states provided above.

$$p_{cap} = \min(p_{lim,c1}, p_{lim,shear}) \quad (79)$$

Before carrying out a safe speed assessment using the direct line load criteria, an FE model should be used to verify the limit state formulations described by equations (67) through (79) for various load patch sizes and orientations. Examples of verification efforts are outside the current scope of this project.

#### 4.6.3. Large Deflection Criteria

Numerical simulations (e.g. nonlinear finite element analysis) can be used to develop more complex structural response functions that consider, for example, the effects of structural deformation energy and limit conditions beyond the notional plastic capacity of a frame (e.g. large denting or collapse behavior). These methods require quite specific information on the scantlings and arrangements and a fairly in-depth analysis to derive the response functions. DDePS\_2a\_Safe\_Check has an option to deal with large

deflection limits states but the user must define additional parameters after a dedicated numerical analysis of the representative structural arrangement. This is currently outside the scope of this project and therefore not presented in detail in this report. Some applications of this approach are described in Section 3.2.3.

#### **4.7. DDePS Validation**

The validation of an analytical tool like DDePS for scenarios applicable to light ice-strengthened government ships presents an obvious challenge. While conventional ice impact load data has been gathered from instrumented icebreakers and high ice class ships (i.e. icebreaking hull forms with strong local structures), no existing suitable validation data sets exist for light ice class or non-ice strengthened hulls in ice conditions. Furthermore, the majority of previous ice load measurement campaigns have generally targeted relatively challenging ice conditions (i.e. thick first year ice, multi-year ice, high concentrations, etc.) to better understand the nature of extreme ice loads and the limits of vessel performance capabilities.

Unfortunately comprehensive validation data is not currently available and would be prohibitively expensive to obtain in the field. There has been some efforts on the validation of the DDePS by the developers of the tool. Data from *USCG POLAR SEA* trials in the high Arctic and the Bering Sea (1980s) have been used to compare force vs. speed estimates computed by DDePS. Under some basic, but quite reasonable assumptions, the computed load levels compare well with the measured data. The presentation of these validation efforts are outside the current scope of this project.

## 5. Case Study – Ice Class PC5 Patrol Vessel

An example case study is presented in this section of the proposed safe speed methodology applied to a 5000 ton, Ice Class PC5 Patrol Vessel. The assessment follows the established procedure outlined in Section 4 using the existing software tool *DDePS\_2a\_Safe\_Check*.

### 5.1. Hull Form

The ship design is conceptual and developed by the project team based on sample ships of similar hull forms and structural arrangements. Ice Class PC5 is a relatively light ice class in the IACS Unified Requirements for Polar Class Ships with a nominal ice description - “year-round operation in medium first-year ice which may include old ice inclusions” (IACS, 2011). The ship features a moderate icebreaking hull form as shown in Figure 47. The lines are used to determine the hull angles and impact locations in the bow area for the ice load assessments. Table 7 shows the input deck for DDePS with all of the assumed ship particulars and hull data.

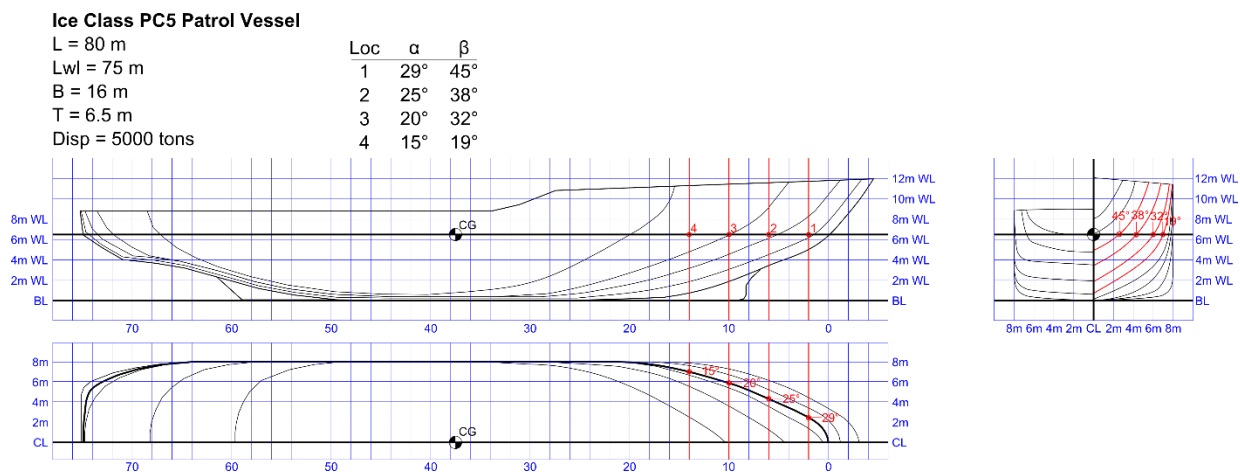


Figure 47: Hull particulars, lines, and bow hull angles for Ice Class PC5 Patrol Ship

Table 7: DDePS input deck – main particulars and hull data

Main Particulars			
ship type	--	ST	PV
ice class	--	IC	PC5
length overall	m	Loa	80.0
length between perpendiculars	m	Lbp	75.0
beam	m	B	16.00
draft	m	T	6.50
height (depth)	m	H	9.00
block coef.	--	CB	0.625
waterplane coef.	--	Cwp	0.895
midship coef.	--	Cm	0.95
displacement	tons	M	5000.00
Hull Data			
region	--	HA	1
frame number	--	FN	2
longitudinal distance from CG	m	x	35.50
transverse distance from CG	m	y	2.50
vertical distance from CG	m	z	0.00
waterline angle	deg	$\alpha$	29.00
frame angle	deg	$\beta$	45.00

	1	2	3	4
region	Bow	Bow	Bow	Bow
frame number	2	6	10	14
longitudinal distance from CG	35.50	31.50	27.50	23.50
transverse distance from CG	2.50	4.30	5.80	7.00
vertical distance from CG	0.00	0.00	0.00	0.00
waterline angle	29.00	25.00	20.00	15.00
frame angle	45.00	38.00	32.00	19.00

## 5.2. Hull Structural Design

A representative bow structural arrangement was developed and is provided in Figure 48. The icebelt consists of transverse frames spaced 610 mm apart and supported by primary decks. The scantlings of the framing and plating are indicated on the drawing and comply with minimum requirements of Ice Class PC5. The decks and bulkheads were also dimensioned along with stiffening arrangements according to typical ice belt designs. The figure also highlights the extent of a finite element model that is described in the following section. Table 8 presents the frame information that is used in DDePS. It should be reiterated that this is a conceptual structural design developed to demonstrate the technical safe speed methodology. Actual structural details of a real ship are more sophisticated and dimensions/scantlings may differ from frame to frame. In this simplification, each of the neighboring frames are assumed to be identical and the finite element model was developed for one of the bow locations (between #3 and #4).

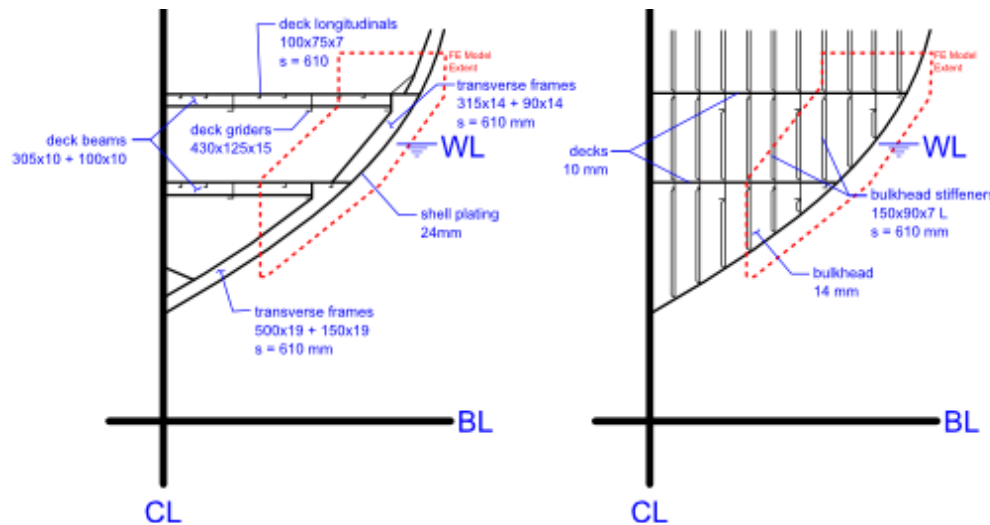


Figure 48: Representative structural arrangement for bow region of Ice Class PC5 Patrol Ship – frame section (left) and bulkhead section (right)

Table 8: DDePS input deck – frame data

Offered Ice Frame Data			1	1	1	1
frame orientation angle (to waterline)	deg	OA	90°	90°	90°	90°
frame orientation type	--	FO	Transverse	Transverse	Transverse	Transverse
frame attachment parameter	--	j	2	2	2	2
yield strength - framing material	MPa	Fy_f	355	355	355	355
yield strength - plating material	MPa	Fy_p	355	355	355	355
main frame span	mm	a	2000	2000	2000	2000
main frame spacing	mm	s	610	610	610	610
plate thickness (gross offered)	mm	tp_ofrd	24.0	24.0	24.0	24.0
offered frame	--	ofrd_frm	Built Section	Built Section	Built Section	Built Section
web angle	deg	fiw	90	90	90	90
web height	mm	hw	315	315	315	315
web thickness (gross)	mm	tw_gr	14	14	14	14
flange width	mm	wf	90	90	90	90
flange thickness (gross)	mm	tf_gr	14	14	14	14
flange offset distance	mm	bw	0	0	0	0

### 5.3. Finite Element Mesh

A finite element model was developed based on the structural design presented above. The model, shown in Figure 49, is used for characterizing the response of the representative structure to various ice load scenarios and verifying the limit state equations described in Section 4.6. The finite element mesh for the hull plating, decks, bulkheads, frames, and all types of stiffening (including both webs and flanges) must be capable of capturing nonlinear material and geometric behavior. For this reason, the entire mesh consists only of shell elements.

The longitudinal extent of the model (~4.5m) includes two transverse bulkheads (yellow) with 5 transverse icebelt frames (blue) that are supported by two primary decks (green). The vertical extent of the model is ~6.5m. The boundary conditions include fixed nodes at the longitudinal and vertical extents, as well as the inboard extents of the bulkheads, decks, and deck beams. A mesh size of ~3-4 cm edge length was found to be sufficient to remove load-deflection behavior dependence on mesh size. For the loading conditions considered in this study, these modeling assumptions are appropriate.

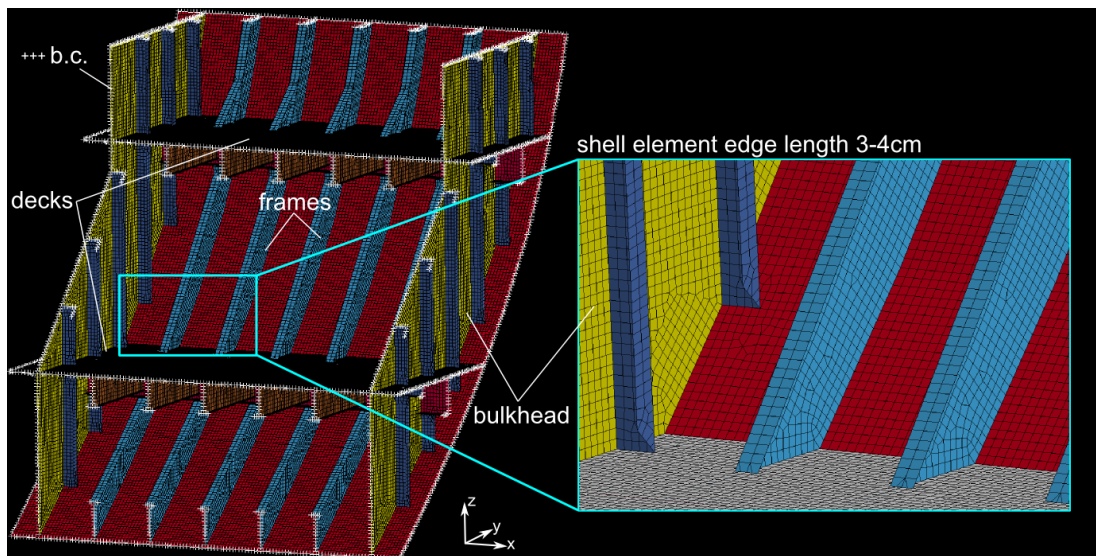


Figure 49: Structural finite element model of representative bow structure – Ice Class PC5 Patrol Ship

The structure is assumed to be composed of high tensile steel with a nominal yield strength of 355 MPa, which is typically used for ice strengthened ships. For the finite element analysis of the nonlinear response to ice loads, it is common to use bilinear plastic-kinematic hardening material model; which requires the selection of a tangent modulus that describes the strain-hardening behavior. Methods of selecting the tangent modulus differ. Preferred practice of the project team is to make a (successively refined) estimate of the range of strain experienced by highly deformed finite elements, and to choose a tangent modulus that best predicts the strain in that range, while ensuring that stress is not over-predicted. The assumed material properties used in this study are provided in Table 9.

Table 9: Assumed material properties and bilinear plastic-kinematic model parameters

Material Properties			
Density	$\rho$	7,850	kg/m <sup>3</sup>
Yield Strength	$\sigma_Y$	355	MPa
Young's Modulus	$E$	204	GPa
Poisson's Ratio	$\nu$	0.3	--
Tangent Modulus	$E_T$	1.0	GPa

## 5.4. Structural Response to Various Patch Loads

In order to characterize the overload response of the representative structure, a series of patch loads were applied to the FE model via quasi-static nonlinear finite element simulations. Four load patches of different sizes and aspect ratios were applied at several locations on the structure, as shown in Table 10, and Figures 50 and Figure 51. In each run, the force was gradually increased from 0 to approximately 10 MN (over the load patch area). The objective of these force-controlled simulations was to observe the overload capacity of the structure, well beyond the notional yield point of the material.

In addition, the results are used to verify the Polar UR nominal frame limits for different load patch orientations. These limits can be considered notional “capacities” but in reality are well below any ultimate strength due to strain hardening, membrane and other effects. The results demonstrate it is reasonable to use the Polar UR frame criteria as a ‘safety point’ in an ice capability assessment.

Load cases included loads centered on a transverse frame, shell plating, and the bulkhead. The load patch sizes and aspect ratios were selected to show the different response to concentrated local loads (A), longitudinally distributed loads (B & C), and vertically distributed loads (D).

Table 10: Patch load cases

run	description	load patch	force, F (MN)	pressure, P (MPa)	width, w (m)	height, b (m)
P_001	load cases centered on transverse frame	A	11.5	45.6	0.61	0.41
P_002		B	10.5	8.8	1.83	0.65
P_003		C	10.4	9.3	1.22	0.92
P_004		D	10.0	20.0	0.47	1.06
P_005	load cases centered on plating	A	11.5	45.6	0.61	0.41
P_006		B	10.5	8.8	1.83	0.65
P_007		C	10.4	9.3	1.22	0.92
P_008		D	10.0	20.0	0.47	1.06
P_009	load cases centered on bulkhead	A	11.5	45.6	0.61	0.41
P_010		B	10.5	8.8	1.83	0.65
P_011		C	10.4	9.3	1.22	0.92
P_012		D	10.0	20.0	0.47	1.06

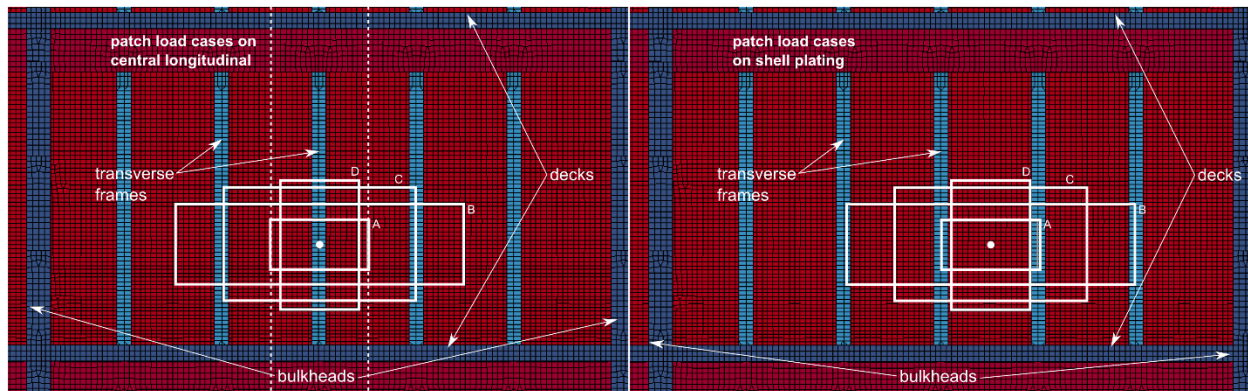


Figure 50: Load cases centered on transverse frame (left); Load cases centered on plating (right)

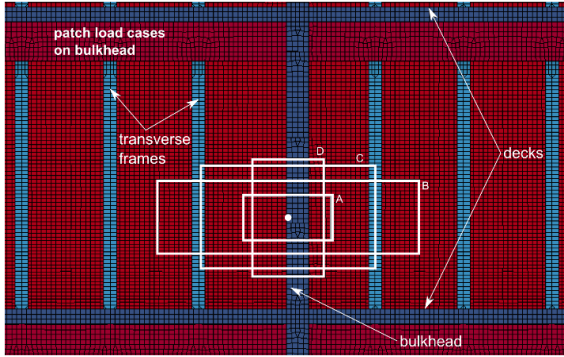


Figure 51: Load cases centered on bulkhead

The load vs. displacement curves (FEA results) for all of the patch load cases are shown in Figures 52 and 53. In these plots, the load is expressed as a line load  $[Q = \frac{F}{w}]$  as it increases during the simulation, and displacement is the measured resultant displacement at the center of the load patch on the plating. For the frame load cases (black curves), the Polar UR nominal frame limits are also identified. While the frame response varies for each case, the limit state equations consistently predict a point prior to any major loss of frame stiffness. At these load levels, there is plasticity but, the observable permanent deformation of the frame would be quite small.

For the same load patches centered on the plating, the response (red) can be quite different. At the frame limit loads, the plating exhibits some minor permanent deformation (indicated on the plots), but these are still relatively small compared to the thickness of the plating. Two example von-Mises stress distribution plots are shown in Figure 54 for cases P\_004 (patch D on frame) and P\_008 (patch D on plating) at the frame limit load. Areas highlighted in red indicate where the stress has exceeded the material yield point (355 MPa).

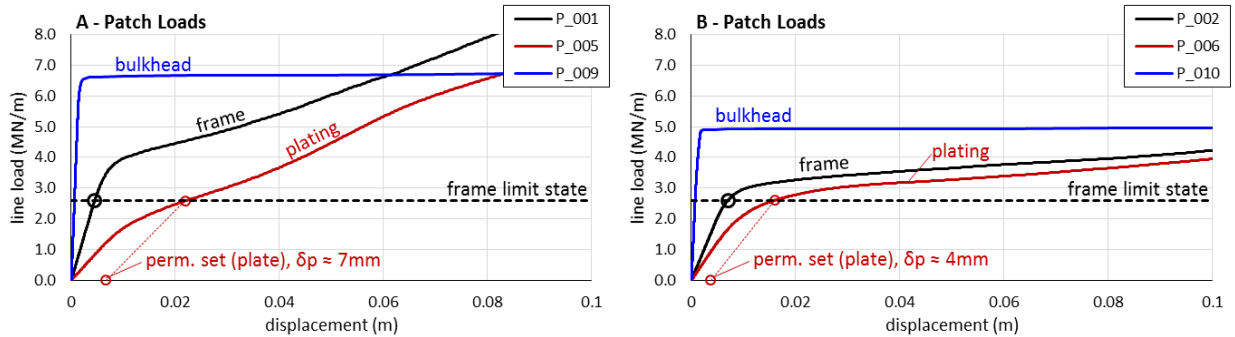


Figure 52: FEA results of structure response to various patch loads

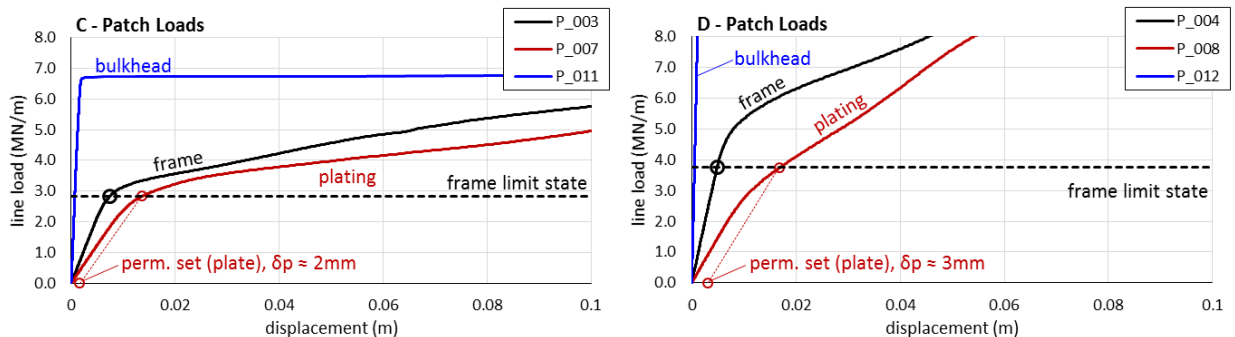


Figure 53: FEA results of structure response to various patch loads

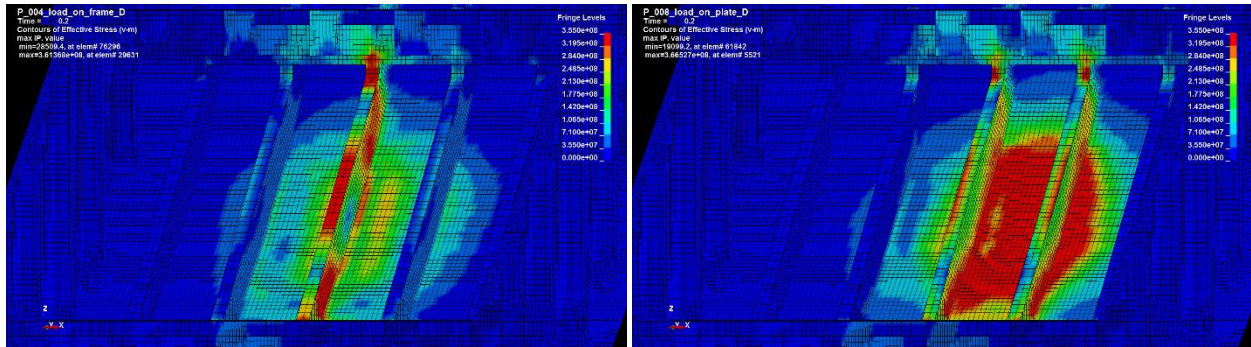


Figure 54: von-Mises stress distribution plots for cases P\_004 (left) and P\_008 (right) at the frame limit load

The bulkhead response to patch loads is substantially stiffer than the frames and plating. At the frame limits for each case, the bulkhead remains more or less elastic. However at higher load levels, the bulkhead web plating exhibits a rapid loss in capacity. This is caused by a post-yield instability of the bulkhead between supporting stiffeners. The contour plot in Figure 55 shows the stress distribution at the bulkhead collapse point in load case P\_009. The transverse frames would reach their limit state at much lower load levels ( $Q \approx 2 \sim 4$  MN/m, depending on the patch size), so it is not necessary to define a specific limit for these large members.

It should be noted that the frame limit state equations only consider an idealized single frame in isolation. In these analyses there is a load shedding effect to neighboring frames and other supporting members. Nevertheless, the equations predict quite reasonable load levels to set a safety point in a safe speed analysis.

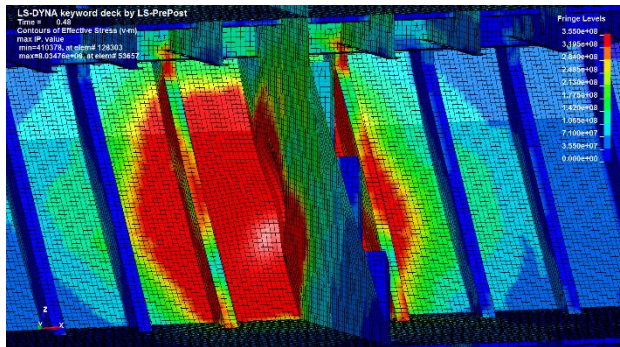


Figure 55: von-Mises stress distribution at web frame collapse point – load case P\_009

## 5.5. Safe Speed Assessment

In the safe speed assessment of the sample ship, DDePS is used to calculate load parameters for a series of conditions. Floe size, ice thickness, and impact location are systematically varied. As described in Section 4.3 the ice floe is assumed to be oriented normal to the point of contact. For the purposes of computing the mass and moments of inertia, the floe is idealized as a square with uniform thickness. The wedge shape at the impact point is simply used for the contact model. At each realization of the model, the frame scantlings are checked against the load parameters. If the load (expressed as line load) exceeds the defined limit state for the transverse frame, a limit is established.

As a way to demonstrate the procedure some example outputs of DDePS are presented in the following sections. Figure 56 illustrates several impact scenarios that will be used for the safe speed assessment and identifies 4 example cases (i.e. individual realizations of the model). Figure 57 shows the forces vs. speed results for 10 m, 20 m, 50 m, and 100 m floes. Thickness is varied in each plot from 15 cm to 3 m. The example cases are also identified on the respective plots. As a general reference, recall from the previous section that the nominal frame limit loads are  $\sim 2\text{-}4$  MN/m.

### 5.5.1. Example DDePS Outputs

The time history outputs for each example case are provided in Figures 58 through Figure 61. The time histories are solved using a fairly simple numerical integration scheme incrementing the normal velocity and position changes, starting from initial conditions. The algorithm calculates the ship's position (normal to collision) at each time step from the position and velocity at the previous time step.

The flexural failure modes are included to stop the integration scheme once a flexural limit is exceeded. In each example DDePS output, the time histories of total force, patch dimensions (width and height), average pressure, and line load are provided. On the line load plots, the frame capacity is also shown (black line). The capacity is a function of the frame limit load divided by the effective load width which explains why the frame capacity reduces as the patch load becomes larger.

These four cases were selected in order to highlight different ice collision scenarios that produce loads which are close to the frame limit states (either slightly exceeding or below). They also represent different ice failure modes and limit conditions in the model (i.e. ice crushing/momentum limit or flexural bending limit).

- **Case 1** is a 6 knot impact with a 25m floe that is 3m thick. This impact is limited by momentum and there is no flexural limit in the ice. This scenario slightly exceeds the limit state of the frame.
- **Case 2** is 4 knot collision with a 50m floe that is 1 m thick. This scenario is also limited by momentum and the final line load is almost exactly at the frame limit state.
- **Case 3** is a higher speed collision with a large but relatively thin floe (100m x 50cm). The load is limited by a flexural failure in the ice, i.e. there is enough downward breaking force to break the ice in flexure for these thickness levels. The time history output for line load also shows the frame limit state is not exceeded.
- **Case 4** is a fast collision (10 knots) of a vast, thin floe (500m x 30cm). Again, the load is limited by a flexural failure in the ice and is below the frame limit state.

In the time history plots the subscript “\_d” represents the final value for the respective parameter. For example  $F_d$  is the maximum force and  $p_d$  is the final pressure. These are the final values at the end of the integration scheme.

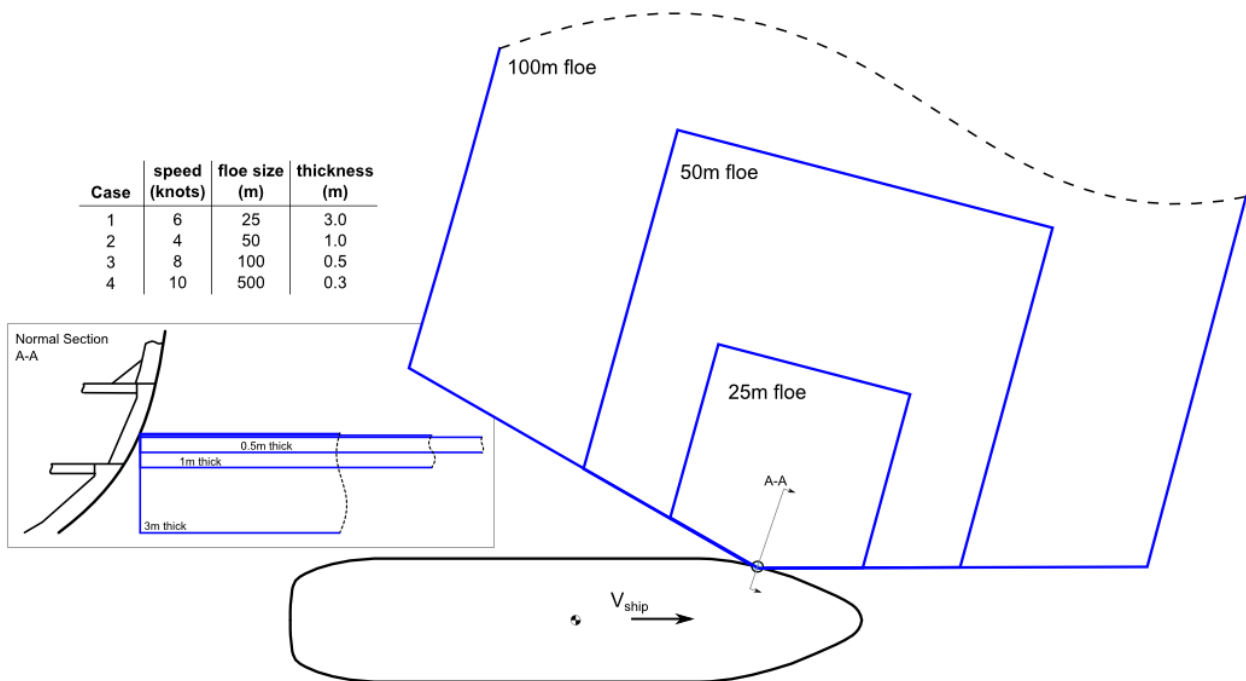


Figure 56: Sample DDePS calculation scenarios

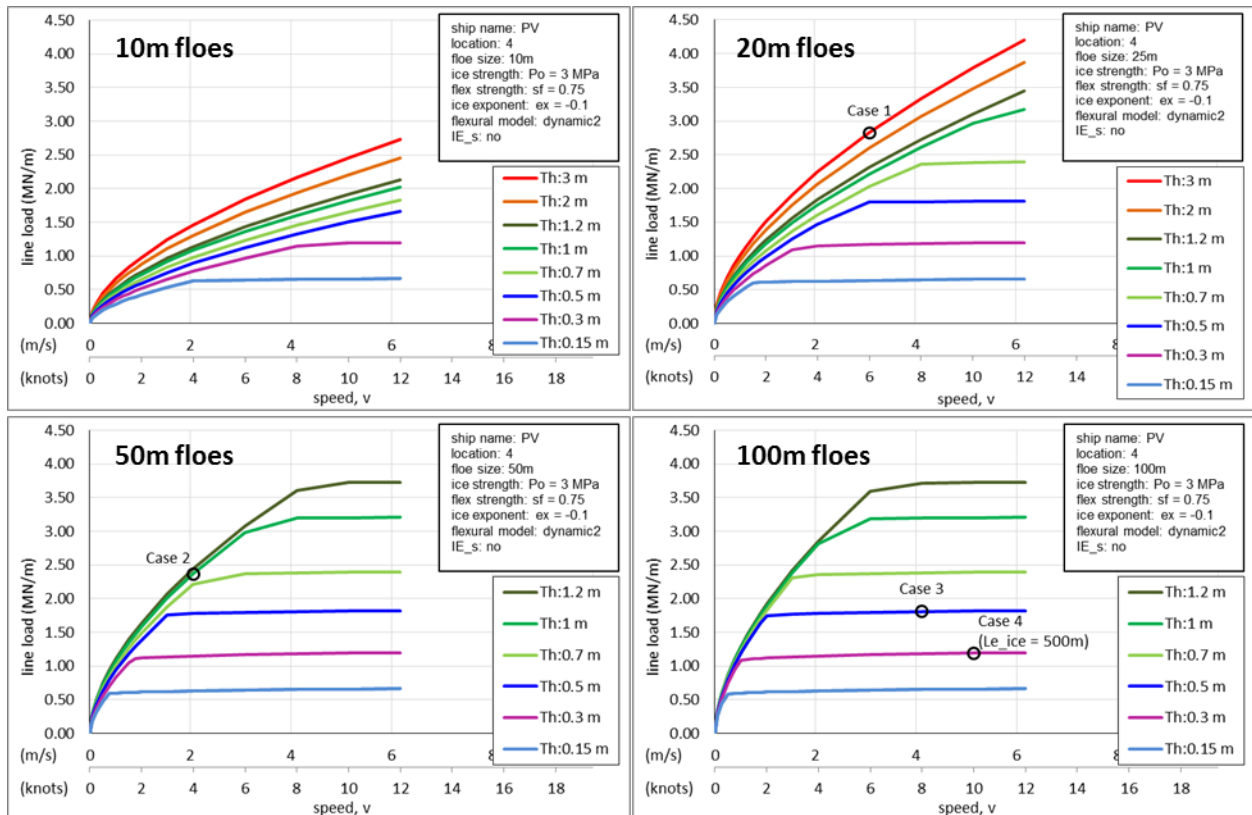


Figure 57: Load vs. speed results varying floe size and ice thickness (expressed in line load)

### Case 1

$V_s = 6$  knots

$L_{ice} = 25$  m

$H_{ice} = 3.0$  m

$P_0 = 3$  MPa,  $ex = -0.1$ ,  $\sigma_f = 0.75$  MPa

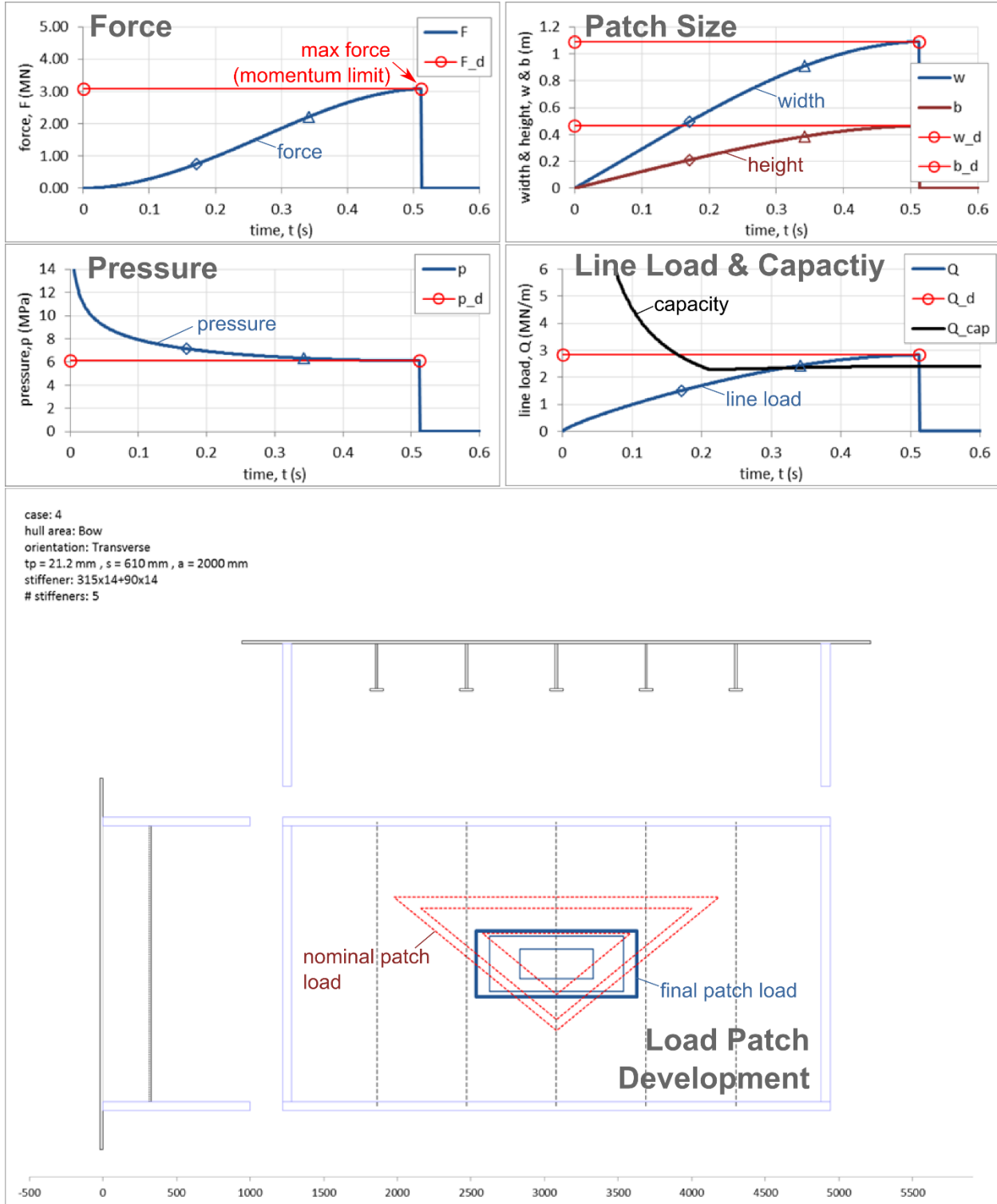


Figure 58: Case 1 - DDePS Outputs

## Case 2

$L_{ice} = 50 \text{ m}$

$H_{ice} = 1.0 \text{ m}$

$V_s = 4 \text{ knots}$

$P_o = 3 \text{ MPa}$ ,  $ex = -0.1$ ,  $\sigma_f = 0.75 \text{ MPa}$

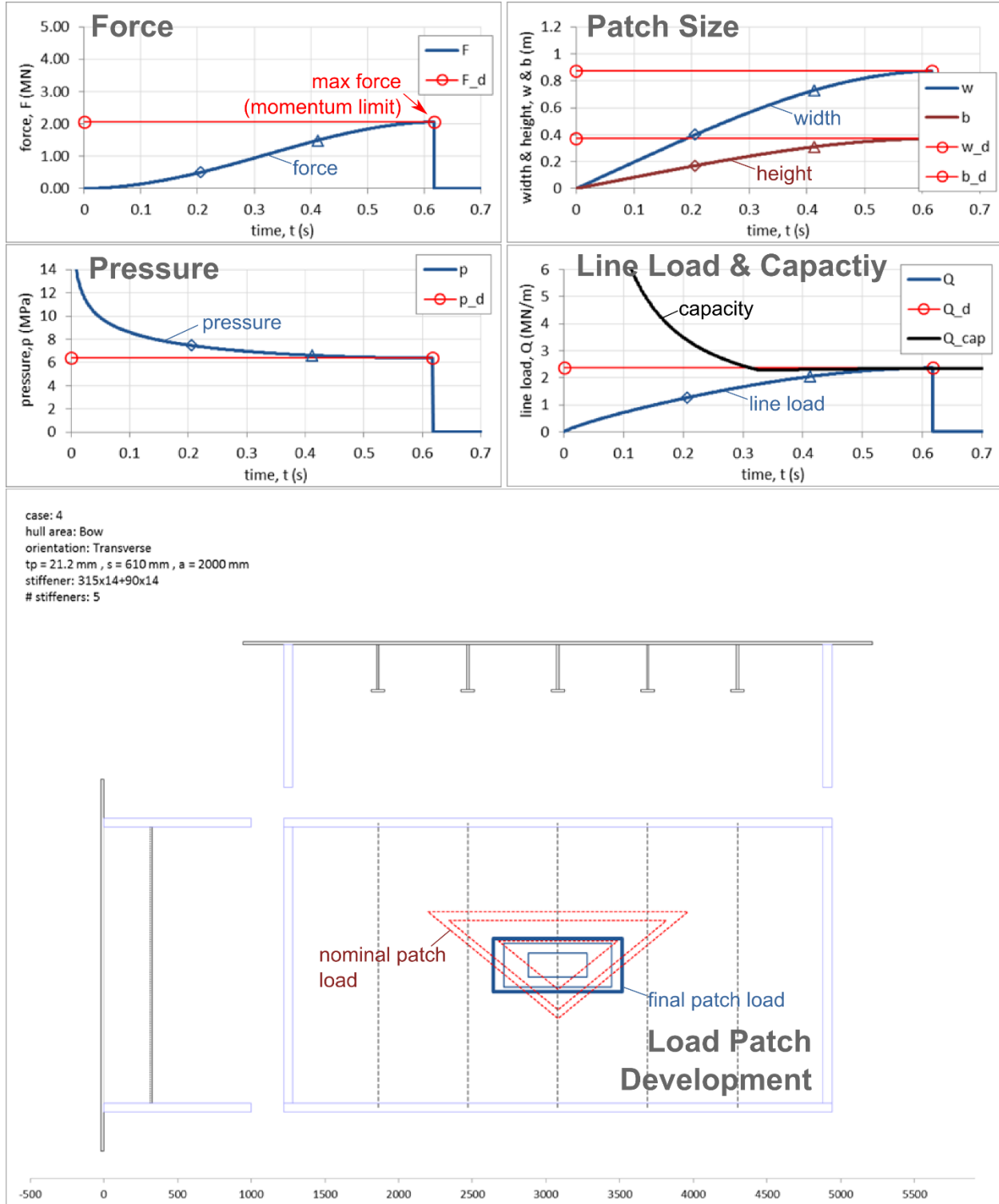


Figure 59: Case 2 - DDePS Outputs

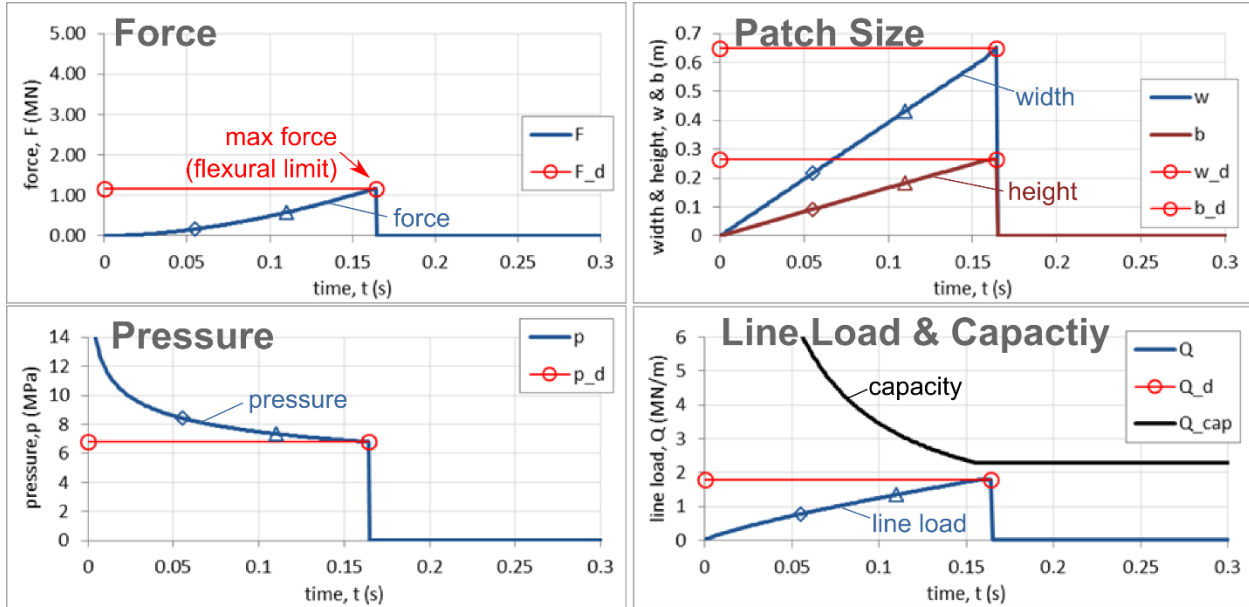
### Case 3

$L_{ice} = 100$  m

$H_{ice} = 0.5$  m

$V_s = 8$  knots

$P_o = 3$  MPa,  $ex = -0.1$ ,  $\sigma_f = 0.75$  MPa



case: 4  
hull area: Bow  
orientation: Transverse  
 $tp = 21.2$  mm,  $s = 610$  mm,  $a = 2000$  mm  
stiffener: 315x14+90x14  
# stiffeners: 5

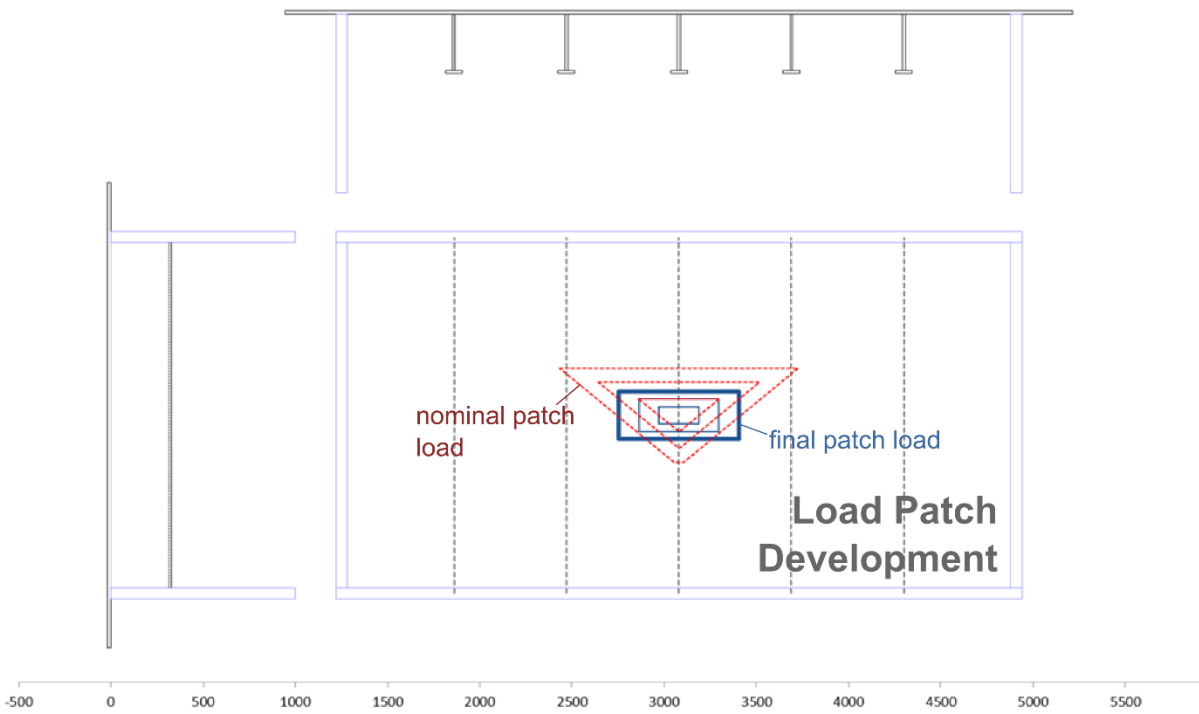


Figure 60: Case 3 - DDePS Outputs

**Case 4**

$L_{ice} = 500$  m

$H_{ice} = 0.3$  m

$V_s = 10$  knots

$P_o = 3$  MPa,  $ex = -0.1$ ,  $\sigma_f = 0.75$  MPa

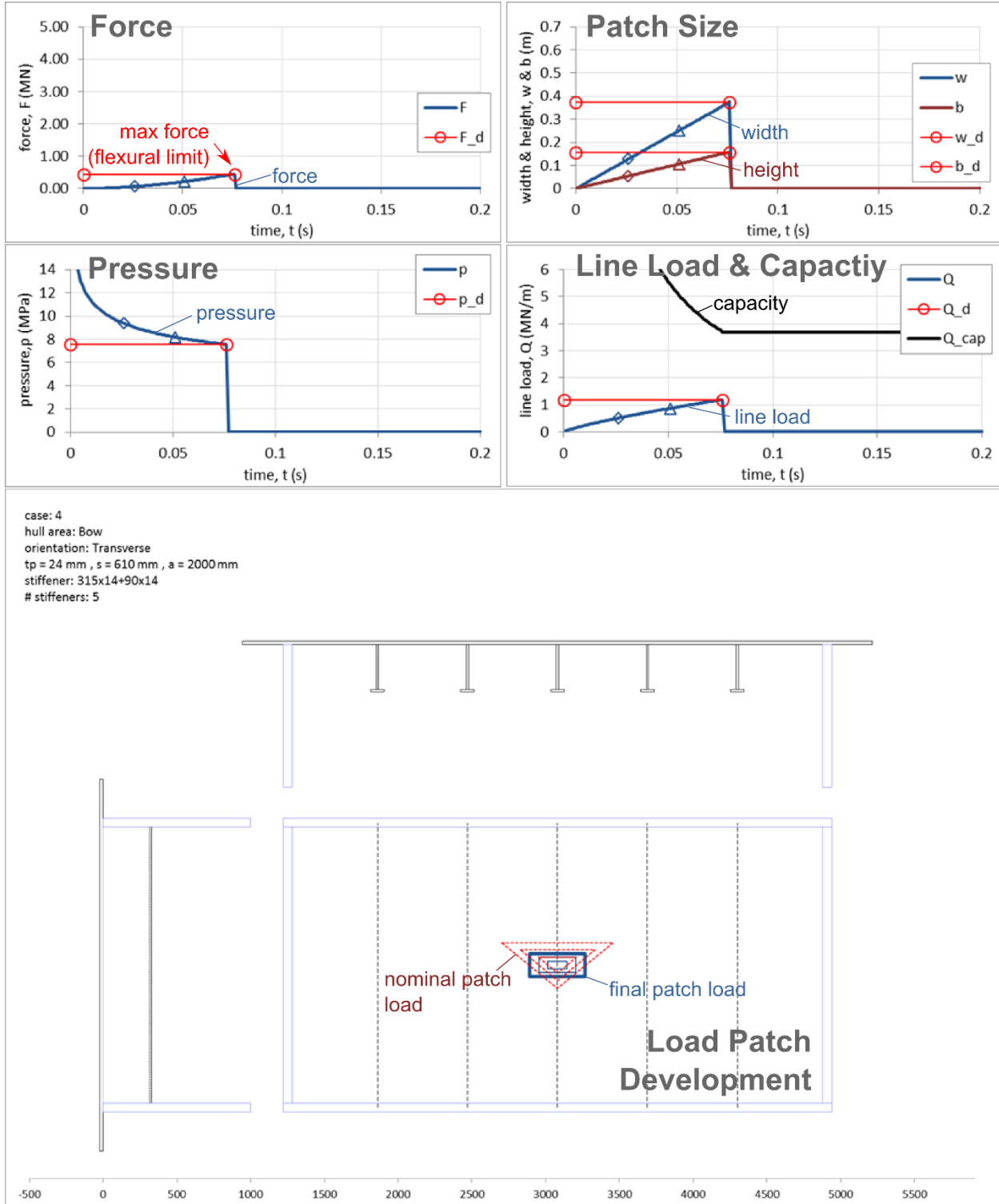


Figure 61: Case 4 - DDePS Outputs

### 5.5.2. Safe Speed Results

The DDePS program computes technical speed limits based on all combinations of ice parameters and several locations on the hull. The previous examples are just individual realizations of the model. Limits are established when the load exceeds the frame capacity. For the purposes of this study, line load (Q) is used as the basis for comparison and establishing the technical safe speed limits. Line load is the closest parameter that relates to the load encountered by a single frame. As previously described, the limit state is the formation of a 3 hinge plastic mechanism of a side shell frame under a patch load. This was shown to produce plasticity in the frame but without any major observable permanent dent size.

Figure 62 presents the technical safe speed results for the ships assuming the following parameters. In each plot, there are four curves representing different limits for different frame locations.

Ice crushing strength:  $P_o = 3 \text{ MPa}$  (ex = -0.1)  
 Ice flexural strength:  $\sigma_f = 0.75 \text{ MPa}$   
 Floe size:  $L_{ice} = 25 \text{ m} - 200 \text{ m}$   
 Thickness:  $h_{ice} = 15 \text{ cm} - 3 \text{ m}$   
 Speeds:  $V_s = 1 \text{ knot} - 16 \text{ knots}$   
 Locations: # 1, 2, 3, 4 (see Figure 47)

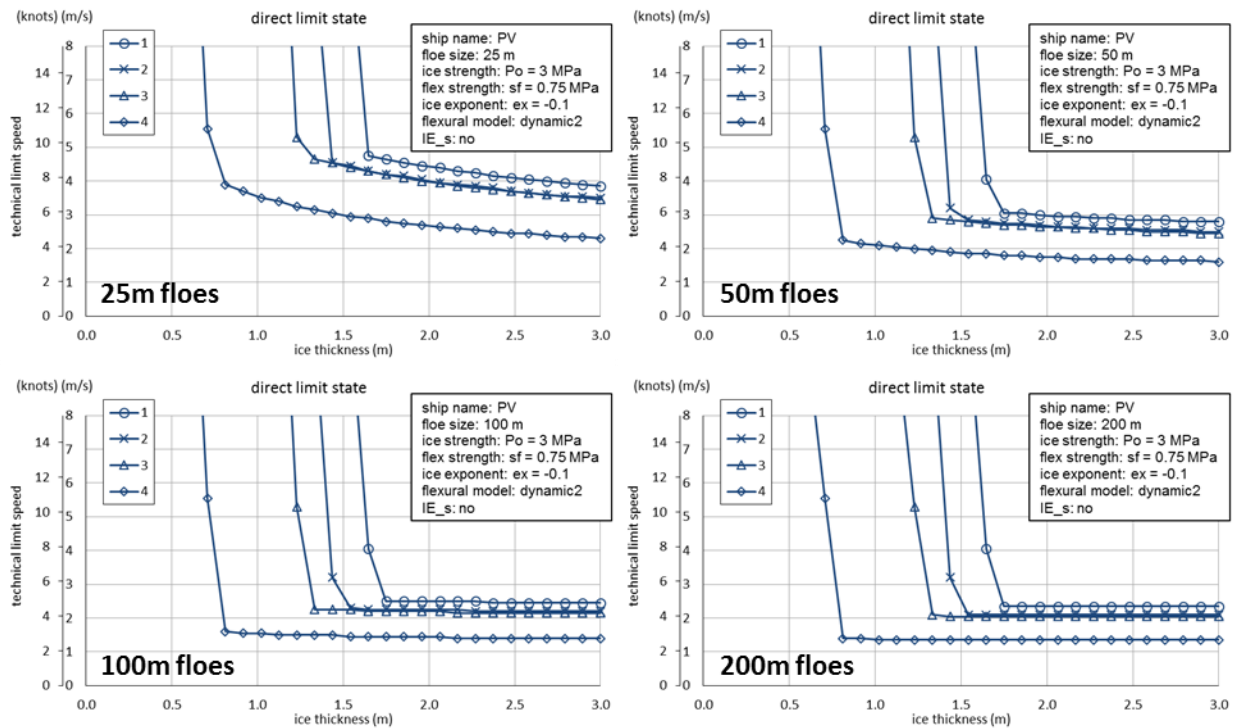


Figure 62: Technical safe speeds vs ice thickness for different floe sizes

Figure 63 is a summary plot of all the technical safe speed curves. For each impact scenario (combination of floe size and thickness), the minimum limit speed was taken of all the impact locations. The results suggest speed limitations for this ship at ice thicknesses greater than 0.5m. Below this thickness level, the flexural failure of the ice governs and the load magnitudes are lower than the frame limits. At approximately 0.75 m, the results suggest slow speed operations (< 5 knots) for floe sizes greater than 50m.

The nominal operational description for Ice Class PC5 is “year-round operation in **medium first-year ice** which may include old ice inclusions”. According to WMO nomenclature (referencing Table 1 in this report), the thickness range for medium first-year ice is 0.7-1.2 m. The outcome of this assessment is generally consistent with notional description of the ice class but offers additional information about the risks at different speeds for more combinations of conditions.

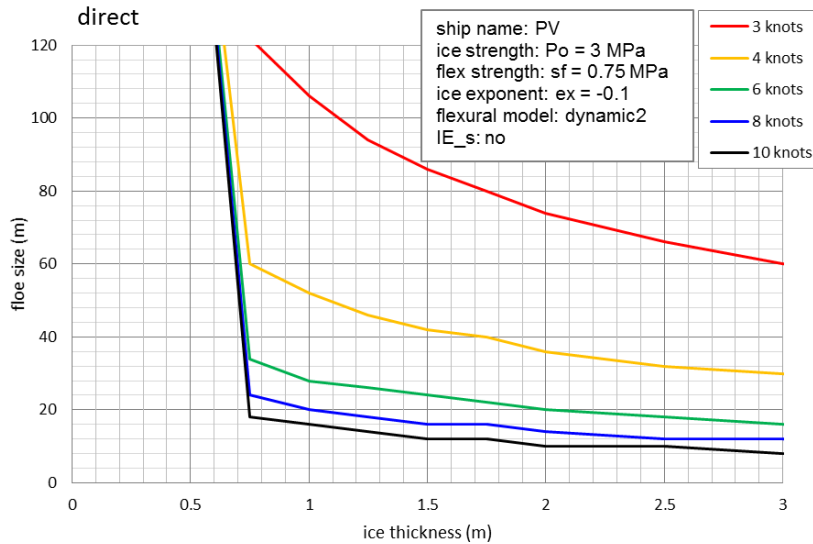


Figure 63: Summary plot of safe speed curves

Figure 64 demonstrates the influence of the ice strength terms (crushing,  $P_o$  and flexural,  $\sigma_f$ ) on the safe speed calculation results. As indicated in the figure the crushing strength is the dominating ice failure mode thicker ice regimes and the flexural limit dominates for thinner conditions. In this comparison the crushing strength is increased to 6 MPa, which is the assumed strength used in the design point for Ice Class PC1, and the flexural strength is increased to 1 MPa (used in the design point for Ice Class PC5).

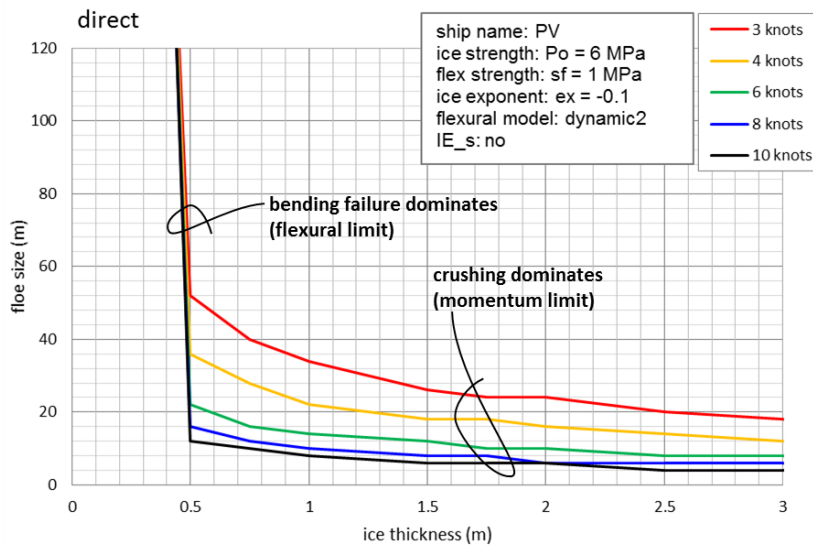


Figure 64: Summary plot of safe speed curves (stronger ice -  $P_o = 6 \text{ MPa}$ ,  $\sigma_f = 1.0 \text{ MPa}$ )

## 6. Conclusions and Future Work

This report presents an overview of safe speeds in ice and outlines the key operational hazards that should be considered in an evaluation of a ship's ice capability. A review of many existing approaches for establishing operational limitations of ships in ice is also presented. This includes simplified risk-based control regimes as well as technical ship-specific deterministic approaches.

A detailed technical methodology for determining safe speeds has been derived and proposed based on an assumed ice-ship interaction scenario, a mathematical model of ice collision mechanics, different ice failure modes including crushing and flexural bending failure, and structural response criteria.

Finally the technical methodology has been demonstrated using a 5000 ton Ice Class PC5 Patrol Vessel. The results are consistent with the nominal ice description for PC5 but offer additional information about the risks at different speeds for more combinations of conditions. These operational envelopes are useful in understanding a ship's structural capability in a variety of ice types.

It should be emphasized that speeds presented in this report are termed "technical safe speeds" in order to clarify that the speeds are derived by a simple set of calculations for specific technical assumptions. An actual safe speed would need to take a variety of other factors into account, including various uncertainties, levels of training, field experience and organizational risk tolerance.

Through the course of this effort, and through several parallel projects, a number of recommendations have come up that should be further studied to improve the technical approach and reduce uncertainties. Several assumptions have been made, most of which are believed to be conservative, but the results of the case study help narrate a discussion of uncertainties in the modeling approach and highlight critical gaps for future development.

### 1) Develop a stronger link between ice crushing terms and actual ice properties

As described in Section 2.4, there is a disconnect between the uniaxial ice crushing strength, which is most commonly reported from field measurements, and the process pressure-area relationship used to represent ice strength in the proposed technical methodology. The pressure-area approach is empirical and parameters are typically derived from full scale measurements of instrumented icebreakers. In the case of this study, the crushing terms were drawn from the assumed values used for design points in the Polar Rules. Unfortunately little work has been done to draw a link between the two representations of crushing strength. A combination of dedicated laboratory experiments and a focused review of reported field testing programs and in-situ ice measurements could greatly improve this link.

### 2) Modeling moving loads and the resulting structural response

The model employed in this study is based on Popov collision mechanics, which assumes the collision process is quick and there is no sliding along the hull. Up to the limit states explored in this study (on set of plastic deformations), this assumption is reasonable. However, for more severe limit states (e.g. larger deformation cases), moving load effects should be carefully considered. Quinton (2015) has demonstrated numerically and physically (experimental laboratory tests) the adverse effects of scoring action on a structure's ability to withstand a load, in particular when already subject to plastic damage. This is an area currently under further investigation in a parallel effort supported by ONR.

### 3) Continued development of thin-ice mechanics

The assessment presented in this report made use of methods that do not account for the flexural elasticity of the ice edge as an energy absorption mechanism. For ships operating in thin ice conditions

the edge flexibility may have a significant effect on the development of the ice force and pressure distributions on the hull structure. Especially in the case of floe diameters exceeding 20x the thickness, the impacts may be over-estimated. This is another area currently under further investigation in a parallel effort supported by ONR.

#### **4) Maneuvering operations and the influence on load severity**

The technical methodology currently only considers pure forward motion with impacts on the bow structure. Maneuvering through pack ice results in impacts with various degrees of lateral speed and at different positions along the hull. Maneuvering operations will affect the loads both positively and negatively. Further study of the navigation in pack ice is warranted. A new software technology called GPU Event Mechanics (GEM) has been used to explore natural variability in ice loads during different operational modes, including maneuvering. GEM is a novel modeling capability developed at Memorial University that makes use of the kind of formulations used in DDePS, but implements them in the context of a general vessel navigation simulation (Daley, Alawneh, Peters, & Colbourne, 2014). GEM remains under continuous development and new features are regularly being incorporated into the model. Future work may apply the GEM software more extensively to further evaluate loads on ships from more natural operation conditions.

## 7. References

- ABS. (2015). *ABS Technical Report - USCG WMSL Class - Operational Capabilities and Limitations in Ice*. Houston, TX, USA.
- Canadian Coast Guard. (2012). *Ice Navigation in Canadian Waters*. Ottawa, ON, Canada: Icebreaking Program, Maritime Services, Canadian Coast Guard Fisheries and Oceans Canada.
- Colbourne, B. (1989). *A three component method of analyzing icebreaking resistance (IR-1989-07)*. St. John's, NL, Canada.
- Daley, C. (1999). Energy based ice collision forces. *Port and Ocean Engineering under Arctic Conditions, POAC'99*. Espoo, Finland.
- Daley, C. (2000). *IACS Unified Requirements for Polar Ships - Background Notes to Design Ice Loads*.
- Daley, C. (2002a). Application of plastic framing requirements for polar ships. *Marine Structures, 15*(6), 533–542. doi:10.1016/S0951-8339(02)00018-7
- Daley, C. (2002b). Derivation of plastic framing requirements for polar ships. *Marine Structures, 15*(6), 543–559. doi:10.1016/S0951-8339(02)00019-9
- Daley, C. (2015). *Ice Impact Capability of DRDC Notional Destroyer*.
- Daley, C., Alawneh, S., Peters, D., & Colbourne, B. (2014). GPU-Event-Mechanics Evaluation of Ice Impact Load Statistics (OTC 24645). *Arctic Technology Conference, ATC'14*. Houston, TX, USA.
- Daley, C., & Hermanski, G. (2009). *Investigation of Plastic Limit States for Design of Ship Hull Structures - Ship Frame Research Program - A Experimental Study of Ship Frames and Grillages Subjected to Patch Loads (Ship Structure Committee Report SSC-457)*. Washington, DC, USA.
- Daley, C., & Kendrick, A. (2011). *Safe Speeds in Ice (BMT Report 6931DFR.Rev00)*.
- Daley, C., Kendrick, A., & Appolonov, E. (2001). Plating and Framing Design in the Unified Requirements for Polar Class Ships. *Port and Ocean Engineering under Arctic Conditions, POAC'01*. Ottawa, ON, Canada.
- Daley, C., Kendrick, A., & Quinton, B. W. T. (2011). *Safe Speeds in Ice (errata)*.
- Daley, C., & Kim, H. (2010). Ice Collision Forces Considering Structural Deformation. *International Conference on Offshore Mechanics and Arctic Engineering, OMAE'10*. Shanghai, China.
- Daley, C., & Liu, J. J. (2009). *DDePS for Ship Ramming Infinite / Finite Ice*.
- Daley, C., & Liu, J. J. (2010). Assessment of Ship Ice Loads in Pack Ice. *International Conference and Exhibition on Performance of Ships and Structures in Ice, IceTech'10*. Anchorage, AK, USA.
- DeBord, F., McAllister, T., Cleary, C., Dolny, J., & Kawamoto, R. (2015). Design considerations for operation of Coast Guard cutters and combatants in the Arctic. *SNAME World Maritime Technology Conference, WMTC'15*. Providence, RI, USA.
- Dolny, J., Yu, H., Daley, C., & Kendrick, A. (2013). Developing a Technical Methodology for the Evaluation of Safe Operating Speeds in Various Ice Conditions. *Port and Ocean Engineering under Arctic Conditions, POAC'13*. Espoo, Finland.
- Finland, Sweden, Kolari, K., & Kurkela, J. (2012). DE 57/INF.3: Simulation of ship-ice interaction. *IMO Sub-Committee on Ship Design and Equipment, 57th Session, Agenda Item 11, Development of a Mandatory Polar Code*.
- IACS. (2011). *IACS Unified Requirements Concerning Polar Class*. London, UK: International Association of Classification Societies.

- Kendrick, A., & Daley, C. (2000). *IACS Unified Requirements for Polar Ships - Background Notes to Derivation and Use of Formulations for Framing Design*.
- Kendrick, A., & Daley, C. (2006a). *Ice Interaction Scenarios and Load Modeling Approaches (BMT Report 6007A.DFR submitted to ABS)*.
- Kendrick, A., & Daley, C. (2006b). *Ice Loads for Structural and Vibration Analysis of Large Arctic LNG Carriers – Phase II (BMT Report 6055 DR submitted to ABS)*.
- Kendrick, A., & Daley, C. (2009). *DDPS for Stern Impacts with Ice (BMT Report 6512D.FR submitted to ABS and DSME)*.
- Kendrick, A., & Daley, C. (2011). *Structural Challenges Faced by Arctic Ships (Ship Structure Committee Report SSC-461)*.
- Kim, H., Dolny, J., & Daley, C. (2015). An experimental study of the design and overload capacity of structural grillages subjected to ice loads. *Port and Ocean Engineering under Arctic Conditions, POAC'15*. Trondheim, Norway.
- Kurdyumov, V. A., & Kheisin, D. E. (1976a). Hydrodynamic Model of the Impact of a Solid on Ice (Translated). *Applied Mechanics*, 12(10), 103–109.
- Kurdyumov, V. A., & Kheisin, D. E. (1976b). Hydrodynamic Model of the Impact of Solid Body Impact Against Ice. *International Applied Mechanics*, 12(10), 1063–1068.
- Likhomanov, V. A., Timofeev, O. Y., Stepanov, I., Kashtelyan, V. I., Iltchuk, A., Krupina, N., & Klenov, A. (1997). *Scientific Basis and Methodology of the Development of an Ice Passport*. St. Petersburg, Russia.
- Likhomanov, V. A., Timofeev, O. Y., Stepanov, I. V., & Kashtelyan, V. I. (1998). Ice Passport for Icebreaker Pierre Radisson and Passport's Concept: Further Development. *International Offshore and Polar Engineering Conference, ISOPE'98* (Vol. 2, pp. 566–571). Montreal, Canada.
- Makutov, D. D., & Popov, Y. N. (1981). Development and Implementation of Ship Ice Certificates. *Second International Conference on Icebreaking & Related Technologies, IceTech'81*. Ottawa, ON, Canada.
- Manual, M., Gudimelta, P. S. R., Daley, C., & Colbourne, B. (2013). Controlled Plastic Deformation of a Grillage Using Artificial Freshwater Ice at a Large Scale. *Port and Ocean Engineering under Arctic Conditions, POAC'13*. Espoo, Finland.
- Popov, Y. N., Faddeyev, O. V., Kheisin, D. E., & Yalovlev, A. (1967). *Strength of ships sailing in ice* (FSTC-HT-23.). Leningrad: Sudostroenie Publishing House, U.S. Army Foreign Science and Technology Center (Translation).
- Popov, Y. N., Faddeyev, O. V., Kheysin, D. Y., & Yakovlev, A. A. (1967). *Strength of Ships Sailing In Ice (Translated)*, F3TC-HT-23-96-68 (Technical.). Leningrad, USSR: Sudostroyeniye Publishing House.
- Quinton, B. (2015). *Experimental and Numerical Investigation of Moving Loads on Hull Structures*. Memorial University of Newfoundland.
- Riska, K., & Kämäräinen, J. (2012). Comparison of Finnish-Swedish and IACS ice class rules. *RINA International Conference on Ice Class Ships* (pp. 43–62). London, UK.
- Sazidy, M. (2014). *Development of Velocity Dependent Ice Flexural Failure Model and Application to Safe Speed*. Memorial University of Newfoundland.
- Sazidy, M., Daley, C., & Colbourne, B. (2014). A Mathematical Model of Icebreaking for Safe Speed Assessment. *International Conference and Exhibition on Performance of Ships and Structures in Ice, IceTech'14* (pp. 1–8). Banff, AB, Canada.

- Sazidy, M., Daley, C., Colbourne, B., & Wang, J. (2014). Effect of Ship Speed on Level Ice Edge Breaking. *International Conference on Offshore Mechanics and Arctic Engineering, OMAE'14*. San Francisco, CA, USA.
- Timco, G. W., & Weeks, W. F. (2010). A review of the engineering properties of sea ice. *Cold Regions Science and Technology*, 60(2), 107–129. doi:10.1016/j.coldregions.2009.10.003
- Tunik, A. (2000). Safe Speeds of Navigation in Ice as Criteria of Operational Risk. *International Journal of Offshore and Polar Engineering*, 10(4).
- Tunik, A. L., Kheisin, D. E., & Kurdyumov, V. A. (1990). Probabilistic Concept of Safe Speeds for Arctic Shipping. *Ice Technology for Polar Operations: Proceedings of the Second International Conference on Ice Technology* (pp. 295–306). Cambridge, United Kingdom.
- Valanto, P. (1996). On the transient response of a floating ice cover to an advancing ship. *International Conference on Offshore Mechanics and Arctic Engineering, OMAE'96* (pp. 24–40). Florence, Italy.
- VARD. (2015). *Safe Speed in Ice (305-000-01, Report for Transport Canada)*.

## Appendix A - Description of Popov Terms

This appendix provides the technical derivations for the effective mass terms for the ship and ice that are used in DDePS. This approach was first developed by Popov et al. (1967).

### A.1 Popov Terms for Ship

A collision taking place at point 'P' (see Figure 65), will result in a normal force  $F_n$ . Point P will accelerate, and a component of the acceleration will be along the normal vector, with a magnitude  $\ddot{\zeta}$ . The collision can be modeled as if point P were a single mass (a 1 degree of freedom system) with an equivalent mass  $M_e$  of;

$$M_e = F_n / \ddot{\zeta} \quad (80)$$

The equivalent mass is a function of the inertial properties (mass, radii of gyration, hull angles and moment arms) of the ship. The equivalent mass is linearly proportional to the mass (displacement) of the vessel, and can be expressed simply by the following equation.

$$M_{e_{ship}} = \frac{M_{ship}}{C_o} = \frac{1}{\frac{l^2}{M_{sx}} + \frac{m^2}{M_{sy}} + \frac{n^2}{M_{sz}} + \frac{\lambda^2}{I_{sx}} + \frac{\mu^2}{I_{sy}} + \frac{\nu^2}{I_{sz}}} \quad (81)$$

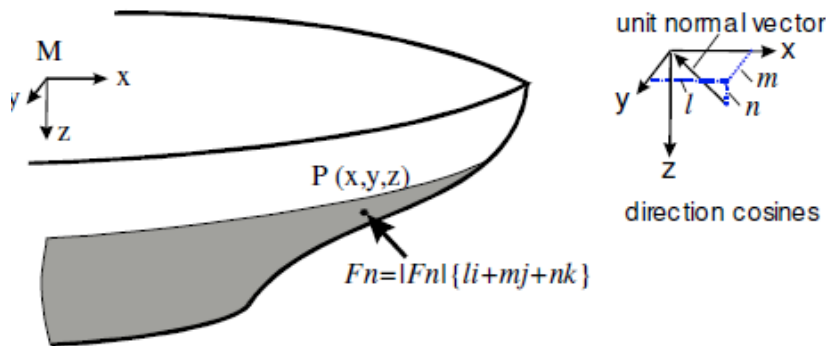


Figure 65: Collision point geometry

The inertial properties of the vessel are as follows;

Hull angles at point P:

$\alpha$  : waterline angle

$\beta$  : frame angle

$\beta'$  : normal frame angle

$\gamma$  : sheer angle

The various angles are related as follows:

$$\tan(\beta) = \tan(\alpha) \tan(\gamma) \quad (82)$$

$$\tan(\beta') = \tan(\beta) \cos(\alpha) \quad (83)$$

Based on these angles, the direction cosines  $l$ ,  $m$ , and  $n$  are:

$$l = \sin(\alpha) \cos(\beta') \quad (84)$$

$$m = \cos(\alpha) \cos(\beta') \quad (85)$$

$$n = \sin(\beta') \quad (86)$$

and the moment arms are;

$$\lambda = ny - mz \quad (\text{roll moment arm}) \quad (87)$$

$$\mu = lz - nx \quad (\text{pitch moment arm}) \quad (88)$$

$$\eta = mx - ly \quad (\text{yaw moment arm}) \quad (89)$$

The added mass terms for the ship are represented by the following geometric relationships (from Popov);

$$AM_x = 0 \quad (\text{added mass factor in surge}) \quad (90)$$

$$AM_y = 2 T/B \quad (\text{added mass factor in sway}) \quad (91)$$

$$AM_z = 2/3 (B C_{wp}^2)/(T(C_B(1 + C_{wp}))) \quad (\text{added mass factor in heave}) \quad (92)$$

$$AM_{roll} = 0.25 \quad (\text{added mass factor in roll}) \quad (93)$$

$$AM_{pit} = B(T/(3 - 2C_{wp})(3 - C_{wp})) \quad (\text{added mass factor in pitch}) \quad (94)$$

$$AM_{yaw} = 0.3 + 0.05 L/B \quad (\text{added mass factor in yaw}) \quad (95)$$

The mass radii of gyration (squared) are;

$$rx^2 = C_{wp}B^2/(11.4 C_m) + H^2/12 \quad (\text{roll}) \quad (96)$$

$$ry^2 = 0.07 C_{wp}L^2 \quad (\text{pitch}) \quad (97)$$

$$rz^2 = L^2/16 \quad (\text{yaw}) \quad (98)$$

The six force (moment) actions on the six degrees of freedom of the vessel's center of gravity are;

$$F_x = F_n l \quad (\text{force in surge}) \quad (99)$$

$$F_y = F_n m \quad (\text{force in sway}) \quad (100)$$

$$F_z = F_n n \quad (\text{force in heave}) \quad (101)$$

$$M_{rol} = F_n \lambda \quad (\text{moment in roll}) \quad (102)$$

$$M_{pit} = F_n \mu \quad (\text{moment in pitch}) \quad (103)$$

$$M_{yaw} = F_n \eta \quad (\text{moment in yaw}) \quad (104)$$

There are six accelerations at the center of gravity which are:

$$a_x = F_n l/(M(1 + AM_x)) \quad (\text{acceleration in surge}) \quad (105)$$

$$a_y = F_n m/(M(1 + AM_y)) \quad (\text{acceleration in sway}) \quad (106)$$

$$a_z = F_n n/(M(1 + AM_z)) \quad (\text{acceleration in heave}) \quad (107)$$

$$a_{rol} = F_n \lambda/(M rx^2(1 + AM_{roll})) \quad (\text{acceleration in roll}) \quad (108)$$

$$a_{pit} = F_n \mu/(M ry^2(1 + AM_{pit})) \quad (\text{acceleration in pitch}) \quad (109)$$

$$a_{yaw} = F_n \eta / (M r z^2 (1 + AM_{yaw})) \quad (\text{acceleration in yaw}) \quad (110)$$

Each of these accelerations contributes to the acceleration of the point of ice contact. The total acceleration at the point of contact can be expressed as;

$$\ddot{\zeta} = F_n C_o / M_{ship} \quad (111)$$

where;

$$C_o = \frac{l^2}{1+AM_x} + \frac{m^2}{1+AM_y} + \frac{n^2}{1+AM_z} + \frac{\lambda^2}{rx^2(1+AM_{roll})} + \frac{\mu^2}{ry^2(1+AM_{pit})} + \frac{\eta^2}{rz^2(1+AM_{yaw})} \quad (112)$$

The collision applies an impulse  $I_e$  to the vessel at the point of contact. The changes in velocity at the center of gravity are;

$$dV_x = I_e l / (M(1 + AM_x)) \quad (\text{velocity change in surge}) \quad (113)$$

$$dV_y = I_e m / (M(1 + AM_y)) \quad (\text{velocity change in sway}) \quad (114)$$

$$dV_z = I_e n / (M(1 + AM_z)) \quad (\text{velocity change in heave}) \quad (115)$$

$$dV_{rol} = I_e \lambda / (M \cdot rx^2 (1 + AM_{roll})) \quad (\text{velocity change in roll}) \quad (116)$$

$$dV_{pit} = I_e \mu / (M \cdot ry^2 (1 + AM_{pit})) \quad (\text{velocity change in pitch}) \quad (117)$$

$$dV_{yaw} = I_e \eta / (M \cdot rz^2 (1 + AM_{yaw})) \quad (\text{velocity change in yaw}) \quad (118)$$

## A.2 Popov Terms for Ice

In the Popov model, the ice floe is regarded as a special ship with similar dimensional definitions. The formulations for the ship added mass terms depend on empirical formulas based on the ship experimental data. In this report, the added mass terms for the ice are selected based on expected reasonable values for ice floes. In the future, more rational derivations of ice added mass terms may be developed. The ice floe equivalent mass can be expressed as:

$$M_{ice} = \frac{1}{\frac{l^2}{M_{ix}} + \frac{m^2}{M_{iy}} + \frac{n^2}{M_{iz}} + \frac{\lambda^2}{I_{ix}} + \frac{\mu^2}{I_{iy}} + \frac{\nu^2}{I_{iz}}} \quad (119)$$

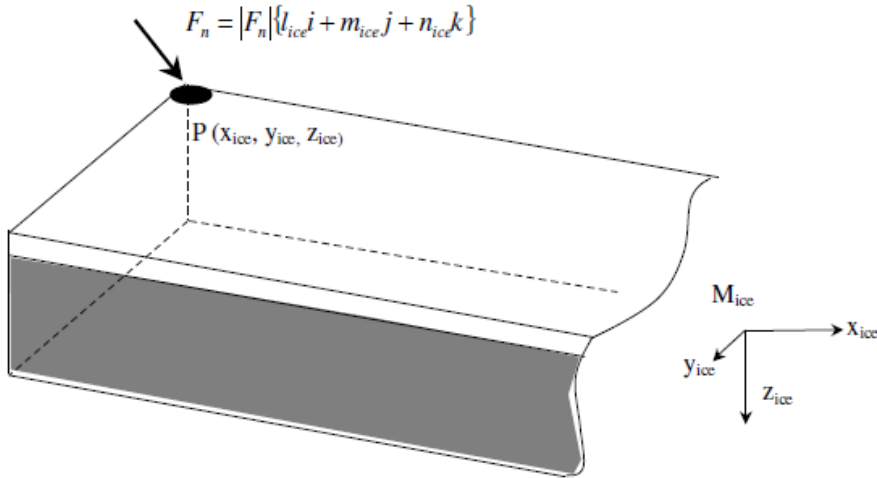


**Figure 66: Ice collision point geometry**

For the ice block the direction cosines  $l$ ,  $m$ , and  $n$  are:

$$l_{ice} = -\cos(\beta') \quad (120)$$

$$m_{ice} = 0 \quad (121)$$

$$n_{ice} = -\sin(\beta') \quad (122)$$

and the moment arms are;

$$\lambda_{ice} = n_{ice}y_{ice} - m_{ice}z_{ice} \quad (\text{roll moment arm}) \quad (123)$$

$$\mu_{ice} = l_{ice}z_{ice} - n_{ice}x_{ice} \quad (\text{pitch moment arm}) \quad (124)$$

$$\eta_{ice} = m_{ice}x_{ice} - l_{ice}y_{ice} \quad (\text{yaw moment arm}) \quad (125)$$

The added mass terms for the ice are assumed as follows;

$$AM_{x_{ice}} = 0.05 \quad (\text{added mass factor in surge}) \quad (126)$$

$$AM_{y_{ice}} = 0.05 \quad (\text{added mass factor in sway}) \quad (127)$$

$$AM_{z_{ice}} = 1.0 \quad (\text{added mass factor in heave}) \quad (128)$$

$$AM_{roll_{ice}} = 1.0 \quad (\text{added mass factor in roll}) \quad (129)$$

$$AM_{pit_{ice}} = 1.0 \quad (\text{added mass factor in pitch}) \quad (130)$$

$$AM_{yaw_{ice}} = 0.05 \quad (\text{added mass factor in yaw}) \quad (131)$$

The mass radii of gyration (squared) are;

$$rx_{ice}^2 = L^2/12 \quad (\text{roll}) \quad (132)$$

$$ry_{ice}^2 = L^2/12 \quad (\text{pitch}) \quad (133)$$

$$rz_{ice}^2 = L^2/9 \quad (\text{yaw}) \quad (134)$$

The six force (moment) actions on the six degrees of freedom of the vessel's center of gravity are;

$$F_{x_{ice}} = F_n l_{ice} \quad (\text{force in surge}) \quad (135)$$

$$F_{y_{ice}} = F_n m_{ice} \quad (\text{force in sway}) \quad (136)$$

$$F_{z_{ice}} = F_n n_{ice} \quad (\text{force in heave}) \quad (137)$$

$$M_{roll_{ice}} = F_n \lambda_{ice} \quad (\text{moment in roll}) \quad (138)$$

$$M_{pit_{ice}} = F_n \mu_{ice} \quad (\text{moment in pitch}) \quad (139)$$

$$M_{yaw_{ice}} = F_n \eta_{ice} \quad (\text{moment in yaw}) \quad (140)$$

There are six accelerations at the center of gravity are;

$$a_{x_{ice}} = F_n l / (M(1 + AM_x)) \quad (\text{acceleration in surge}) \quad (141)$$

$$a_{y_{ice}} = F_n m / (M_{ice}(1 + AM_y)) \quad (\text{acceleration in sway}) \quad (142)$$

$$a_{z_{ice}} = F_n n / (M_{ice}(1 + AM_z)) \quad (\text{acceleration in heave}) \quad (143)$$

$$a_{roll_{ice}} = F_n \lambda_{ice} / (M_{ice} r x_{ice}^2 (1 + AM_{roll_{ice}})) \quad (\text{acceleration in roll}) \quad (144)$$

$$a_{pit_{ice}} = F_n \mu_{ice} / (M_{ice} r y_{ice}^2 (1 + AM_{pit_{ice}})) \quad (\text{acceleration in pitch}) \quad (145)$$

$$a_{yaw_{ice}} = F_n \eta_{ice} / (M_{ice} r z_{ice}^2 (1 + AM_{yaw_{ice}})) \quad (\text{acceleration in yaw}) \quad (146)$$

Each of these accelerations contributes to the acceleration of the point of ice contact. The total acceleration at the point of contact can be expressed as;

$$\ddot{\zeta}_{ice} = F_n C_{o_{ice}} / M_{ice} \quad (147)$$

where;

$$C_o = \frac{l_{ice}^2}{1+AM_x} + \frac{m_{ice}^2}{1+AM_y} + \frac{n_{ice}^2}{1+AM_z} + \frac{\lambda_{ice}^2}{r x_{ice}^2 (1+AM_{roll})} + \frac{\mu_{ice}^2}{r y_{ice}^2 (1+AM_{pit})} + \frac{\eta_{ice}^2}{r z_{ice}^2 (1+AM_{yaw})} \quad (148)$$